Theoretical studies of elastic effects in segregation of small molecules in complex polymer mixtures-Impact on consumer goods industry

CROCE, SALVATORE

Theoretical studies of elastic effects in segregation of small molecules in complex polymer mixtures

Impact on consumer goods industry

Salvatore Croce

A Thesis presented for the degree of
Doctor of Philosophy

Department of Mathematical Sciences
Durham University
United Kingdom

October 2017-January2018

Theoretical studies of elastic effects in segregation of small molecules in complex polymer mixtures

Impact on consumer goods industry

Salvatore Croce

Submitted for the degree of Doctor of Philosophy

October 2017-January2018

Abstract: When a polymer mixture of two types of polymers having different molecular weights are left to equilibrate, the polymer having the lower molecular weight migrates to the free interface. This phenomenon is known as surface migration. We present a theoretical framework to explain this phenomenon and to quantitatively predict the amount of material that migrates to the interface. In what follows, we provide a review of the background literature, emphasizing the phenomenology behind such a segregation process, the different theoretical developments including variational methods and self consistent field theory as well as the experimental techniques that have been used to measure the amount of material leeches as a function of parameters e.g. temperature, surface tension and the mixing parameter (that determines whether the bulk polymeric phase is mixed or phase separated). The main hypothesis presented in this thesis is that the elasticity of the polymer matrix through which the low molecular weight species migrates to the free interface is an important parameter that has not been taken into account so far. This raises

the interesting possibility of controlling surface migration by tuning matrix rigidity by changing polymer elasticity with broad industrial applications. The structure of the thesis is as follows:

- Chapter 1 presents the fundamental properties of Gaussian chains, the phenomenology of migration and the bulk thermodynamics for polymer mixtures, together with the surface thermodynamics of fluids;
- Chapter 2 reviews the mean field theories for surface migration (Variational method and self consistent field theory);
- Chapter 3 introduces the elasticity as a property of the matrix and analyses the impact of different properties for manipulating polymer nanofilms;
- Chapter 4 presents the design of experiments as a tool for the subsequent comparison theory-experiments, a statistical analysis and some insights from computational simulations with C.U.L.G.I. (Chemistry Unified Language Graphics Interface);
- Chapter 5 reviews the Locally Correlated Lattice Theory (LCL) for the correct description of the bulk thermodynamics of compressible mixtures as well as the combination LCL migration theory needed for going beyond the limitation of Flory-Huggins and mean field theories;
- Chapter 6 reviews the content of the thesis, discussing the conclusions, some future research perspectives and open questions;

Declaration

The work in this thesis is based on research carried out within the Biomathematics group, the Department of Mathematical Sciences, Durham university, England and the Procter & Gamble Research & Development centre in Schwalbach am Taunus, Germany. No part of this thesis has been submitted elsewhere for any other degree or qualification and it is all my own work unless referenced to the contrary in the text. The work is based on the following collaborative research papers:

- Krawczyk, J., Croce, S., McLeish, T.C.B. & Chakrabarti, B. (2016); 'Elasticity dominated surface segregation of small molecules in polymer mixtures', Physical Review Letters 116(20): 208301;
- S. Croce,J. Krawczyk,G.Schäfer, T.Lindner, B. Chakrabarti; 'Surface segregation and wetting in binary polymeric gels' (2018, manuscript in preparation)
- S.Croce, B. Chakrabarti; 'Surface segregation and locally correlated lattice theory' (2018, manuscript in preparation)

Acknowledgements

I would like to thank all the people who supported me during this wonderful experience across countries. First amongst them my parents Maria Luisa and Franco who listened to and encouraged me through Skype in the dark times. My brother Piergiorgio who put new fire in my enthusiasm for science. My supervisor Dr Buddhapriya Chakrabarti, who taught me Soft Matter and Polymer Physics, had patience and supported me in my attempts to achieve the high standards required to publish in leading scientific journals, even working remotely for a very long time. The rest of my family who was always curious about what I was doing in this "PhD", in particular my uncle Mario and my relatives from Tocco da Casauria. I would like to thank all the people in the department of Mathematics for useful discussions across all the subjects of Mathematics, in particular Prof. Anne Taormina for supporting me during the last months of the PhD. Thank you to all the MICSED people as well, from the Department of Chemistry, among them Prof. John S.O. Evans and Miss Julie McLoughlin for having made the MICSED project real and Elise, Benjamin, Anna and Niamh for sharing with me this experience. The group of Theoretical Soft Condensed Matter in Physics, in particular Prof. Tom McLeish, for useful discussions on science. Thank you also to the people from my college St. John's, in particular the MCR, for giving me a wonderful experience as international student. Another thank you to all the amazing people I have met in Germany in P& G, among them my supervisors Dr. Gabriela Schäfer and Dr. Torsten Lindner for teaching me how to be an industrial scientist and Dr. Mattias Schmidt for inspiring discussions about industrial innovation. A big thank to all the P&G new hires, but also the

people from Wella, now in Coty for sharing with me the P&G *Frankfurter* experience. Last but not least all the Durham and Frankfurt Italian friends for continuously bringing me a little piece of my country. All of you are brilliant.

"La filosofia scritta in questo grandissimo libro che continuamente ci sta aperto innanzi a gli occhi (io dico l'universo), ma non si può intendere se prima non s'impara a intender la lingua, e conoscer i caratteri, ne' quali scritto. Egli scritto in lingua matematica, e i caratteri son triangoli, cerchi, ed altre figure geometriche, senza i quali mezzi impossibile a intenderne umanamente parola; senza questi un aggirarsi vanamente per un oscuro laberinto."
Trad:"Philosophy is written in this very big book that is continuously open in front of our eyes (I say universe), but one cannot understand if does not understand the language, know the characters, in which it is written. It is written in mathematical language and the characters are triangles, circles and other geometrical figures and without them it would be impossible to understand anything of that; without them it would be like wandering around an obscure labyrinth."

— from *Il Saggiatore* by G. Galilei

"Das allgemeine vorzgliche Kennzeichen der griechischen Meisterstcke ist endlich eine edle Einfalt, und eine stille Grüe, sowohl in der Stellung als im Ausdrucke. So wie die Tiefe des Meers allezeit ruhig bleibt, die Oberflche mag noch so wten, ebenso zeiget der Ausdruck in den Figuren der Griechen bei allen Leidenschaften eine groe und gesetzte Seele."
Trad:"The general preeminence of Greek masterpieces is, finally, a noble simplicity, and a stillness, both in position and in expression. As the depth of the sea is always calm, the surface may still be so, the expression shows in the figures of the Greeks, a great and established soul in all passions."

— from *Gedanken über die Nachahmung der griechischen Werke in der Malerei und Bildhauerkunst* by J.J. Winckelmann

Dedicated to

The Millennials, a generation with
a high level of education, but low
job perspectives.
I wish you to be as lucky as me in
finding your ideal job and path

Contents

Chapter 1

Introduction

We describe the phenomenon of surface segregation of the low molecular weight component of a polymer mixture to a surface that is open to atmosphere. In this chapter we introduce some fundamental properties of random chains, describe the phenomenology of migration and the different experimental techniques which have been used to explore the phenomenon, e.g. IBA-Ion Beam Analysis, NR-Neutron Reflectometry, XPS-X rays Photoemission Spectroscopy and the pendant drop for measuring the surface energy. Finally we review the theories for bulk and surface thermodynamics of polymer mixtures.

1.1 Polymers and random chains

Polymers are macromolecules, i.e. very large molecules made of repeated units (monomers) arranged in a chain. The number of units, which we denote by N, is called the "degree of polymerization". We speak about polymers if the chain molecules are made of more then 100 monomers, in other words, when the degree of polymerization is greater than 100. It is easy to find natural systems with a degree of polymerization of up to $10^7 - 10^9$ (DNA and biologycal systems). Polymers exhibit properties which are in between normal fluids and solid and they are classified in the middle world of "soft materials". Several complex formulations are mixtures of

such long chains molecules and it is extremely difficult to connect the macroscopic properties of such mixtures to microscopic features of molecules that make up the mixture. In particular, the segregation and migration to the surface of polymer mixtures is an interesting phenomenon with varied applications in everyday life. Binary mixture migration, which occurs when the lower molecular weight component of a two-component polymer mixture travels to the surface, results in a phase separation that may decrease the functionality of certain products. Many polymeric materials such as plastics, adhesives and even chocolate [82] and food packaging [6] are affected by this phenomenon which, despite many studies, is not yet well understood.

In this section, we briefly review some basic concepts and physical properties of polymer chains.

Ideal polymer chain and random walk

The simplest model to describe a polymer is the ideal chain model, where the monomers (units) are represented by rigid rods, all of length b (the Kuhn length). If the polymer is made of N monomers, its total length is therefore $L = Nb$. Each rod is joined to the next by a perfectly flexible joint. It is assumed that the orientation of any particular rod is independent of the orientation and location of neighbouring rods in the chain, and in particular, two rods can occupy the same space in an ideal chain model.

The description of the exact state of a polymer at a particular time, and how it evolves subsequently, requires a vast number of parameters. For instance, one would need to take into account the angles of every chemical bond. The complexity of the task makes it impossible to provide accurate predictions on the exact state of a polymer at any time t, but it is possible to predict average properties of a given polymer's shape by treating each configuration in a series of "snapshots" taken at consecutive times as a 3-dimensional random walk.

To describe the random walk, one considers the polymer as a chain on a cubic lattice, where each joint sits at one of the corners of a cube centred on the previous joint in the chain. Let the cube have sides of length 2λ. In this set up, the rods have Kuhn length $b = \sqrt{3}\lambda$. Considering $\mathbf{R}$ as the vector connecting the two ends of the polymer and $\mathbf{r}_n$ as the random vector representing rod n, we can write:

$$\mathbf{R} = \sum_{n=1}^{N} \mathbf{r}_n. \tag{1.1.1}$$

We notice that the average value $\langle \mathbf{R} \rangle$ of the vector $\mathbf{R}$ is zero. Indeed, although the two ends of the polymer do not coincide, they fluctutate randomly around each other. Since N is considered to be very large, one can use the central limit theorem, which, given that the vectors $\mathbf{r}_n$ are all independent of each other, yields a mean-square distance between the ends of the chain:

$$\left\langle \mathbf{R}^2 \right\rangle = \sum_{n=1}^{N} \left\langle \mathbf{r}_n^2 \right\rangle = Nb^2. \tag{1.1.2}$$

We immediately notice that the size of an ideal polymer chain is proportional to $\sqrt{N}$, so it scales with the square root of the degree of polymerisation. It is easy to calculate the probability distribution function of $\mathbf{R}$. For a polymer with N monomers and one end fixed at the origin, let $P(\mathbf{R}, N)$ be the probability of the other end to be at position $\mathbf{R}$. Let z be the coordination number of the lattice, i.e. the number of nearest neighbour lattice sites of any particular joint. Following Doi [29] and denoting by $\mathbf{b}_i (i = 1, ..., z)$ the possible vectors that link a joint to its nearest neighbours in the chain polymer, the probability of the polymer end being at position $\mathbf{R}$ can be written as:

$$P(\mathbf{R}, N) = \frac{1}{z} \sum_{i=1}^{z} P(\mathbf{R} - \mathbf{b}_i, N - 1). \tag{1.1.3}$$

If the polymer is very long, we can expand eq. (1.1.3) into a Taylor series and in this way, using the central limit theorem, the probability distribution function will be:

$$P(N, \mathbf{R}) = \left(\frac{3}{2\pi N b^2} \right)^{\frac{3}{2}} \exp\left(-\frac{3\mathbf{R}^2}{2Nb^2} \right). \tag{1.1.4}$$

We immediately notice that the function is a Gaussian. Actually, *random chains* and *Gaussians* are the core of the classic approach to Polymers, see [44, 29, 105]. We can calculate the free energy for ideal chains by taking the logarithm of the probability distribution, obtaining:

$$F(N, \mathbf{R}) = \frac{3\mathbf{R}^2}{2Nb^2} k_B T + F(N, 0) \tag{1.1.5}$$

where $F(N, 0)$ is the free energy of the chain with both ends at the same point. Within this framework we speak about Gaussian chains. Polymer models are equivalent to the random walk model when we consider b as an effective length. Deviation from this ideal behaviour can be analysed with scaling arguments. In our model we are considering only short-range interactions and the system could be quite different with long-range interaction. For example one of the long-range effect is the excluded volume, simply because occupying the same volume at the same time is forbidden. Considering the Gaussian chains we can also introduce the bead-spring model where we consider that each part of the chain is linked by a spring, with a harmonic potential:

$$U = \frac{1}{2} k \sum_{n=1}^{N} (\mathbf{R}_n - \mathbf{R}_{n-1})^2 \tag{1.1.6}$$

where the spring constant is $k = \frac{3k_B T}{b^2}$ as in Doi [29].

Deviation from Gaussian behaviour

In a real system we should consider that polymers cannot overlap. So considering an interaction potential $U(\mathbf{r})$ between polymers at a fixed distance of each other, we can define the Mayer-f function for the overlapping probability:

$$f(\mathbf{r}) = \exp\left(-\frac{U(\mathbf{r})}{k_B T}\right) - 1 \tag{1.1.7}$$

which is zero for $\mathbf{r} \to 0$ and decreases very rapidly for higher values. The excluded volume of the system will be:

$$v = \int d\mathbf{r} f(\mathbf{r}) \tag{1.1.8}$$

with $f(\mathbf{r}) < 0$ when $U(\mathbf{r}) > k_B T$ and $f(\mathbf{r}) > 0$ when $U(\mathbf{r}) < k_B T$.
Considering a virial expansion of the free energy density, the excluded volume will be the coefficient of the second order. Adding also the entropic contribution we obtain the function:

$$F = F_{int} + F_{ent} = k_B T \left(v \frac{N^2}{R^3} + \frac{R^2}{N b^2} \right) \tag{1.1.9}$$

and minimizing it we obtain the contribution of the self-avoiding to the dimension of the system:

$$R \sim R_0 N^{\frac{3}{5}} \tag{1.1.10}$$

that is different from the expression in eq.(1.1.2). In the general case the formula for considering the excluded volume is:

$$R \sim N^{\nu} b \tag{1.1.11}$$

where the experimental value of ν is 0.588, very similar to the theoretical value. The value gives us a ratio as a scaling argument, of the deviation from ideal behaviour. Scaling will be important across our work, as we shall see in the next chapters.

1.2 Experiments and phenomenology of migration

The pioneer study of segregation in polymer mixtures has been performed in the early '80s by Pan et al.[95] with the X-ray Photo Emission Spectroscopy (XPS), analysing the X-Ray interaction with the interface of a blend of polystyrene (PS) and poly(vynil methyl ether)PVME on an aluminium substrate heated above the critical solution temperature. Measuring the peaks of C_{1s}, the carbon emission spectra, they compared the results with a model by Prigogine et al. [100], that we will study

in more detail in Chapter 2, but without a proper fit of the experimental data. Following that study Bhatia et al. [4] combined the XPS and the surface tension measurements, improving the resolution of the segregation profile, but still lacking in a perfect explanation of the subject. Both studies introduced the concentration of migrants as a function of the distance z from the wall, defined as:

$$\phi_j = \frac{V_j}{\sum_i V_i} \tag{1.2.1}$$

where V_j is the volume of a single component and $\Sigma_j V_j$ is the total volume. In both studies the research groups were not able to obtain high resolutions results. A big step forward has been made by Jones and co-workers [66] with the introduction of a new experimental technique, neutron reflectivity (NR). NR is a technique which makes use of the reflection of electrons in the first layers of an interface. It is particularly good for studying nanofilms ($h \leq 100nm$) and in particular organic compounds, partially transparent to X-rays, such as polymers. A few years later Steiner et al.[118] studied not only segregation systems, but they also paid attention to the existence of wetting, as a macroscopic layer at the polymer air interface. After that measurement a comparison between experiments and theory was performed by Jones' group [66]. We can see a comparison between measurements obtained by XPS and NR in fig.(1.1). We shall describe the fundamental thermodynamic properties in the next sections.

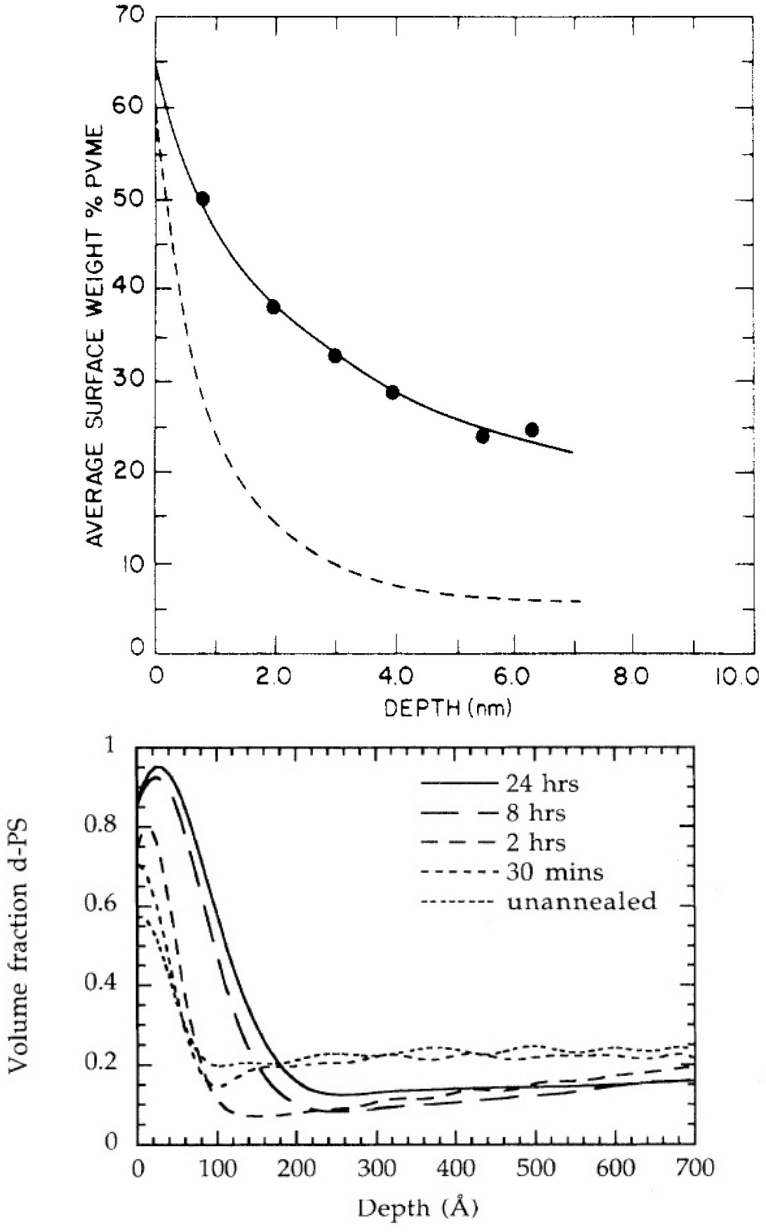

Figure 1.1: XPS results on the top [5] with experimental data (points) and Prigogine's model (dashed line). Fraction of volume as function of time from NR at the bottom [66]. We notice a significant improvement of the resolution. Figures reproduced from the papers.

System study

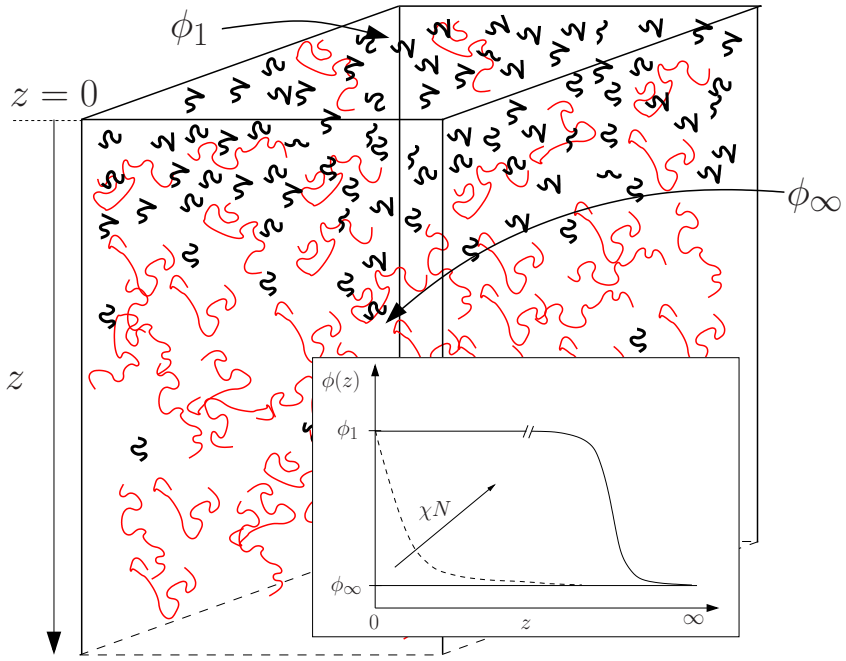

Figure 1.2: Schematic of the system .

Fig.(1.2) shows a schematic representation of the system having two components, a large polymer matrix (red) and small molecules (black) in a box, migrating from the bulk ($z \to \infty$) to the surface ($z = 0$). ϕ_1 is the amount of migrant molecules at the surface while ϕ_∞ is the amount of migrant molecules in the bulk. The segregation and wetting are driven by increasing N, the entropy, and χ, the enthalpy. The next two sections summarise the thermodynamics of the bulk of this system and of the additional effects present at the surface separating the bulk polymer mixture from the atmosphere.

1.3 Bulk properties for polymer mixtures: Flory-Huggins theory

We describe the thermodynamics of polymer mixtures with Flory-Huggins theory, the analog for polymer systems of the Bragg-Williams theory [10] applied to metal alloys.

Following Rubinstein and Colby [105] we start by considering a mixture of polymers of two different types a and b. The theory is put on a finite lattice containing n sites, and we denote by v_0 the volume of a lattice site, which corresponds to the volume of a monomer (here, we assume that all monomers of both polymer types have the same volume). With N_a and N_b the degrees of polymerization and n_a, n_b the number of polymers of type a and b respectively, the volume occupied by all polymers of each type is given by $V_i = n_i\, N_i v_0$, $i = a, b$, so that the total volume of the lattice is $V_a + V_b$ and the total number of lattice sites is

$$n = \frac{V_a + V_b}{v_0}. \tag{1.3.1}$$

In this simplified lattice theory called the Flory-Huggins (FH) theory, one assumes that the two polymer types mix at constant volume, so that in order to determine the thermodynamical equilibrium of the mixture, one needs to minimize the Helmholtz free energy of mixing per lattice site, $\Delta\bar{F}_{mix}$, which is an intrinsic thermodynamic quantity. This free energy receives a contribution from the mixing entropy of the system, $\Delta\bar{S}_{mix}$, and from the energy change on mixing, $\Delta\bar{U}_{mix}$. An important parameter in the binary system we study is ϕ, which is called the composition and which controls the volume fractions $\phi_i = \frac{V_i}{V_a+V_b}$, $i = a, b$ of both types of polymers:

$$\phi_a = \phi \ , \ \phi_b = 1 - \phi. \tag{1.3.2}$$

This parametrisation is derived from the assumption of incompressibility we have made, namely $\phi_a + \phi_b = 1$. With these definitions, one notes that all polymers of type i in the mixture occupy $n\phi_i = \frac{V_i}{v_0}$ sites, and therefore, the number of states

that a single polymer of type i can be in before mixing, Ω_i, is equal to the number of lattice sites occupied by all polymers of type i, i.e. $\Omega_i = n\phi_i$. Furthermore, in an homogeneous mixture of the two types of polymers, each polymer can be in $\Omega_{ab} = n$ states. Since the entropy is generically the product of the Boltzmann constant k_B by the natural logarithm of the number of states accessible to all components of a system, in our model the entropy change on mixing for a single polymer of type i is given by the difference between the entropy of that polymer in the homogeneous mixture of polymers of type a and b and the entropy of that polymer in pure state i (before mixing):

$$\Delta S_{mix,i} = k_B(\log \Omega_{ab} - \log \Omega_i) = k_B \log \frac{n}{n\phi_i} = -k_B \log \phi_i, i = a, b. \tag{1.3.3}$$

The total entropy of mixing per lattice site is therefore

$$\Delta \bar{S}_{mix} = \frac{1}{n} \sum_{i=a,b} n_i \Delta S_{mix,i} = \sum_{i=a,b} \frac{\phi_i}{N_i} \Delta S_{mix,i} = \\ - k_B \left\{ \frac{\phi}{N_a} \log(\phi) + \frac{1-\phi}{N_b} \log(1-\phi) \right\}. \tag{1.3.4}$$

Since the degrees of polymerisation are assumed to be very large, the mixing entropy is very small. The Helmoltz free energy per lattice site is given by

$$\Delta \bar{F}_{mix} = \Delta \bar{U}_{mix} - T \Delta \bar{S}_{mix}, \tag{1.3.5}$$

and we now derive $\Delta \bar{U}_{mix}$, which is the energy change per lattice site on mixing. This contribution to the free energy depends on the strength of interactions between type a (χ_{aa}) or type b (χ_{bb}) monomers, and between type a and b ($\chi_{ab} = \chi_{ba}$) monomers. It is assumed that all energies of interaction are between pairs of monomers occupying adjacent lattice sites. The average pairwise interaction of a monomer of type i with one neighbouring monomer (which can be of type a or b) is

$$U_i = \chi_{ii}\phi_i + \chi_{ij}\phi_j, \ i \neq j \text{ and } i, j \in \{a, b\} \tag{1.3.6}$$

with no summation on i and j. From these quantities, one builds the total interaction energy of the mixture as

$$U_{after\ mix} = \frac{z}{2} \sum_{i=a,b} U_i n\phi_i \tag{1.3.7}$$

where z is the coordination number of the lattice and where the factor of $\frac{1}{2}$ compensates for the double-counting of pairwise interactions. Recall that $n\phi_i$ is the number of sites occupied by all polymers of type i. Using eq.(1.3.2) and eq.(1.3.6), one obtains the total interaction energy of a mixture of two polymer types on a lattice with n sites as

$$U_{after\ mix} = \frac{zn}{2} \left\{ \chi_{aa}\phi^2 + 2\chi_{ab}\phi(1-\phi) + \chi_{bb}(1-\phi)^2 \right\}. \tag{1.3.8}$$

On the other hand, before mixing, the total energy of polymers of type i is

$$U_{ii} = \frac{zn}{2} \chi_{ii}\phi_i, \ \ i = a, b \tag{1.3.9}$$

since there is no neighbouring site of a monomer of type i that could be of a different type (pure state), and end-of-chain effects are neglected as the chains are very long (N_i very large). Hence before mixing, the total interaction energy of the system is

$$U_{before\ mix} = \frac{zn}{2} \sum_{i=a,b} \chi_{ii}\phi_i. \tag{1.3.10}$$

Finally, the total interaction energy change per lattice site on mixing is given by

$$\Delta\bar{U}_{mix} = \frac{1}{n}(U_{after\ mix} - U_{before\ mix}) = \frac{z}{2}\phi(1-\phi)(2\chi_{ab} - \chi_{aa} - \chi_{bb}). \tag{1.3.11}$$

This energy can be rewritten in terms of the Flory-Huggins interaction parameter χ,

$$\chi = \frac{z(2\chi_{ab} - \chi_{aa} - \chi_{bb})}{2k_BT} \tag{1.3.12}$$

which represents the mean field pairwise interaction for the surrounding polymers. With the help of eq.(1.3.4), eq.(1.3.11), eq.(1.3.12) and eq.(1.3.2), we arrive at the following expression for the Helmoltz free energy per lattice site eq.(1.3.5):

$$\Delta\bar{F}_{mix} = k_BT \left\{ \frac{\phi}{N_a} \log(\phi) + \frac{1-\phi}{N_b} \log(1-\phi) + \chi\phi(1-\phi) \right\}, \tag{1.3.13}$$

which is the Flory-Huggins equation describing the bulk properties of a mixture of two polymer types a and b.

Free energy curves can be used to determine the most stable state for a system, i.e. the phase or phase mixture with the lowest free energy for a given temperature T and composition ϕ. As a first example, fig.(1.3) shows the function $\Delta\bar{F}_{mix}(\phi)/k_BT$, with a volume equal to one, for different values of the F-H constant χ. In particular if we consider only the energetic contribution ($T = 0$) for $\chi < 0$ the mixtures are stable, while for $\chi > 0$ the mixtures are not stable [44]. Let us study the qualitative

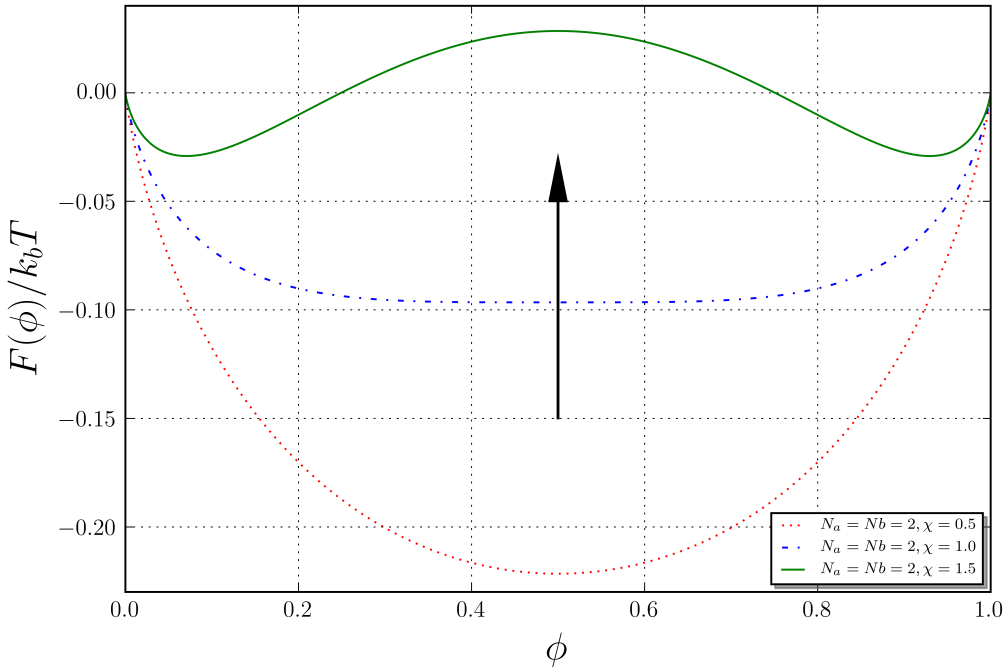

Figure 1.3: F-H free energy, in units of k_BT, as a function of the composition ϕ for systems with same degree of polymerisation, but different interaction parameter χ, increasing in the direction of the arrow ($\chi_c = 1$). We notice a single phase for $\chi < \chi_c$, a plateau at $\chi = \chi_c$ and two different phases for $\chi > \chi_c$.

shape of the free energy curve $\Delta\bar{F}_{mix}(\phi)$ in the interval $0 \leq \phi \leq 1$ at different temperatures. We first note that

$$\frac{\partial \Delta\bar{F}_{mix}}{\partial\phi} = k_BT\left\{\frac{1}{N_a}\log\phi - \frac{1}{N_b}\log(1-\phi) + \frac{1}{N_a} - \frac{1}{N_b}\right\} + k_BT\chi(1-2\phi), \quad (1.3.14)$$

which shows that the slope of the curve tends to $-\infty$ as ϕ tends to 0, and tends to ∞ when ϕ tends to 1. This behaviour is driven by the entropic contribution to the free energy and it implies that small amounts of type a polymers (when $\phi \sim 0$) and small amounts of type b polymers (when $\phi \sim 1$) will always mix and provide stable states, even if the energy interactions are less than favourable. For intermediate compositions, there is a competition between the entropic contribution and the interaction energy contribution, and the local stability of the two polymer types mixture is determined by the sign of the second derivative of the free energy at a given composition. A positive sign corresponds to an instability while a negative sign corresponds to a stable state. One has

$$\frac{\partial^2 \Delta \bar{F}_{mix}}{\partial \phi^2} = k_B T \left\{ \frac{1}{N_a \phi} + \frac{1}{N_b(1-\phi)} - 2\chi \right\}. \tag{1.3.15}$$

At high temperatures, the entropic contribution dominates, which results in all compositions being stable, but as the temperature decreases, the interaction energy of mixing increases at the expense of the entropic contribution, and the free energy curve "bulges" at intermediate compositions, presenting a region where it becomes concave, with a local maximum, between two values of composition, say ϕ_α and ϕ_β, which are determined through the construction of "common tangent". Mathematically, ϕ_α and ϕ_β must solve the two equations

$$\left.\frac{\partial \Delta \bar{F}_{mix}}{\partial \phi}\right|_{\phi_\alpha} = \left.\frac{\partial \Delta \bar{F}_{mix}}{\partial \phi}\right|_{\phi_\beta} \tag{1.3.16}$$

and

$$\Delta \bar{F}_{mix}(\phi_\alpha) - m\phi_\alpha = \Delta \bar{F}_{mix}(\phi_\beta) - m\phi_\beta, \tag{1.3.17}$$

using the formulas eq.(1.3.13) and eq.(1.3.14). Once the solution $(\phi_\alpha, \phi_\beta)$ is found, set $m \equiv \left.\frac{\partial \Delta \bar{F}_{mix}}{\partial \phi}\right|_{\phi_\alpha}$ and $c \equiv \Delta \bar{F}_{mix}(\phi_\alpha) - m\phi_\alpha$ and the sought common tangent has equation

$$t(\phi) = m\phi + c. \tag{1.3.18}$$

The physical significance of this common tangent will be explained later on. Note

that the points ϕ_α and ϕ_β are called "binodal points". At temperatures lower than a critical temperature (or equivalently, at values of the F-H parameter χ higher than a critical value χ_c), there are two other significant points on the Helmoltz free energy curve: its points of inflection, i.e. the points with compositions $\phi^{(1)}_{\text{spin}}$ and $\phi^{(2)}_{\text{spin}}$ solving the equation

$$\frac{\partial^2 \Delta \bar{F}_{mix}}{\partial \phi^2} = k_B T \left\{ \frac{1}{N_a \phi} + \frac{1}{N_b (1-\phi)} - 2\chi \right\} = 0. \tag{1.3.19}$$

The points $(\phi^{(1)}_{\text{spin}}, \Delta \bar{F}_{mix}(\phi^{(1)}_{\text{spin}}))$ and $(\phi^{(2)}_{\text{spin}}, \Delta \bar{F}_{mix}(\phi^{(2)}_{\text{spin}}))$ are called the spinodal points of the Helmoltz free energy curve at a given fixed temperature or F-H parameter. Plots of $\Delta \bar{F}_{mix}(\phi)$ at various values of the F-H parameter χ are presented in fig.(1.3) for a symmetric F-H theory (i.e. with $N_a = N_b \equiv N$) and in fig.(1.5) for an asymmetric theory (dashed blue curve). In fig.(1.3), one observes that, as the F-H parameter decreases, the two binodal points visible on the green curve merge to one in the blue and red curves, and once they have merged, the spinodal points disappear. A similar phenomenon is present in asymmetric F-H theories. This type of data, i.e. the data of free energy curves as functions of the composition at various F-H parameter values (keeping N_a and N_b fixed) can be encoded in a phase diagram where the phase boundaries are determined by the so-called spinodal and binodal curves. But before we draw such a diagram, let us study the stability of states in an asymmetric F-H theory for a specific Helmholtz energy curve with F-H parameter larger than χ_c. In this regime, the free energy curve is given by an asymmetric double-well curve, with qualitative features as in fig. (1.4). If we consider a mixture of composition ϕ_0 on that plot, its free energy is higher than the free energy of mixtures in phases α and β. The system will therefore attempt to reduce its free energy through existing as a mixture of two distinct phases at compositions ϕ_0^α and ϕ_0^β, where ϕ_0^β is determined from the knowledge of ϕ_0^α by drawing a straight line parallel to the common tangent $t(\phi)$ and through the points $(\phi_0^\alpha, G(\phi_0^\alpha))$ and $(\phi_0^\beta, G(\phi_0^\beta))$ (magenta dots on fig. (1.4)). Given ϕ_0, this "phase splitting" may occur for any composition ϕ_0^α in the range $[\phi_\alpha, \phi_0[$, using the common tangent rule to determine the corresponding ϕ_0^β. Note that the new energy curve defined as $\tilde{G}(\phi) = G_\phi - t(\phi)$

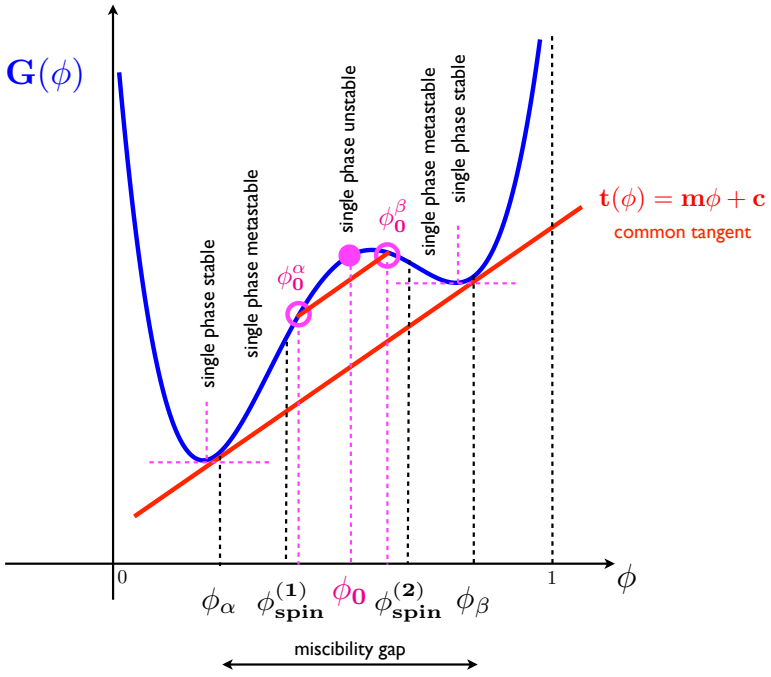

Figure 1.4: Qualitative features of the Helmoltz free energy G at F-H parameter larger than χ_c and common tangent construction.

has local minima ϕ_α and ϕ_β at the same energy level. This is illustrated in fig. (1.5) for the F-H asymmetric theory. The interval $[\phi_\alpha, \phi_\beta]$ bounded by the binodal points

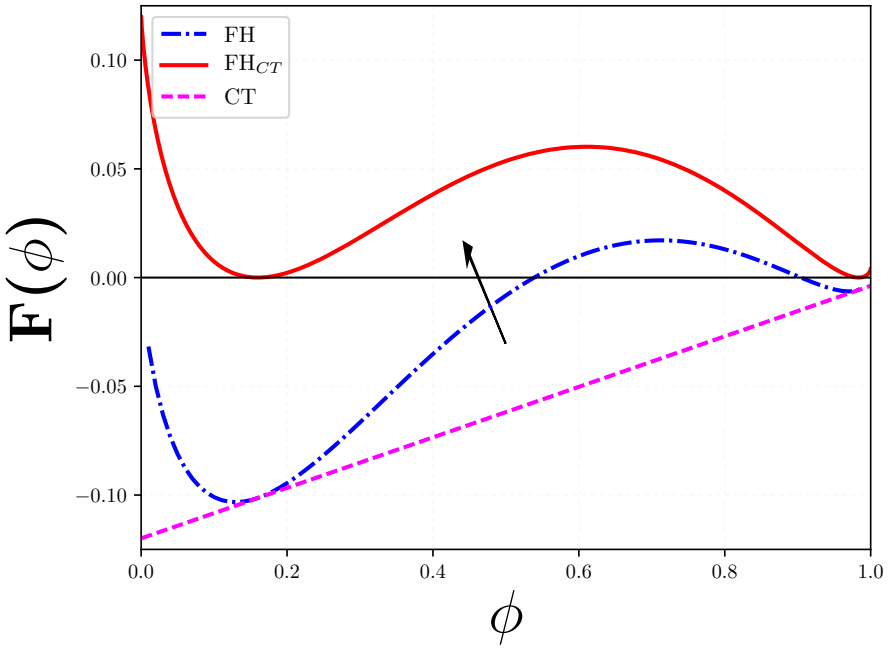

Figure 1.5: Common tangent construction calculated numerically for an asymmetric Flory-Huggins (FH) free energy with $N_a = 1, N_b = 4$ and $\chi = 1.7$. By construction, after subtraction of the common tangent (CT) from the FH free energy, the resulting function of composition (FH_{CT}) has two local minima at the same energy level.

is called the miscibility gap, while the interval $[\phi^{(1)}_{\text{spin}}, \phi^{(2)}_{\text{spin}}]$ determines the spinodal region, which is an unstable region. Indeed, in that region the second derivative of the free energy is negative, and the mixed state is unstable, as the tiniest fluctuations in composition lead to phase separation. This is called "spinodal decomposition". In the remainder of the miscibility gap, the mixed state is locally stable to small fluctuations in composition, and this region is metastable. In the regions outside the miscibility gap, the mixed states are stable, as was justified after eq.(1.3.14). Note that, since the common-tangent construction minimizes the free energy of mixing over some range of compositions, namely in the domain of miscibility $[\phi_\alpha, \phi_\beta]$, and since the equilibrated system over this range consists of the two phases α and β, then these two phases, being at equilibrium, must have the same chemical potential for each polymer type.

We end this section by presenting the phase diagram summarising the regions of stability, metastability and instability as the F-H parameter χ varies in the expression eq.(1.3.13) for $\Delta\bar{F}_{mix}$ for all possible compositions. For this, we need to calculate the boundary curves between these different regions, wich are called "binodal and spinodal curves". The binodal curve contains all pairs of binodal points $(\phi_\alpha, \Delta\bar{F}_{mix}(\phi_\alpha), (\phi_\beta, \Delta\bar{F}_{mix}(\phi_\beta))$, each pair corresponding to the binodal points of a Helmoltz free energy curve at fixed parameter χ. Its derivation is simpler in the symmetric case, where it is clear that the slope of the common tangent is zero, and hence the compositions ϕ_α and ϕ_β correspond in this case to the local minima of the Helmoltz free energy $\Delta\bar{F}_{mix}$, which are found by solving

$$\frac{\partial\Delta\bar{F}_{mix}}{\partial\phi} = 0 \tag{1.3.20}$$

for ϕ. In other words, the values ϕ_α and ϕ_β are solutions of

$$k_BT\left\{\frac{1}{N}\log\phi - \frac{1}{N}\log(1-\phi)\right\} + k_BT\chi(1-2\phi) = 0 \tag{1.3.21}$$

at given $N_a = N_b = N$ and F-H parameter χ. But one can also solve eq.(1.3.21) for χ as a function of the composition ϕ, yielding the binodal curve for symmetric F-H theory,

$$\chi_{\text{bin}}(\phi) = \frac{\log\phi - \log(1-\phi)}{N(2\phi-1)}. \tag{1.3.22}$$

This curve is plotted in fig.(1.6) for $N = 1$ and $N = 5$ as a function of the composition.

The spinodal curve can easily be derived in the more general asymmetric theory by setting eq.(1.3.15) to zero and solving for χ. This yields

$$\chi_{\text{spin}}(\phi) = \frac{1}{2}\left(\frac{1}{N_a\phi} + \frac{1}{N_b(1-\phi)}\right). \tag{1.3.23}$$

The minimum of the function $\chi_{\text{spin}}(\phi)$ is the critical point ϕ_c, which in turn yields the value of the critical interaction parameter χ_c above which the homogeneous mixed phase is unstable and the two type polymer mixture is phase-separated. One easily

obtains the critical composition and the critical F-H parameter as

$$\phi_{\rm c} = \frac{\sqrt{N_b}}{\sqrt{N_a}+\sqrt{N_b}} \tag{1.3.24}$$

$$\chi_{\rm c} = \frac{1}{2}\left(\frac{1}{\sqrt{N_a}}+\frac{1}{\sqrt{N_b}}\right)^2. \tag{1.3.25}$$

In the symmetric case, it is sufficient to set $N_a = N_b = N$ in the above expressions and in particular, eq. (1.3.24) and eq.(1.3.25) simplify as:

$$\phi_c = \frac{1}{2} \tag{1.3.26}$$

$$\chi_c = \frac{2}{N}. \tag{1.3.27}$$

Fig. (1.6) reproduces two phase diagrams for $N_a = N_b = 1$ and $N_a = N_b = 5$. The metastable regions are in-between the binodal and the spinodal curves in each case, while the region within the spinodal curves is unstable. The region under the binodal curve is stable.

Finally in the very special cases of low concentrations, $\phi \to 0$, $\phi \to 1$, we can find solutions of the F-H equation in the bulk. In particular with the first approximation we can expand the logarithm in a power series, obtaining a mixing energy:

$$\frac{F_{\rm mix}}{k_B T} = \left[\frac{\phi}{N_a}\log\phi + \phi(\chi - \frac{1}{N_b}) + \phi^2(\frac{1}{N_b} - 2\chi) + \frac{\phi^3}{6N_b} + ...\right] \tag{1.3.28}$$

which is an expression similar to a Ginzburg-Landau [53] free energy for the phase transition of a system.

The F-H theory outlined above presents some limitations, such as the incompressibility constraint ($\sum_i \phi_i = 1$). We will see how to avoid this weakness in Chapter 5 with the Locally Correlated Lattice (LCL) theory.

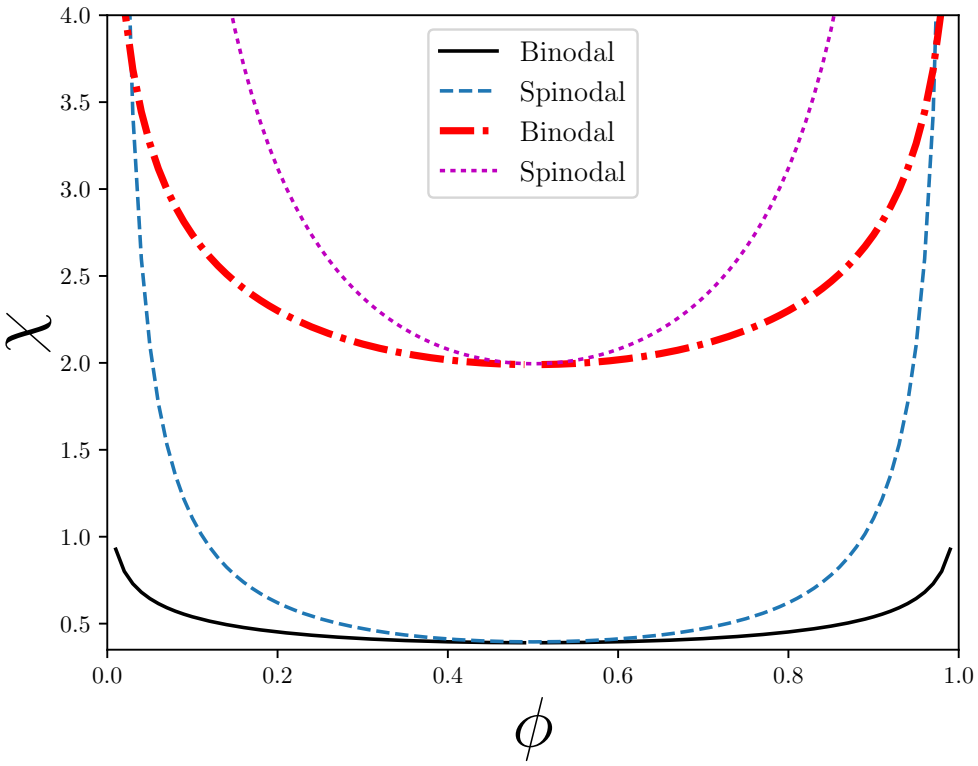

Figure 1.6: Values of the F-H constant in the binodal region for different degrees of polymerization, as a function of the fraction of volume ϕ (top), and comparison between the different χ on the binodal, spinodal and critical cases for a symmetric system (bottom).

1.4 Surface Properties: Cahn's theory of wetting

While the Flory-Huggins (FH) theory qualitatively captures the basic features of the thermodynamics of polymer mixtures, there are limitations adapting it to real polymers. A framework similar to FH theory has been applied to real gases that involve a phase transition. In particular for unstable regions of the P-V curve, for liquid-gas systems in the vicinity of a phase transition, one uses the gas equation [103] in conjunction with a graphic method introduced by Maxwell [85] with equal area construction. A similar approach has been introduced by Cahn [19] in the case of wetting transitions. There are different types of wetting behaviours [43, 9] and

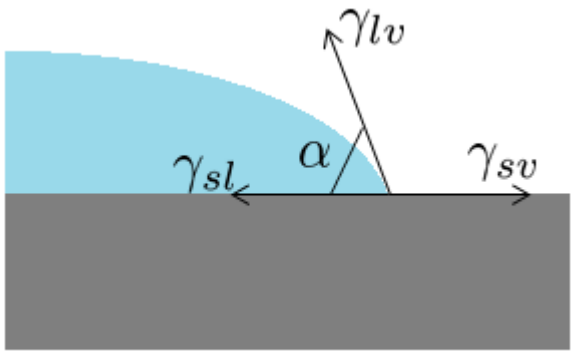

Figure 1.7: Sessile drop with different surface tensions for solid-liquid, solid-vapour and liquid-vapour interfaces. Adapted from Bonn et al.[9].

they can be classified depending on the balance between the surface tensions of the different phases. In fig.(1.7) we see a schematic with a sessile drop, the contact angle α and the surface tensions, i.e. solid-liquid (γ_{sl}), liquid-vapour (γ_{lv}) and solid-vapour (γ_{sv}) by means of the Young-Dupré equation:

$$\gamma_{sv} = \gamma_{sl} + \gamma_{lv} \cos \alpha_{eq} \tag{1.4.1}$$

where all quantities are measured in Nm and the angle α is at equilibrium. There are three possible wetting behaviours for the system:

- $\gamma_{sv} < \gamma_{sl} + \gamma_{lv}$ corresponds to partial wetting;
- $\gamma_{sv} = \gamma_{sl} + \gamma_{lv}$ corresponds to complete wetting;

- if $\gamma_{sv} > \gamma_{sl} + \gamma_{lv}$ the surface is completely dry;

as shown in fig.(1.8).

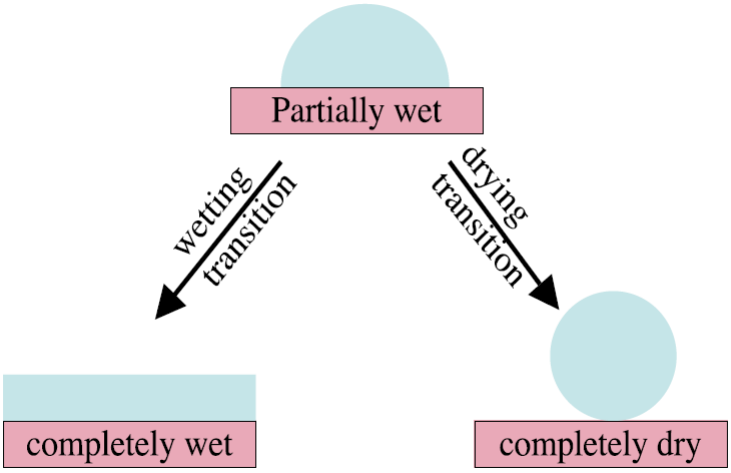

Figure 1.8: Different wetting scenarios, adapted from Bonn et al. [9]

Considering the thermodynamics in more details, it is possible to give a quantitative description of the wetting transition in terms of the free energy of the system.

We refer back to the schematic diagram introduced in fig. (1.2), with a semi-infinite liquid (that will be a two-type polymer mixture later on) for $z > 0$ in contact with a plane solid surface localized at $z = 0$). As in fig. (1.2), we denote by ϕ_1 the composition of the liquid at the surface, which for us will be the volume fraction of the small migrating polymers at the surface, ϕ_1 and by ϕ_∞ the volume fraction of the migrant polymers deep in the bulk ($z \to \infty$).

In this section, we summarise aspects of Cahn's theory of wetting that will be useful later. This material is based on [19, 43]. We make the following assumptions in deriving the theory of wetting applied to fluid systems:

- we describe the solid/liquid interface within the framework of a continuum theory where the liquid composition $\phi(z)$ varies smoothly as a function of the distance z. This is a reasonable assumption if the system is studied near the critical temperature;

- we consider only short range forces between the liquid and the solid, which can be described by adding a surface energy contribution $F_s(\phi_1)$ to the energy $F_d(\phi)$ produced by the distortions in the $\phi(z)$ composition profile of the system. Although the Cahn's construction we are summarising below allows for a more general form of the functional $F_s(\phi_1)$, we will use the following simple polynomial form,

$$F_s(\phi_1) = -\mu_1\phi_1 - \frac{g}{2}\phi_1^2, \tag{1.4.2}$$

where μ_1 is the surface chemical potential and g measures the change in bulk interactions due to the surface (missing neighbours).

- we simplify the distortion energy contribution by taking

$$F_d(\phi) = \int_{z_{surf}}^{z_{bulk}} dz\, \mathcal{L}(\phi, d_z\phi) = \int_{z_{surf}}^{z_{bulk}} dz \left(\Delta F(\phi) + k \left(\frac{d\phi}{dz} \right)^2 \right) \tag{1.4.3}$$

where $z_{surf} = 0, z_{bulk} = z \to \infty$ and

$$\Delta F(\phi) = \Delta \bar{F}_{mix}(\phi) - \Delta \bar{F}_{mix}(\phi_\infty) - \mu(\phi - \phi_\infty), \tag{1.4.4}$$

with $\Delta \bar{F}_{mix}$ being the asymmetric double-well Flory-Huggins bulk free energy in eq.(1.3.13) and μ being the chemical potential $\Delta \bar{F}_{mix}(\phi)$ as reviewed in Section 1.3. Hence, the functional $\Delta F(\phi)$ is a symmetric double-well functional, i.e. its two minima are at the same energy level for the two equilibrium compositions ϕ_l (liquid) and ϕ_v (vapour). The integrand $\mathcal{L}(\phi, d_z\phi)$ is known as the square gradient approximation of the free energy functional, where $\Delta F(\phi)$ is a mean field expression for the free energy and where the square gradient $k \left(\frac{d\phi}{dz} \right)^2$ takes into account the fluctuation at the interface with the local variation of ϕ. The parameter k is taken as a positive constant. Such an approximation is valid in the situation where only short range interactions are considered, as is the case here.

With the assumptions listed above, the total energy per unit area of solid/liquid

interface and unit temperature can be defined by:

$$\frac{F[\phi,\phi_1]}{Ak_BT} = F_s(\phi_1) + F_d(\phi). \tag{1.4.5}$$

The aim is now to calculate the liquid composition at the surface, ϕ_1. This is done by minimising $\frac{F[\phi,\phi_1]}{Ak_BT}$ given by eq.(1.4.5) using the standard variational calculus. We first minimize $F_d(\phi)$ given in eq.(1.4.3) using the Euler-Lagrange equation, i.e.

$$\frac{\partial \mathcal{L}}{\partial \phi} = d_z \frac{\partial \mathcal{L}}{\partial (d_z\phi)} \tag{1.4.6}$$

where $d_z \equiv \frac{d}{dz}$. This yields

$$\frac{d\Delta F(\phi)}{d\phi} = 2kd_z^2\phi. \tag{1.4.7}$$

Integrating eq. (1.4.7) once with respect to ϕ, one gets

$$\Delta F(\phi) = k(d_z\phi)^2 + c, \tag{1.4.8}$$

where the integration constant is fixed to the value zero by the boundary condition at $z \to \infty$. Indeed, one assumes that deep in the bulk, the composition ϕ_∞ is constant as it corresponds to the other local minimum of the energy, and hence $\left.\frac{d\phi}{dz}\right|_{z\to\infty} = 0$. Since $\Delta F(\phi_\infty) = 0$, as can be seen immediately from eq.(1.4.4), one must have $c = 0$. Inserting the solution

$$\Delta F(\phi) = k(d_z\phi)^2 \tag{1.4.9}$$

in eq.(1.4.3), one gets

$$F_{dmin} = 2k\int_0^\infty dz(d_z\phi)^2 = -2k\int_{\phi_\infty}^{\phi_1} d\phi\, d_z\phi \equiv F_d(\phi_1;\phi_\infty) \tag{1.4.10}$$

where F_{dmin} is $F_d(\phi)$ evaluated at the minimum obtained via the Euler-Lagrange equation, and we have introduced the notation $F_d(\phi_1;\phi_\infty)$ to emphasize its dependence on ϕ_1 (recall that ϕ_∞ is taken as constant). The last step is to find the minimum of the total energy

$$\frac{F[\phi_1]}{Ak_BT} = F_s(\phi_1) + F_d(\phi_1;\phi_\infty) \tag{1.4.11}$$

as a functional of ϕ_1. This gives the condition

$$\frac{d}{d\phi_1}\left(\frac{F[\phi,\phi_1]}{Ak_BT}\right) = \frac{dF_s(\phi_1)}{d\phi_1} + \frac{dF_d(\phi_1;\phi_\infty)}{d\phi_1} = 0, \tag{1.4.12}$$

where $\frac{dF_d(\phi_1;\phi_\infty)}{d\phi_1} = -2k(d_z\phi)\Big|_{\phi=\phi_1}$ if one uses eq.(1.4.10), so that the condition above becomes

$$\frac{dF_s(\phi_1)}{d\phi_1} = 2k(d_z\phi)\Big|_{\phi=\phi_1}. \tag{1.4.13}$$

If on the other hand, one uses eq.(1.4.9) to rewrite

$$F_d(\phi_1;\phi_\infty) = -2k\int_{\phi_\infty}^{\phi_1} d\phi\, d_z\phi = \pm\int_{\phi_\infty}^{\phi_1} d\phi\sqrt{k\Delta F(\phi)}, \tag{1.4.14}$$

then the condition eq.(1.4.12) becomes

$$\frac{dF_s(\phi_1)}{d\phi_1} = -\frac{dF_d(\phi_1;\phi_\infty)}{d\phi_1} = \pm 2\frac{d}{d\phi_1}\int_{\phi_\infty}^{\phi_1} d\phi\sqrt{k\Delta F(\phi)} = \pm 2\sqrt{k\Delta F(\phi_1)}. \tag{1.4.15}$$

The ambiguity in sign introduced by taking a square root can be lifted by demanding that $\phi_1 \geq \phi \geq \phi_\infty$. This corresponds to choosing $\frac{dF_s(\phi_1)}{d\phi_1}$ negative, which, according to eq.(1.4.13), leads to negative $(d_z\phi)\Big|_{\phi=\phi_1}$. Hence the boundary condition at the surface, which determines ϕ_1, is

$$\frac{dF_s(\phi_1)}{d\phi_1} = -2\sqrt{k\Delta F(\phi_1)}. \tag{1.4.16}$$

We note, for future reference, that the chosen sign yields

$$F_d(\phi_1;\phi_\infty) = 2\int_{\phi_\infty}^{\phi_1} d\phi\sqrt{k\Delta F(\phi)} \tag{1.4.17}$$

and

$$d_z\phi = -\left(\frac{\Delta F(\phi)}{k}\right)^{1/2}, \tag{1.4.18}$$

which is consistent with eq.(1.4.9). Integrating eq.(1.4.18),

$$-\int_{\phi_1}^{\phi} d\tilde{\phi}\left(\frac{k}{\Delta F(\tilde{\phi})}\right)^{1/2} = \int_0^z d\tilde{z} = z(\phi) \tag{1.4.19}$$

we obtain an integral expression for $z(\phi)$ which can be inverted to yield $\phi(z)$, the concentration profile of the migrant.

Finally, using eq.(1.4.11) and eq.(1.4.17), we write the total energy as

$$\frac{F[\phi_1]}{Ak_BT} \overset{(1)}{=} F_s(\phi_1) + 2\int_{\phi_\infty}^{\phi_1} d\phi\sqrt{k\Delta F(\phi)}$$
$$\overset{(2)}{=} F_s(\phi_\infty) + \int_{\phi_\infty}^{\phi_1} d\phi \left\{ \frac{dF_s(\phi)}{d\phi} + 2\sqrt{k\Delta F(\phi)} \right\}, \quad (1.4.20)$$

whose minimum is the equilibrium surface free energy. In eq.(1.4.20), $F_s(\phi_1)$ is the free energy of the solid surface in contact with the liquid, which is at surface composition ϕ_1, and the integral contribution in the first equality (1) is the excess free energy of the non-uniform liquid layer. On the other hand, $F_s(\phi_\infty)$ is the free energy in contact with the homogeneous liquid of bulk composition ϕ_∞, while the integral in the second equality (2) represents the change in the total energy due to the change in surface composition.

We now turn to Cahn's construction, which is a graphical representation that helps understand the nature of the wetting transitions in our system, based on the solutions to the boundary equation at the surface, eq.(1.4.16). With the simplifying assumption eq.(1.4.2), this boundary condition becomes

$$\mu_1 + g\phi_1 = 2\sqrt{k\Delta F(\phi_1)}. \quad (1.4.21)$$

A qualitative graphical solution to eq.(1.4.21) is sketched, at given temperature T, in fig.(1.10) for positive value of μ_1 and negative of g chosen so that the curves $-F_s{}'(\phi_1) = \mu_1 + g\phi_1$ and $2\sqrt{k\Delta F(\phi_1)}$ intersect in four points, but two only correspond to stable solutions of the surface composition, labelled $\phi_1 = \phi'$ and $\phi_1 = \phi''$ (typically, g is small in this regime). At the value $\phi_1 = \phi_1'$, we have a dry solid in contact with the vapour ($\phi_\infty = \phi_v$) and at $\phi_1 = \phi_1''$, we have a wet solid in contact with the liquid ($\phi_\infty = \phi_\ell$) where the vapour composition ϕ_v and the liquid composition ϕ_ℓ (or the two polymer phases as we shall see in the next chapters) are at the intersection points of the x-axis with the bulk curve $2\sqrt{k\Delta F(\phi_1)}$.

One interprets the area under the curve $-F_s{}'(\phi_1)$ as the reduction in free energy due to the reduction in $F_s(\phi_1)$ when ϕ_1 varies, while the area under the curve $2\sqrt{k\Delta F(\phi_1)}$

represents the increase in free energy due to the inhomogeneous surface layer when ϕ_1 varies. The area between these two curves is interpreted as the net reduction in free energy. In fig.1.10, two such areas are labelled S_a and S_b, and we will now give a physical interpretation to their difference, $S_b - S_a$.

A wetting transition may occur every time we have a liquid film on a solid/liquid surface. We can see the three different phases in fig.(1.9).

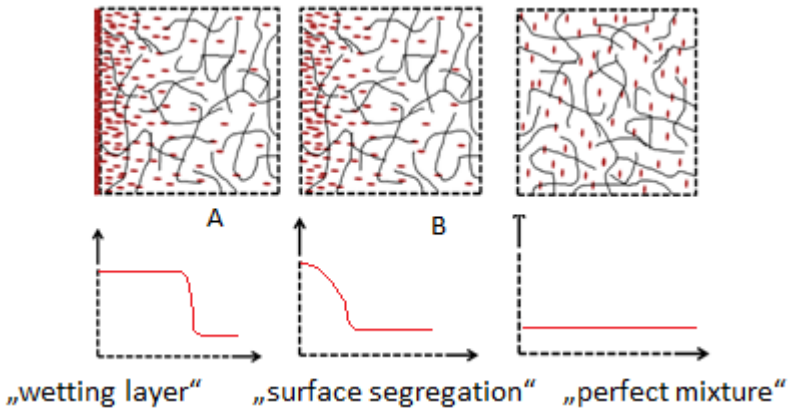

Figure 1.9: Surface phases for total wet, segregation and well mixed with corresponding wetting profiles.

We define the spreading coefficient as

$$S = \gamma_{sv} - \gamma_{s\ell} - \gamma_{\ell v}, \tag{1.4.22}$$

with the energies of the different phases given by

$$\begin{aligned} \gamma_{sv} &= F_d(\phi_1^{'}; \phi_v) + F_s(\phi_1^{'}) \\ \gamma_{s\ell} &= F_d(\phi_1^{''}; \phi_\ell) + F_s(\phi_1^{''}) \\ \gamma_{\ell v} &= F_d(\phi_\ell; \phi_v), \end{aligned} \tag{1.4.23}$$

where F_d is as in eq.(1.4.17). So, for instance,

$$F_d(\phi_1'; \phi_v) = 2\int_{\phi_v}^{\phi_1'} \sqrt{k\Delta F(\phi)}d\phi. \tag{1.4.24}$$

So the spreading coefficient becomes:

$$S = F_d(\phi_1^{'}; \phi_v) - F_d(\phi_1^{''}; \phi_\ell) - F_d(\phi_\ell; \phi_v) + F_s(\phi_1^{'}) - F_s(\phi_1^{''}) \tag{1.4.25}$$

but since $\phi_1^{'} \in (\phi_v, \phi_l)$ and $\phi_l \in (\phi_1^{'}, \phi_1^{''})$ (see fig.1.10), we can rearrange the integration intervals in $F_d(\phi_1^{'}; \phi_v) - F_d(\phi_1^{''}; \phi_\ell) - F_d(\phi_\ell; \phi_v)$. We choose to rewrite

$$\int_{\phi_v}^{\phi_1'} - \int_{\phi_\ell}^{\phi_1''} - \int_{\phi_v}^{\phi_\ell} \equiv - \int_{\phi_1'}^{\phi_{int}} - \int_{\phi_{int}}^{\phi_1''} \tag{1.4.26}$$

where ϕ_{int} corresponds to the unstable minimum near ϕ_ℓ (see see fig. 1.10). Then

$$F_d(\phi_1^{'}; \phi_v) - F_d(\phi_1^{''}; \phi_\ell) - F_d(\phi_\ell; \phi_v) = -F_d(\phi_1^{''}; \phi_{int}) - F_d(\phi_{int}; \phi_1^{'}). \tag{1.4.27}$$

Now if one writes

$$\begin{aligned} - F_s(\phi_1^{''}) &= -F_s(\phi_{int}) + \int_{\phi_{int}}^{\phi_1''} (-F_s'(\phi)) d\phi \\ F_s(\phi_1') &= F_s(\phi_{int}) + \int_{\phi_1'}^{\phi_{int}} (-F_s'(\phi)) d\phi \end{aligned} \tag{1.4.28}$$

the spreading coefficient receives a geometric interpretation:

$$S = \underbrace{\{-F_d(\phi_1^{''}; \phi_{int}) + \int_{\phi_{int}}^{\phi_1''} (-F_s'(\phi)) d\phi\}}_{S_b} + \underbrace{\{-F_d(\phi_{int}; \phi_1^{'}) + \int_{\phi_1'}^{\phi_{int}} (-F_s'(\phi)) d\phi\}}_{-S_a}. \tag{1.4.29}$$

where S_a and S_b are the two (signed) areas trapped between the curves $-F_s'(\phi_1)$ and $2\sqrt{k\Delta F(\phi_1)}$ in the two intervals (ϕ_1', ϕ_{int}) and (ϕ_{int}, ϕ_1''), as illustrated in fig.1.10. If the temperature increases, the relative areas of S_a and S_b change and the spreading coefficient eventually changes sign. This can be understood visually by looking at fig.(1.11) for instance.

In particular we have the following scenario, depending on the temperature of the system:

- $T \ll T_C$ where $S < 0$ with a partial wetting;
- $T = T_w$ where $S = 0$ and we have $\alpha_{eq} = 0$ in eq.(1.4.1);
- $T > T_w$ where $S > 0$ and we can speak about the wetting transition, or complete wetting with the formation of a macroscopic layer L;
- $T \sim T_c$ where there is a jump from a one minimum to a distinct minimum with a first order transition (discontinuity of the derivative of the free energy);

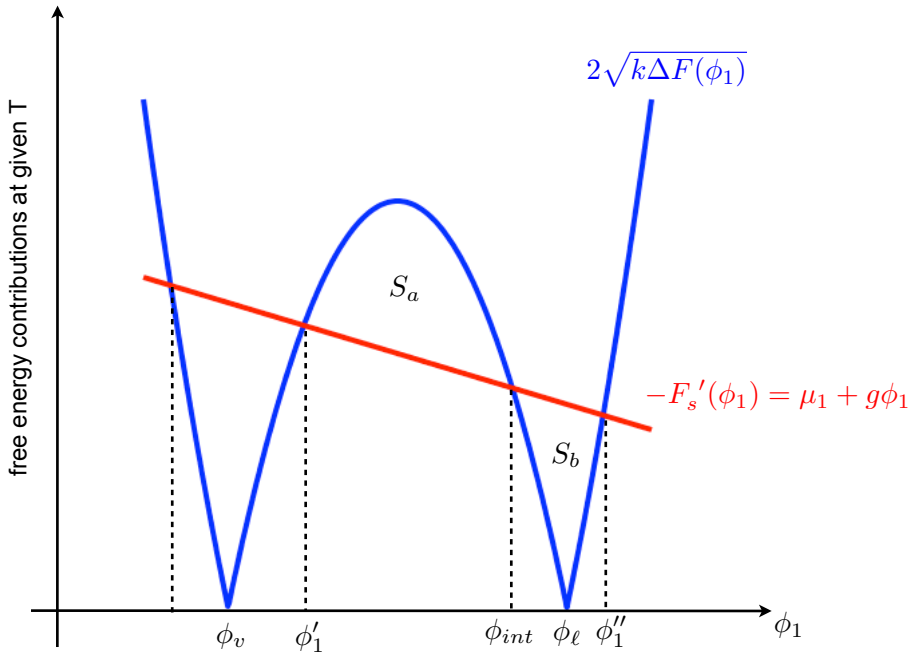

Figure 1.10: Geometric interpretation of the spreading coefficient S using Cahn's construction with $\mu_1 > 0$ and $g < 0$. S is given by the difference between the surface areas S_b and S_a calculated as the differences in areas under the curves $-F_s'(\phi_1)$ and $2\sqrt{k\Delta F(\phi_1)}$ on two intervals (ϕ_1', ϕ_{int}) and (ϕ_{int}, ϕ_1'') delimited by three compositions that minimise the total surface free energy (ϕ_1' and ϕ_1'' are stable minima while ϕ_{int} is unstable).

If the slope of the surface energy function F_s is large at all temperatures, we find only one root from the construction in fig.(1.11). We thus have the following scenario:

- $T < T_w$ we have $\phi_1 < \phi_\ell$ and $S < 0$, so there is partial wetting;
- $T = T_w$, $\phi_s = \phi_\ell$ exactly;
- $T > T_w$, ϕ_S will be higher than ϕ_ℓ, the interface involves a macroscopic layer and we have complete wetting with a continuous second-order wetting

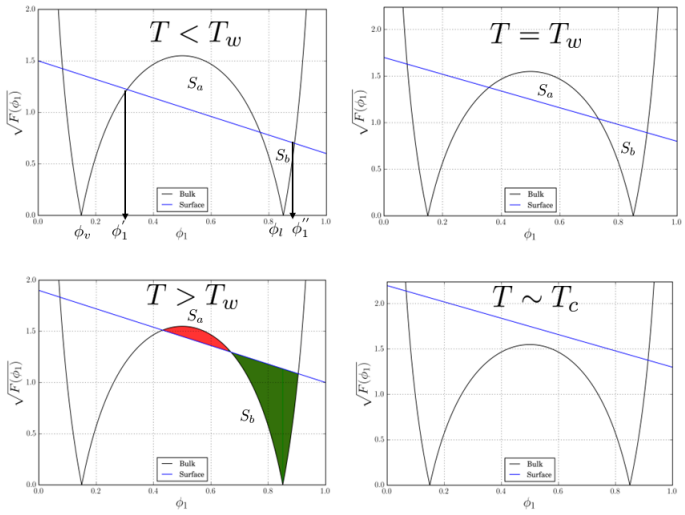

Figure 1.11: Cahn's construction as in eq.(1.4.16) for the free energy as a function of the volume fraction (black double well line) with different values of the surface energy (blue linear function) corresponding to different temperatures. The intersections of the bulk energy $2\sqrt{k\Delta F(\phi_1)}$ with the x-axis represent the vapour phase ϕ_v (left hand side) and the liquid phase ϕ_l (right hand side).The intersections between the bulk energy and the derivative of the surface energy $-F_s'(\phi_1)$ are solutions of eq.(1.4.16) as $\phi_1^{'}$ (dry state, left) and $\phi_1^{''}$ (wet state, right). Adapted from De Gennes [43].

transition, as we can see in fig.1.12.

There are experimental observations of a critical wetting behaviour with long range interaction made by Ragill et al.[102] for pentane on water, where they measured a power law divergence of $(T - T_w)^{\alpha}$ with a change of sign of the Hamaker constant. Evidences of total wetting with short range interaction have been reported by Ross *et al.* [104] for a methanol alkane binary liquid where they found a second order wetting transition.

Conclusions: In this chapter we have seen how to derive the bulk properties of polymer mixtures, with the Flory-Huggins free energy and how the spinodal decomposition allows to determine the stability properties of those systems. Furthermore we described the surface thermodynamics as in Cahn's theory of wetting, which is

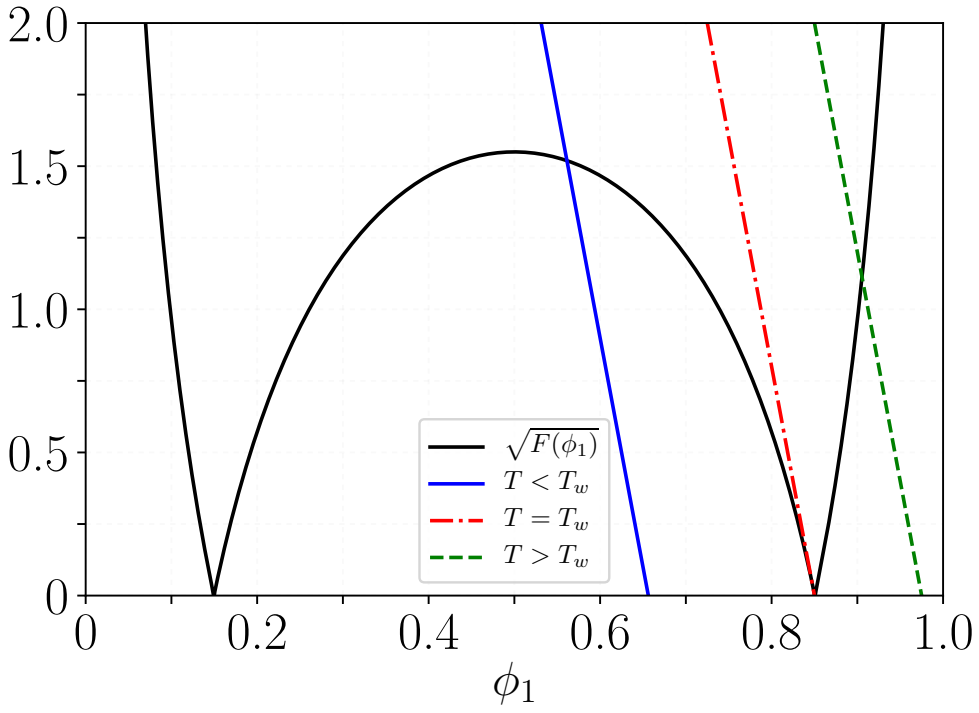

Figure 1.12: Cahn's construction for the free energy as a function of the volume fraction with different values of the surface energy for a second order wetting transition as in De Gennes [43].

not really different from a field theory for phase transitions. Cahn's theory and spinodal decomposition present first and second order phase transitions, depending on where we are on the phase diagram and the balance between bulk energy and surface energy contributions. In the next chapter we shall report on how to combine the bulk and the surface thermodynamics of a polymer system for studying the wetting behaviour.

Chapter 2

Surface segregation models

In this chapter we review the mean field theories for surface segregation in complex fluids. In particular we start with Schmidt-Binder (SB) theory [112], which combines Flory-Huggins (FH) theory and Cahn's theory of wetting. Then we introduce the self-consistent field theory [41] for polymer mixtures with a derivation of the theory and a description of the numerical technique used for solving the equations. Finally we compare the two theories.

2.1 Mean field theories for surface segregation

In the previous chapter we have seen that a first attempt to modelling wetting behaviour in polymer systems was made by Prigogine et al. [100] for describing the interaction layers of a polymeric film with X-rays. The model was interrogated with Pan et al's XPS measurements [95] but it was not possible to explain experimental data for Polystyrene (PS)- Poly Vinyl Methyl Ether (PVME). The most successful theories in this direction are the mean field theories and in particular the SB theory and the self- consistent field theory (SCFT) as we shall see in the next subsections.

2.1.1 Schmidt-Binder theory

Schmidt and Binder [112] have attempted to combine FH and Cahn's theory for describing bulk and surface thermodynamics, with a functional able to describe wetting transitions in polymer mixtures. In particular they use eq.(1.3.13) in conjunction with eq.(1.4.5) in the limit of long wavelength approximation, so small spatial variations compared to the characteristic length of the system as $a^2\nabla^2\phi \ll \frac{1}{N}$. Furthermore, they use the Random Phase Approximation (RPA) [68] for calculating the constant of the square gradient contribution, taking into account fluctuations at the interface. The contribution for the interface is given by:

$$\frac{F_{grad}}{k_bT} = \frac{a^2}{36\phi(1-\phi)}\left(\frac{d\phi}{dz}\right)^2 \tag{2.1.1}$$

where F_{grad} is the gradient in the system, a the Kuhn length and $k = \frac{a^2}{36\phi(1-\phi)}$ is a function of ϕ derived as in the RPA approximation [68], obtained by considering the response and correlations functions of the system. If we consider a system with composition variation only along the z-direction, by means of the variational calculus we can obtain a differential equation describing the concentration of polymers as a function of z, i.e. the distance from the surface to the bulk. The functional per unit surface is:

$$\frac{F[\phi]}{Ak_bT} = F_s(\phi_1) + \int_{z_{surf}}^{z_{bulk}} dz \left(\frac{F_{mix}(\phi)}{k_bT} + k(\phi)\left(\frac{d\phi}{dz}\right)^2 - \Delta\mu\phi\right) \tag{2.1.2}$$

where $F_{mix}(\phi)$ is the Flory Huggins energy and $\Delta\mu$ the chemical potential difference between species, that mathematically speaking is a Lagrange multiplier. The free energy is defined in units of k_bT and per unit surface. If we use the variational calculus, we can find the minimum of the functional in eq.(2.1.2) by solving $\frac{\delta F}{\delta\phi} = 0$, keeping in mind the analogy with Lagrangian Mechanics with the mapping of time t into distance z, q into volume fraction ϕ and momentum $\dot{x}$ into $\dot{\phi}$.

In this way we will obtain a first order differential equation (FODE) as in eq.(1.4.7)

that we can transform into an integral equation:

$$\frac{6z}{a} = \int_{\phi_\infty}^{\phi_s} \frac{d\phi}{\sqrt{\phi(1-\phi)[F(\phi,\chi) - F(\phi_\infty,\chi) - \Delta\mu(\phi-\phi_\infty)]}} \tag{2.1.3}$$

where we set $k_bT = 1$ and $V = 1$ respectively and the bulk free energy is:

$$F(\phi,\chi) = \frac{\phi}{N_a}\log(\phi) + \frac{1-\phi}{N_b}\log(1-\phi) + \chi\phi(1-\phi) \tag{2.1.4}$$

We solve eq.(2.1.3) numerically with the Simpson method, inverting $z(\phi)$ into $\phi(z)$. We plot the numerical solutions in fig.(2.1), which shows segregation profiles $\phi(z)$ that have a value ϕ_1 at the surface, solution of the Cahn construction as in Chapter 1, and decays asymptotically to a value ϕ_∞ in the bulk for different N_a and N_b. We observe a wetting transition in fig.(2.2), with$N_a = N_b$ and $\chi > \chi_c$, as also justified by the Cahn construction, where we observe that the bottom area of intersection is bigger than the top area. The SB theory correctly describes the behaviour

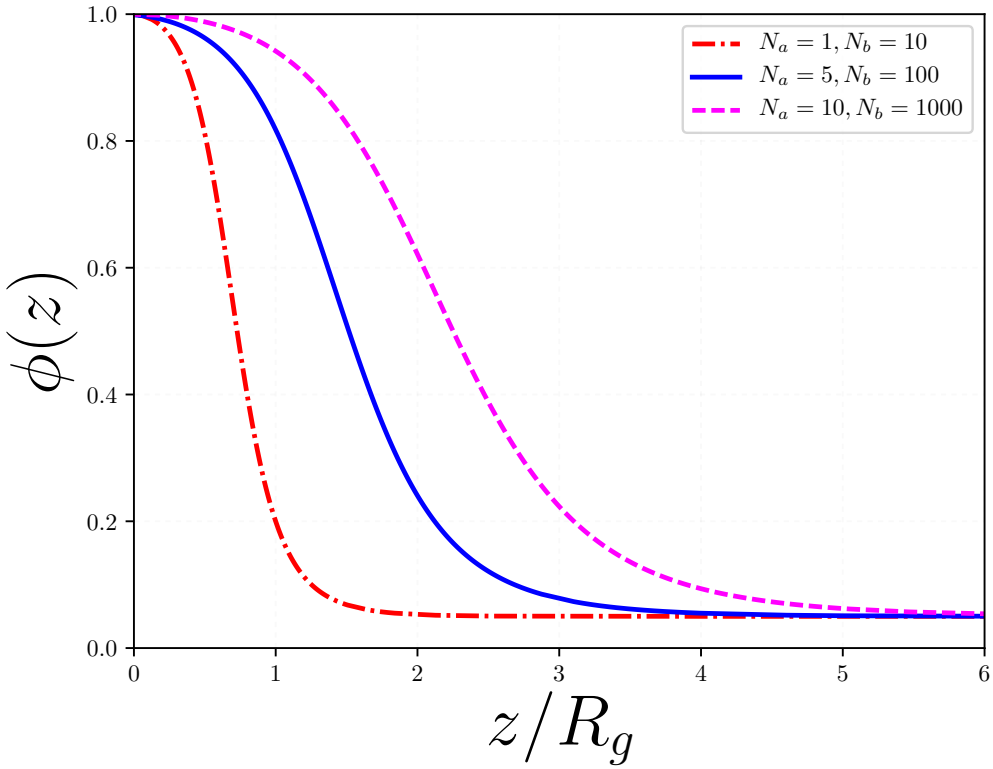

Figure 2.1: Numerical solution of eq.(2.1.3) for different combinations of the degree of polymerisation, showing different segregation profiles for $\Delta\mu = 0$ and $\chi < \chi_c$.

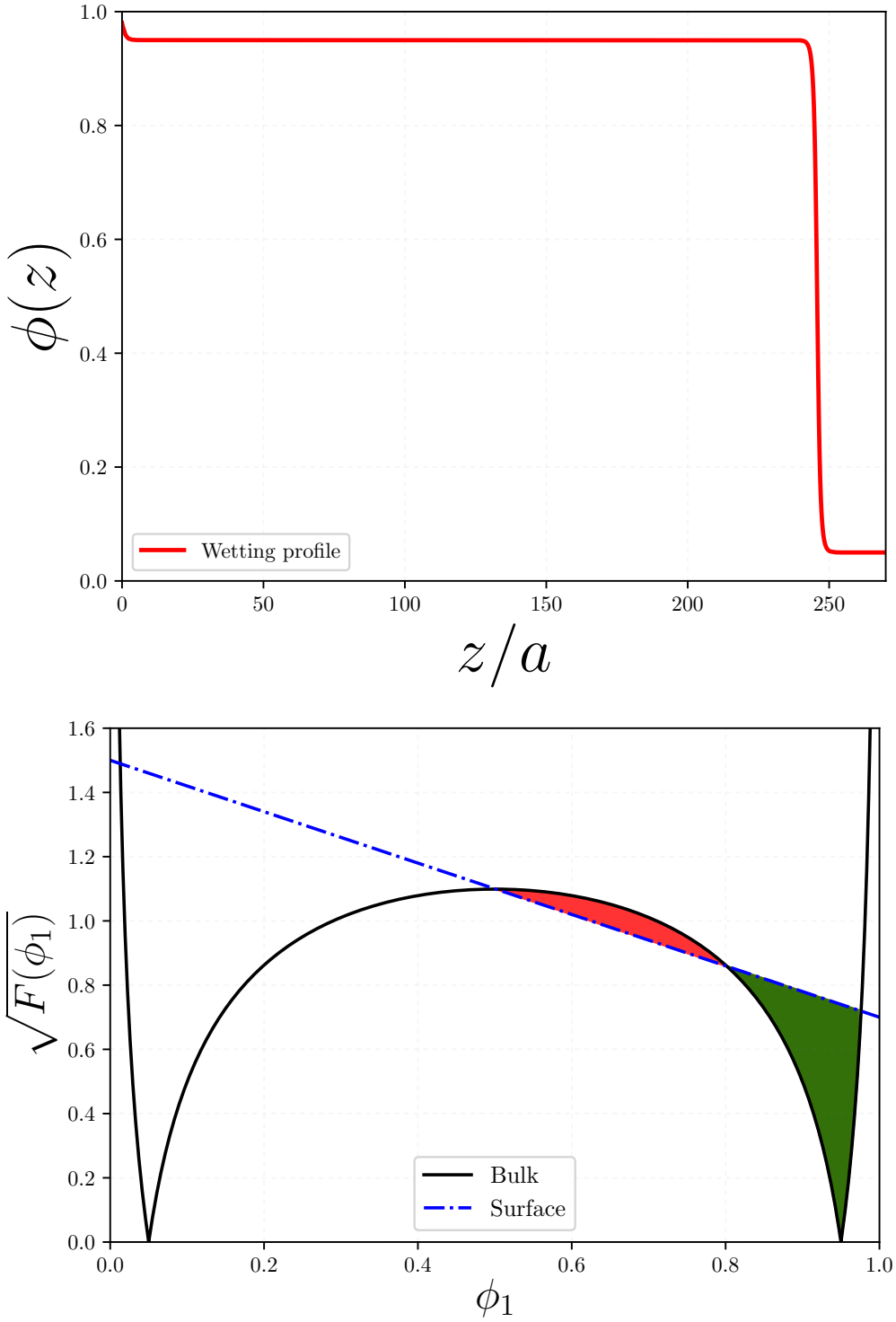

Figure 2.2: Macroscopic wetting layer (top) and Cahn construction (bottom) as in fig.(1.11) for the following parameters: $N_a = N_b = 10$, $\chi = 0.32716$, $\phi_\infty = 0.05$, $\phi_1 = 0.976$ and for the surface energy $\mu = 1.5$ and $g = -0.8$, where $S > 0$ with a wetting transition. In this case $\phi_1 > 1 - \phi_\infty$, so the profiles decreases first from ϕ_1 to $1 - \phi_\infty$ which is a B-rich layer and then after $1 - \phi_\infty$ we find an A-rich macroscopic wetting layer, as reported by Schmidt et al.[112].

of wetting systems, both for segregation and total wetting, but suffers from some limitations. It remains a phenomenological model which has the surface fraction ϕ_1 as an input in the model, as solution of the Cahn construction. Hence the theory has no predictive power for equilibrium properties. Some of those problems can be solved using a more elaborated mean field theory, such as SCFT.

2.1.2 Self Consistent Field Theory

Self Consistent Field Theories (SCFT) is a type of Mean Field Theories (MFT) introduced by Edwards [32] and successfully applied to many topics in Polymer Physics [41, 117, 88]. The key idea is the description of the polymer chains as Gaussian chains, as we have seen in Chapter 1, in an enviroment surrounded by a mean field generated by the other polymers. In particular we have seen the probability distribution of a freely jointed chain to be Gaussian as in eq.(1.1.4). This kind of approximation becomes important for solving the path integrals which allows us to derive the property of the polymer chains, as in the next section.

Derivation

We can treat polymeric systems as random walks and use a Gaussian function as a good approximation for the probability distribution of the system. This is the simplest model we can consider. We can use field theory for describing polymer systems, and we will see that an analogy exists between diffusion and polymer conformation similar to a random walk. In particular we can use self-consistent field methods for obtaining more accurate information about the system.
Writing the partition function of the system as a functional integral of one or more potential fields $w(\mathbf{r})$:

$$Z = \int D[w] \exp\left[-H[w]\right] \tag{2.1.5}$$

where $H[w]$ is the Hamiltonian of the system and it depends on the particular interaction, polymer architecture, polydispersity etc. As a consequence the average

value of some observable G is given by:

$$\langle G[w]\rangle = Z^{-1}\int Dw\, G[w]\exp\left[-H[w]\right] \tag{2.1.6}$$

Using eq.(2.1.6) we can compute all the thermodynamic observables of our system. We can obtain the mean field minimizing the Hamiltonian of the system with respect to the field w, i.e.:

$$\frac{\delta H[w]}{\delta w(\mathbf{r})}\Big|_{w=w^*} = 0 \tag{2.1.7}$$

The field w^* is a field that dominates the other fields and can be seen as a mean field generated by the other surrounding chains. We notice that in this way the partition function of the system and the average of an observable G can be written as:

$$Z \sim \exp\left(-H[w^*]\right)\ ,\ \langle G[w]\rangle \sim G[w^*] \tag{2.1.8}$$

and as a consequence the Helmholtz free energy is:

$$F = \frac{-1}{\beta}\log Z = \frac{-1}{\beta}H[w^*]. \tag{2.1.9}$$

This approximation is valid only at the macroscopic scale, because at the atomic and molecular scales are present fluctuations that cannot be neglected. Furthermore using eq.(2.1.9) and eq.(2.1.7) we can also obtain the Schmidt-Binder free energy with the square-gradient correction to the Flory-Huggins energy by means of the saddle point approximation or steepest descent method[41].

At this level we can define the energy of a polymer configuration r_α with the chain in the interval (l_1, l_2), following Matsen[51] as:

$$\frac{E[r_{\alpha,l_1,l_2}]}{k_bT} = \int_{l_1}^{l_2} dl\left(\frac{3}{2a^2N}|r_\alpha|^2 + w(r_\alpha)\right) \tag{2.1.10}$$

which is a functional involving Gaussian properties and mean field defined as the difference between the chemical potential and the entropy.

We define the partition function for a polymer chain starting at l_1 and finishing at

l_2 as:

$$q(z, l_1, l_2) \propto \int Dr_\alpha \exp\left(\frac{-E[r_{\alpha,l_1,l_2}]}{k_b T}\right)\delta(r_\alpha(0) - l_1)\delta(r_\alpha(l) - l_2) \tag{2.1.11}$$

At this point a careful reader will immediately recognise an analogy with the path integral formulation developed by Feynman[37]. In fact a Gaussian chain in a mean field generated by surrounding chains is like a single particle in an external field $U(z)$. In particular eq.(2.1.10) is the equivalent of the action S and eq.(2.1.11) is the equivalent of a wave function. Thus we can make the following mapping:

$$\begin{aligned} t &\leftrightarrow l \\ m &\leftrightarrow \frac{3}{Na^2} \\ U(z) &\leftrightarrow -w(z) \\ S &\leftrightarrow \frac{E[r_{\alpha,l_1,l_2}]}{k_b T} \\ r_\alpha(t) &\leftrightarrow r_\alpha(l) \\ \hbar &\leftrightarrow -i \\ \Psi(r,t) &\leftrightarrow q(r,l) \end{aligned} \tag{2.1.12}$$

From Feynman[37] we know that the path integral formulation of a particle in a field is equivalent to a time dependent Schrödinger equation:

$$i\hbar\frac{\partial}{\partial t}\Psi(z,t) = \left[-\frac{\hbar^2}{2m}\frac{\partial^2}{\partial z^2} + U(z)\right]\Psi(z,t). \tag{2.1.13}$$

Now thanks to the mapping in eq.(2.1.12) we can write an equivalent equation for a polymer chain in field, which describes the evolution of the distribution function of the polymer. In particular following Jones [68] and Doi [30] we can obtain an analogy between quantum mechanics and Polymer physics. In fact considering the distribution function $q(z,t)$ (here we set $l = t$) of a random walk, we can write the evolution of the system as a diffusion equation [42]:

$$\frac{\partial q(z,t)}{\partial t} = N\frac{a^2}{6}\frac{\partial^2 q(z,t)}{\partial z^2}. \tag{2.1.14}$$

The solution of eq.(2.1.14) is a Gaussian function as in eq.(1.1.4). If our system is affected by a spatial variation potential $w(\mathbf{r})$, we can modify eq.(2.1.14) adding the potential as:

$$\frac{\partial q(z,t)}{\partial t} = N\frac{a^2}{6}\frac{\partial^2 q(z,t)}{\partial z^2} - \beta w(z) q(z,t) \tag{2.1.15}$$

where $\beta = \frac{1}{k_b T}$ and $w(\mathbf{r})$ can be recognized as our mean field derived in eq.(2.1.7) and the eq.(2.1.15) is like the Schrödinger equation in eq.(2.1.13). The diffusion constants are $R_g^2 = N\frac{a^2}{6}$ square radius of gyration for an ideal chain.

The introduction of the mean field of interaction causes a perturbation in the Gaussian chain.

If we consider a polymer mixture of two species A and B, we know that the bulk properties are governed by the FH free energy. If we specialise our mean field as the energy required for placing a segment of volume v_0 into its surroundings, we obtain:

$$w_{a/b}(z) = \frac{\mu_{a/b}(z) - k_b T \log\left(\phi_{a/b}(z)\right)}{N_{a/b}} - \Delta w(z) \tag{2.1.16}$$

where $\phi_{a/b}$ is the fraction volume of species A/B, its logarithm is the entropy, $\mu_{a/b}$ is the chemical potential of one of the two polymers and we had introduced $\Delta w(z)$ for satisfying the constraint that $\phi_b(z) + \phi_a(z) = 1$, being $\Delta w = \frac{1}{\kappa\rho}(1 - \phi_a - \phi_b)$, with ρ density and κ compressibility. The form of the chemical potential in eq.(2.1.16) can be obtained from the following expression where we take into account the difference of the chemical potential of the two species:

$$\mu_{a/b}(z) = N_{a/b}F + N_{a/b}\phi_{b/a}\left[\frac{\partial F}{\partial \phi_{a/b}(z)} - \frac{\partial F}{\partial \phi_{b/a}(z)}\right] \tag{2.1.17}$$

where F is the FH free energy of the system, similar to a Legendre transformation. We have got enough information to calculate the field in eq.(2.1.16) and obtain the profiles of the polymers on the surface. In fact the fraction volume can be computed as:

$$\phi_{a/b}(z) = \frac{e^{\beta\mu_{a/b}(z)}}{N_{a/b}} \int_0^{N_{a/b}} dt\, q(z,t) q(z, N_{a/b} - t) \tag{2.1.18}$$

We notice an analogy with the calculation of observables in quantum mechanics. In fact $q(z,t)$ can be related to a wave function $\psi(z,t)$, considering that both are solutions of a diffusion equation (in the Quantum Mechanics case the diffusion constant is an imaginary number) and the observables are $\phi(z)$ and $|\psi(z,t)|^2$ respectively. All the equations presented about the SCFT of polymer mixtures must be solved numerically, because it is not possible to solve them analytically, with the exception of few cases , as reported by Jones[68], for a "time" independent diffusion equation. We use two distributions, one for the polymer A and one for the polymer B, discretize the equation and obtain a lattice solution. Repeating the calculation multiple times, at large N we obtain a ground state dominance, hence equilibrium, updating the mean field in eq.(2.1.16) each time with the new ϕ. We shall exhibit a numerical solution in the next section.

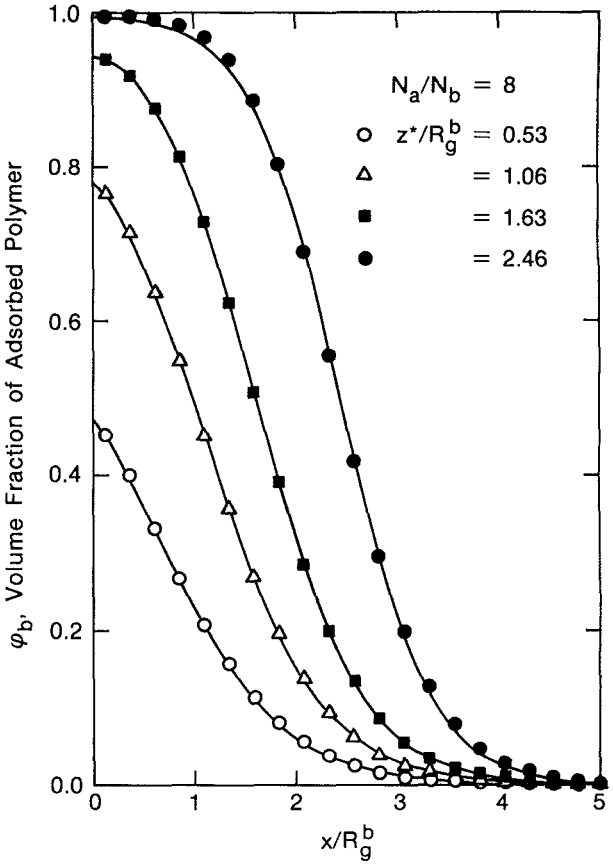

Figure 2.3: Examples of the SCFT results, similar to the square gradient theory. Figure reproduced from Schull[116].

2.1.3 Schull's theory

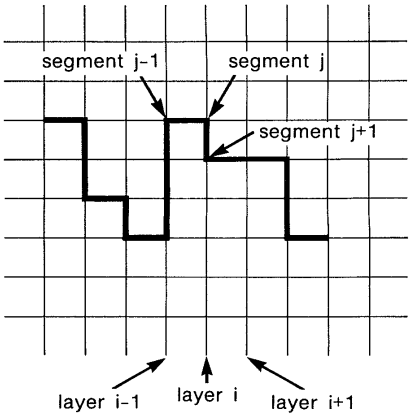

Figure 2.4: Schematic of the lattice solution for the polymeric system from[116].

The essence of SCFT is the description of the distribution of polymer chains as solutions of a diffusion equation. Scheutjens et al.[111] introduced a solution method based on a lattice. In particular polymer chains on a lattice can be described with a matrix formalism. We consider a N-length chain as a random walk of $N-1$ segments on the lattice and we can assign different weights to each of the segments.

Later on Schull [116, 115] introduced a very fast and robust method for solving a lattice version of eq.(2.1.15). We consider a lattice of dimension N, with the j^{th} segment on the i^{th} layer. Following Shull's derivation, we consider three different distributions, one for the polymer matrix, a second for the interacting monomers with the surface (with a growth from bulk to surface) and a third distribution considering the interaction between monomers and the bulk polymer matrix. If we consider the single probabilities of having monomers on the lattice in fig.(2.4), where j is associated to the time (monomer's length) and i is associated to the distance from the wall, z. Saying λ_0 is the probability that a chain segment stays in the same layer, $(1-\lambda_0)/2$ is the probability that it moves into a given adjacent layer. Depending on the lattice type, λ_0 has different values, such as $\frac{1}{2}$ for a hexagonal lattice, $\frac{2}{3}$ for a cubic lattice etc.; if we say $q(i,j)$ is our matrix-probability distribution for the chain,

we shall write it as function of the distributions at the $j-1$ layer as:

$$\begin{aligned} q(i,j) =&[(1-\lambda_0)q(i-1,j-1)/2 + (1-\lambda_0)q(i+1,j-1)/2+ \\ &+ \lambda_0 q(i,j-1)] \exp\left(\frac{-w(i)}{k_b T}\right) \end{aligned} \tag{2.1.19}$$

If $\frac{w(i)}{k_b T} \ll 1$, we can Taylor expand the exponential and so eq.(2.1.19) becomes:

$$q(i,j)[1+\frac{w(i)}{k_b T}] = [(1-\lambda_0)q(i-1,j-1)/2 + (1-\lambda_0)q(i+1,j-1)/2 + \lambda_0 q(i,j-1)] \tag{2.1.20}$$

so rearranging eq.(2.1.20) and considering that i is akin z and j for the time t, we obtain a term $[q(i,j)-q(i,j-1)]/(j-j+1)$ which is a discrete first derivative in time. Furthermore multiplying by δz^2, we have a term $[q(i+1,j-1)+q(i+1,j-1)-2q(i,j-1)]/\delta z^2$ which is a four points discrete second derivative in space. So the two term together looks like:

$$\frac{\partial q(z,t)}{\partial t} = \frac{(1-\lambda_0)}{2}\delta z^2 \frac{\partial^2 q(z,t)}{\partial z^2} - \frac{w(z)q(z,t)}{k_b T} \tag{2.1.21}$$

where with $\delta z^2 = \frac{a}{3(1-\lambda_0)}$, being a the lattice costant, is like the Edwards diffusion equation in eq.(2.1.15). For our purposes we shall consider a simple cubic lattice and fix $\lambda_0 = \frac{2}{3}$. From eq.(2.1.19) we obtain a recursive relation:

$$q_{a,b}(i,j) = [q_{a,b}(i-1,j-1) + q_{a,b}(i+1,j-1) + 4q_{a,b}(i,j-1)]\,\frac{e^{-\beta w_{a/b}(i)}}{6} \tag{2.1.22}$$

where the exponential gives us the thermalization of the system. We can obtain the fraction of volumes by means of eq.(2.1.18) and using eq.(2.1.17) and eq.(2.1.16). With the Flory-Huggins energy we can obtain the mean field and the chemical potential of the species as:

$$\beta\mu_{a/b}(i) = \log\phi_{a/b}(i) + \phi_{b/a}(i)\left(1 - \frac{N_{b/a}}{N_{a/b}}\right) \tag{2.1.23}$$

$$\beta w_{a/b}(i) = \phi_{b/a}(i)\left(\frac{1}{N_{a/b}} - \frac{1}{N_{b/a}}\right) + \chi\phi_{b/a}(i)^2 - \Delta w(i) \tag{2.1.24}$$

where $\Delta w = \frac{1}{\kappa\rho}(1-\phi_a-\phi_b)$ is an incompressibility parameter for conserving the volume, κ the compressibility and ρ the density. In this way we have a set of

coupled equations that we can solve self consistently. The entire approach and methodology is based on solving the diffusion equation, so it needs some boundary conditions. Considering that we are dealing with probability distributions Schull introduced two different kinds of probabilities for dealing with the monomers. He considered the initial condition $q_{b2}(1,0) = e^{-\chi_s}$ for placing monomers on the surface and $q_{b2}(i+1,0) = e^{-\chi_b}$ for placing monomers in the bulk of the system. The other initial condition is $q_{b1}(i,0) = 1$ for all the values of the monomers of the polymer matrix. Furthermore Schull used a random initialization of the values of ϕ, the chemical potential and the mean field before entering into the self-consistent loop , which brings to ground state and equilibrium. A schematic showing the steps of the SCFT implementation is shown in fig.(2.5).

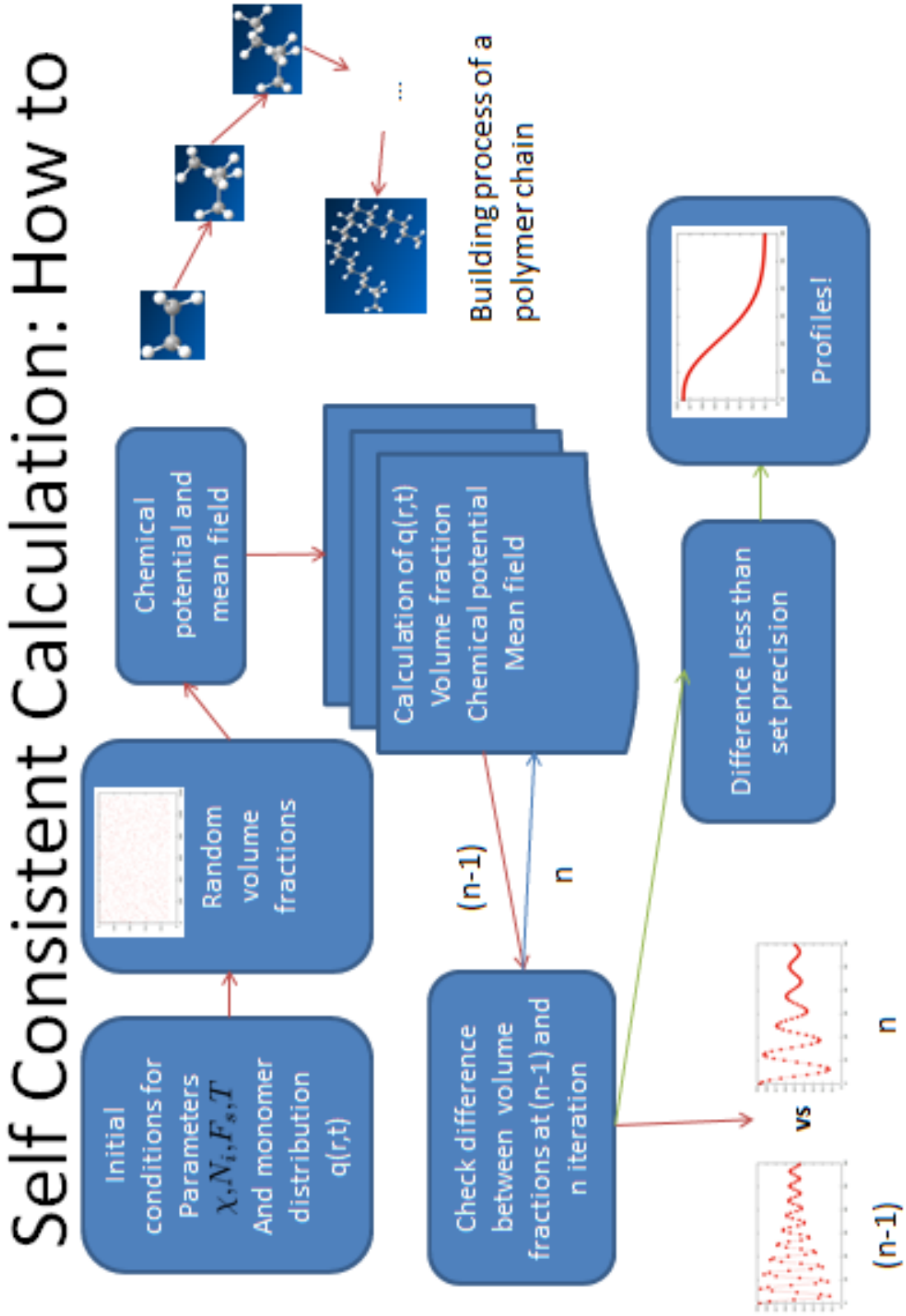

Figure 2.5: Schematic of the execution of the SCFT code, with the parameters, the initial guess for the volume fraction and then the loop with the condition for obtaining the profiles.

2.2 Differences between SB and SCFT mean field theory

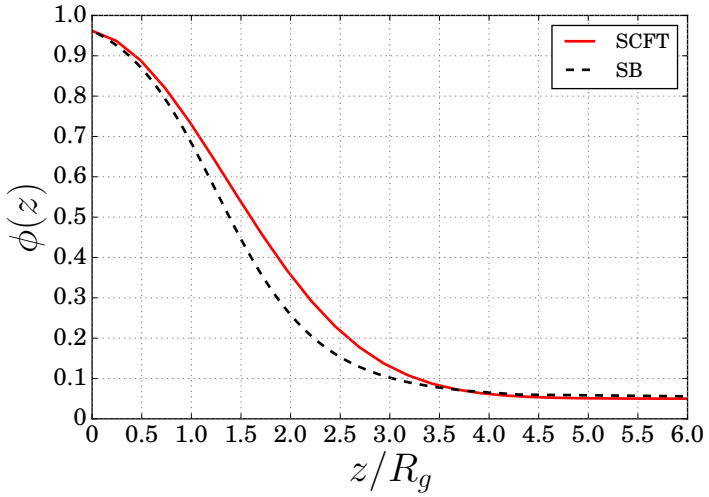

Figure 2.6: Segregation profiles calculated with SB and SCFT theory with $\phi_\infty = 0.05$,$\phi_1 = 0.95$ and correspondent $F_s = -3.3$,$\chi = 0.5$, $N_a = 10$, $N_b = 100$.

We have seen in the previous section how the derivation of the self-consistent field theory for the polymer system is still inside the framework of the mean field description of the system and it can be well justified and understood with the analogy between polymers and quantum mechanics derived from Schroedinger's equation. We will see in this section that there are also many advantages of using SCFT in order to obtain a quantitative comparison with SB theory. To adapt it to our situation we change the boundary conditions for the SCFT equations (since Schull's theory was initially developed for polymer brushes). In particular we use:

$$\begin{aligned} \text{Surface energy: } & F_s \Rightarrow q_{b2}(1,0) = e^{-f_s} \\ \text{Bulk energy: } & \chi_b \to +\infty \Rightarrow q_{b2}(i+1,0) = 0 \\ & \Rightarrow q_{b1}(i,0) = 1, \end{aligned} \tag{2.2.1}$$

where the main difference is a very high value of χ_b, which implies that the bulk thermodynamics is governed by the FH constant and the surface one by f_s, as in SB theory.

This approach will be used across the thesis and it allows a first comparison between mean field theories. In fact we know that for both models it is not possible to have exact analytical solutions and a numerical approach is needed. In particular in fig.(2.6) we see two different profiles generated with the same values of the parameters. Thus so choosing a value of ϕ_1 is equivalent to the one we obtain for a particular value of f_s in SCFT. We notice that there is a small difference in the width and the shape of the profiles obtained by the different methods, probably caused by a systematic underestimation of the profiles by SB, which describes them just at the phenomenological level, without the real chemical potential difference between species. The differences become even more pronounced for the wetting profiles, where SB describes a sharp interface and SCFT calculates a more diffuse one. When we try to calculate higher bulk composition, beyond the critical point of the spinodal diagram, and profiles for very large polymers ($N_i \geq 10^3$), there are significant differences. Indeed SB fails totally in those cases as the quantity in eq.(2.1.2) becomes negative and so we have imaginary solutions and only have solutions for polymers which have an appropriate value of $\Delta\mu$ for compensating the energy loss. However, such solutions do not always correspond to physical values , unless we choose ϕ_1 as solution of Cahn's construction. SCFT works fine and it can calculate the profiles, having $\Delta\mu$ from FH implemented in the mean field.

Making a comparison between the different computational times needed to execute the codes, on the same machine (intel core 2 duo, Majorana), we obtain $\tau \sim 10^2 s$ for the Schmidt-Binder model and $\tau \sim 10^{-1} s$ for the self-consistent field theory, with same parameter conditions. The SCFT method is computationally less intensive and allows for larger system sizes and more complex free energies, to be incorporated within its remit. Other important differences between SB and SCFT concern the use of the surface free energy needed for placing single monomers on the surface, that allows to control directly the final amount of material ϕ_1 as we shall see in more details in Chapter 3.

Conclusions: In this chapter we described two fundamental models for calculating the wetting profiles of a complex fluid, such as SB and SCFT, with both their advantages and limitations. In particular we addressed the differences between the more phenomenological SBMFT and the more coarse grained SCFT. In the next chapter we will apply those migration models to the description of a system including elasticity. We will analyse the bulk thermodynamics and the consequences for migration and surface wetting. Finally we will analyse the effects of the parameters on polymer nanofilm in depth, as well as their possible valuable contribution to industry.

Chapter 3

Effects of elasticity

We present novel results on the migration and segregation of the low molecular weight component polymer in a mixture where the other component is a polymer gel. We recall the theory of elasticity for polymers and gels [105, 123] and then we report a new free energy incorporating elasticity with the SB and SCFT mean field theories. We calculate segregation and wetting profiles, with a comparison between the theories and introduce a novel way for controlling the segregation in those system by changing the matrix elasticity. The chapter is based on the papers by J. Krawczyk et al.[74] and S. Croce et al. [25].

3.1 Flory-Huggins theory and elasticity

When the temperature of a polymer gel is far beyond the gel point, most of the chains are connected to form macroscopic polimeric network. If the glass transition is below the room temperature, the system is a rubber. Rubber like systems exhibit very peculiar mechanical properties under the action of a tensile force. In particular it is interesting to analyse the thermodynamics of rubber [105, 123].
The internal energy of the system can be written with its natural variables as:

$$dU = TdS - pdV + fdL \tag{3.1.1}$$

where dS is the entropy change, dV the volume change, dL the sample length change and f is the force applied to deform this system. Using a Legendre transformation [50, 3, 103], we can write the Helmholtz free energy in term of the internal energy as:

$$F = U - TS \tag{3.1.2}$$

whose differential form is:

$$dF = -SdT - pdV + fdL \tag{3.1.3}$$

considering that T is one of the natural variables of F and it is important in rubber systems. The force applied to deform the network can be found by differentiating F with respect to the deformation L, as:

$$f = \left(\frac{\partial F}{\partial L}\right)_{T,V} = \left(\frac{\partial U}{\partial L}\right)_{T,V} - T\left(\frac{\partial S}{\partial L}\right)_{T,V} \tag{3.1.4}$$

where $\partial V/\partial L \simeq 0$ at fixed volume. We notice that for a soft material such as rubber, the only relevant contribution is the derivative of entropy, since changes in configurational entropy is much larger than the internal energy change, thus $\frac{\partial U}{\partial L} \simeq 0$. This is the opposite behaviour to crystalline and solid state systems where the lattice deformations cause an increased internal energy, but the entropy contribution is negligible because the system is highly ordered [105].

3.1.1 Rubber Elasticity

We can track the rubber elasticity with the deformations along different directions of the system. In particular if $L_{i,0}$ is the length along a direction before applying F, we can define:

$$L_x = \lambda_x L_{x0},\ L_y = \lambda_y L_{y0},\ L_z = \lambda_z L_{z0} \tag{3.1.5}$$

where λ_i represents the percentage of deformation in the i^{th} direction. Considering the projections of a sphere of radius $\mathbf{R}$, for the polymeric gel, we can express the deformation along the directions x, y, z in eq.(3.1.5), and write the elastic entropy

variation for a single component as:

$$S(N,\mathbf{R}) - S(N,\mathbf{R_0}) = -\frac{3k_b}{2}\frac{(\lambda_x^2-1)R_x^2 + (\lambda_y^2-1)R_y^2 + (\lambda_z^2-1)R_z^2}{Nb^2} \tag{3.1.6}$$

where N is the degree of polymerisation and b the Kuhn length. The entropy for the entire system is given as the sum of the elastic entropies for single chains:

$$S_{net} = -\frac{3}{2}\frac{k_b}{Nb^2}\left((\lambda_x^2-1)\sum_{i=1}^{n}(R_{x0})_i^2 + (\lambda_y^2-1)\sum_{i=1}^{n}(R_{y0})_i^2 + (\lambda_z^2-1)\sum_{i=1}^{n}(R_{z0})_i^2\right). \tag{3.1.7}$$

If the system is an ideal network made of cross-linked chains, there is perfect symmetry along the three spatial directions and the average values of the projection radii are:

$$\left\langle R_{x0}^2\right\rangle = \left\langle R_{y0}^2\right\rangle = \left\langle R_{z0}^2\right\rangle = \frac{1}{n}\sum_{i=1}^{n}(R_{z0})_i = \frac{Nb^2}{3}. \tag{3.1.8}$$

thus combining eq.(3.1.8) and eq.(3.1.7) we obtain the expression for the deformation entropy of the network:

$$S_{net} = -\frac{nk_b}{2}(\lambda_x^2 + \lambda_y^2 + \lambda_z^2 - 3) \tag{3.1.9}$$

where n is the density of cross-linked chains. We notice that for a dry system, there are no volume changes, hence no swelling. We will use eq.(3.1.9) in the next chapters. The absence of volume changes can be expressed in term of the deformation constants as:

$$V = \lambda_x\lambda_y\lambda_z V_0 \ , \ \lambda_x\lambda_y\lambda_z = 1. \tag{3.1.10}$$

In this case if we want to satisfy eq.(3.1.10) for a uni-axial deformation along a fixed spatial direction, for example z, we can write the deformation parameters as:

$$\lambda_z = \lambda \ , \ \lambda_x = \lambda_y = \frac{1}{\sqrt{\lambda}}. \tag{3.1.11}$$

So the elastic entropy of the material will transform as:

$$S_{net} = -\frac{nk_b}{2}(\lambda^2 + \frac{2}{\lambda} - 3) \tag{3.1.12}$$

which is the uniaxial deformation elastic energy for an ideal network.

3.1.2 Modified Flory-Huggins theory

The Flory-Huggins theory of eq.(1.3.13) describes the thermodynamics of a system of polymers by means of mixing entropy and enthalpy/mean field. We have seen that for a cross linked system we have to account for an elastic-deformation energy of the network. Thus for a proper description of the thermodynamic behaviour of oligomers in a polymer gel we must include this energy along with the FH one. Using the elastic entropy of eq.(3.1.12) we obtain the correct thermodynamic description for molecules segregating in a polymer gel matrix. Considering eq.(1.3.13), in the limit of a networked system and for the case where the degree of polymerization of the b species is really large compared to the number N_a, as $N_b \gg N_a$. Thus we can neglect the logarithmic contribution, configurational/mixing entropy of the b polymer gel and the biggest energy contribution is the deformation energy as in eq.(3.1.12). In our case we can write the deformation[74] as $\lambda = R/R_0$, with R_0 and R lengths of the polymer before and after the deformation. The correspondent volume fractions are $\phi_b = V_b/V$ and $\phi_{b0} = V_{b0}/V$. So with $\phi_b = 1 - \phi$ and $\phi_{b0} = 1 - \phi_\infty$, the final value of λ as function of the volume fraction ϕ is:

$$\lambda = \left(\frac{1-\phi}{1-\phi_\infty} \right)^{\frac{1}{3}}. \tag{3.1.13}$$

Therefore combining eq.(3.1.12) with eq.(3.1.13, the elastic/deformation energy in units of k_bT for the polymer gel is:

$$S_{el} = \frac{B}{2}(1-\phi_\infty) \left[\left(\frac{1-\phi}{1-\phi_\infty} \right)^{\frac{2}{3}} + 2 \left(\frac{1-\phi_\infty}{1-\phi} \right)^{\frac{1}{3}} - 3 \right] \tag{3.1.14}$$

where B is the elastic modulus of the network and $n = 1-\phi_\infty$ is the number density of chains in the network. The entropy of the system is shown in fig.(3.1). Putting together eq.(3.1.14) with the enthalpic contribution and mixing entropy for the a

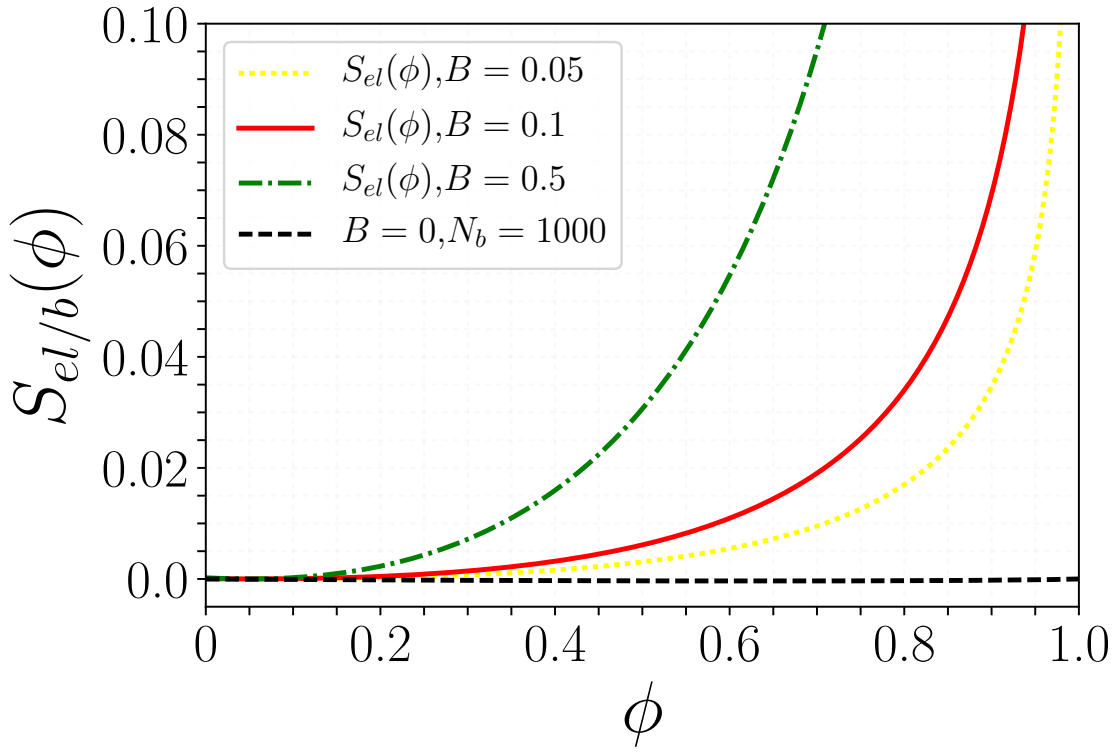

Figure 3.1: Comparison between mixing entropy ($B = 0$) and uniaxial deformation energy ($B \neq 0$) for cross linked systems with $\phi_\infty = 0.05$ and $B = 0.05$, $B = 0.1$ and $B = 0.5$. We notice that for a large polymer ($N_b > 10^3$) the mixing entropy becomes negligible. Increasing the cross linking density, i.e. the elastic modulus, the uniaxial deformation energy dominates over the mixing entropy which justifies the adoption of the model.

polymer, eq.(1.3.13) is given by:

$$\begin{aligned} \frac{F_{fhe}}{k_b T} &= \frac{1}{N_a}\phi \log \phi + \chi\phi(1-\phi) + \\ &+ \frac{B}{2}(1-\phi_\infty)\left[\left(\frac{1-\phi}{1-\phi_\infty}\right)^{\frac{2}{3}} + 2\left(\frac{1-\phi_\infty}{1-\phi}\right)^{\frac{1}{3}} - 3\right] \end{aligned} \tag{3.1.15}$$

where we have an elastic contribution from the network, a configurational entropy contribution for the migrating molecules and a mean field interaction between the oligomers and the polymer matrix by means of the Flory-Huggins constant χ.

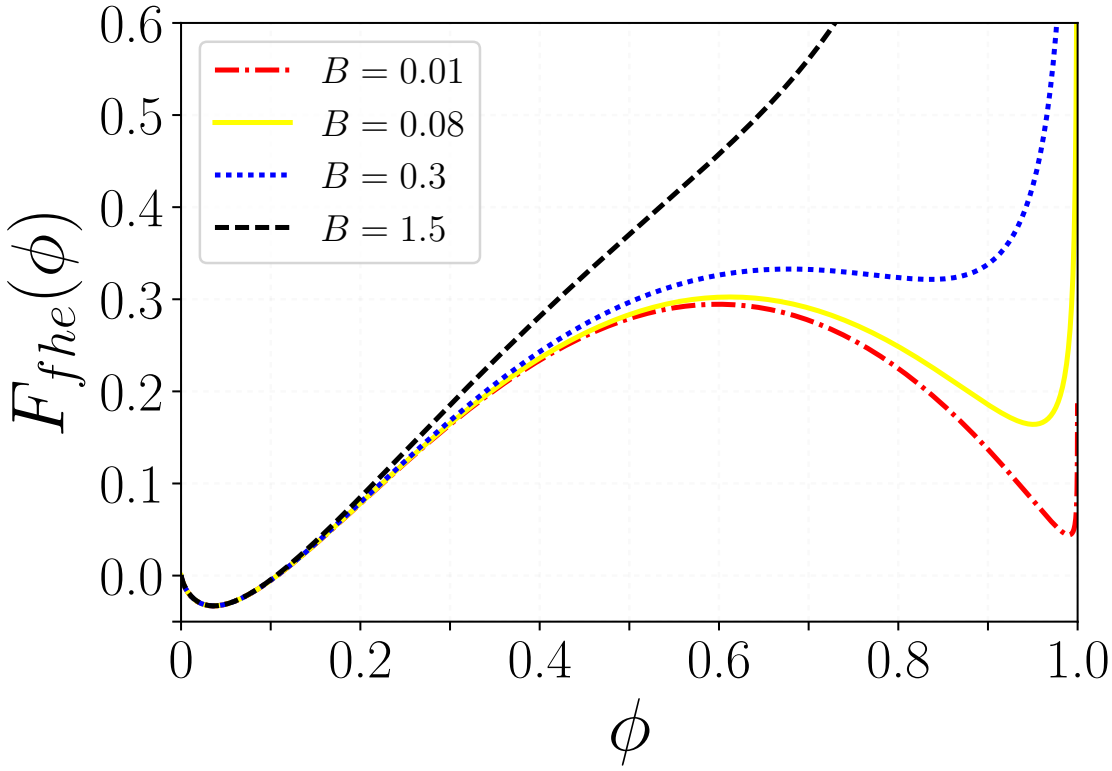

Figure 3.2: Elastic Flory-Huggins free energy for different values of the elastic modulus and $N_a = 1$, $\chi = 2.5$. The system moves from an energy with two minima to an energy with just one, progressively with increasing elastic modulus B, also with $\chi > \chi_c$, where we would expect phase separation.

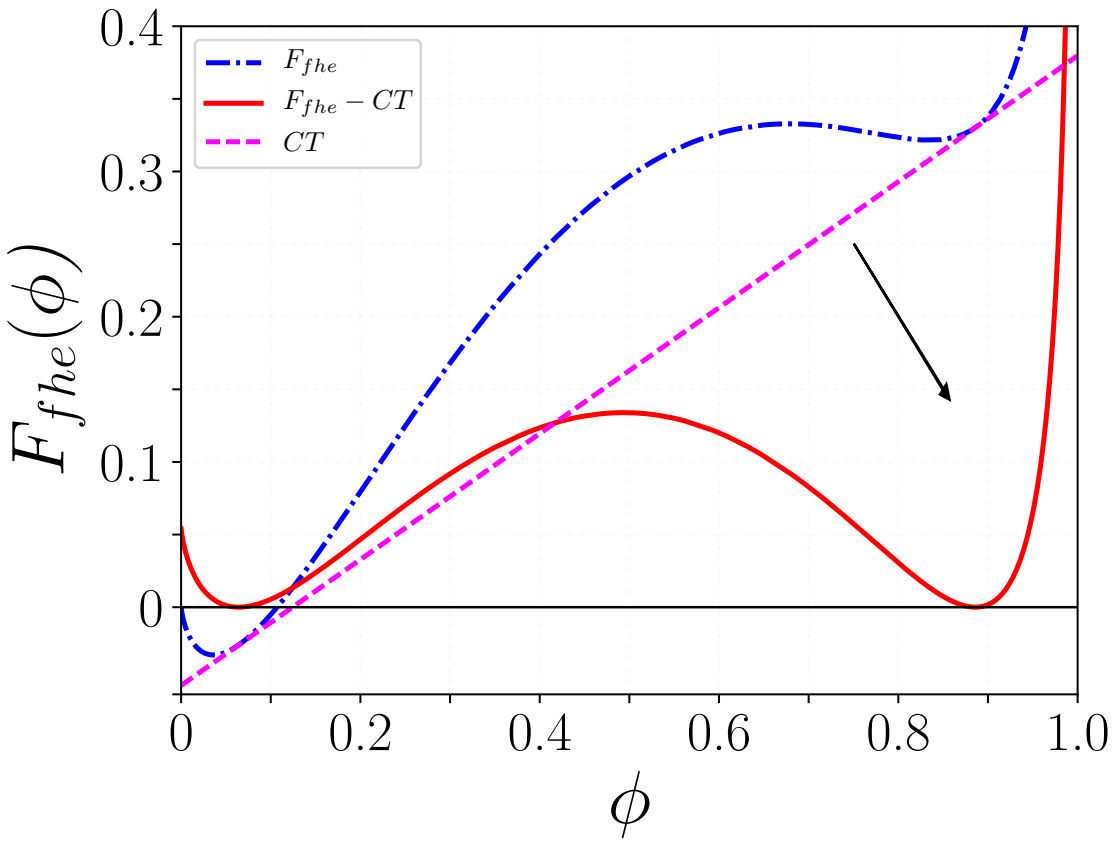

Figure 3.3: The blue(dot-dashed) curve is the elastic Flory-Huggins free energy for $N_a = 1$, $\chi = 2.5$ and $B = 0.3$, the magenta (dashed) curve is the common tangent as in eq.(1.3.18) obtained solving eq.(1.3.16) and eq.(1.3.17). The red curve is the energy minus the common tangent which correctly goes to zero.

3.1.3 Bulk phase diagram

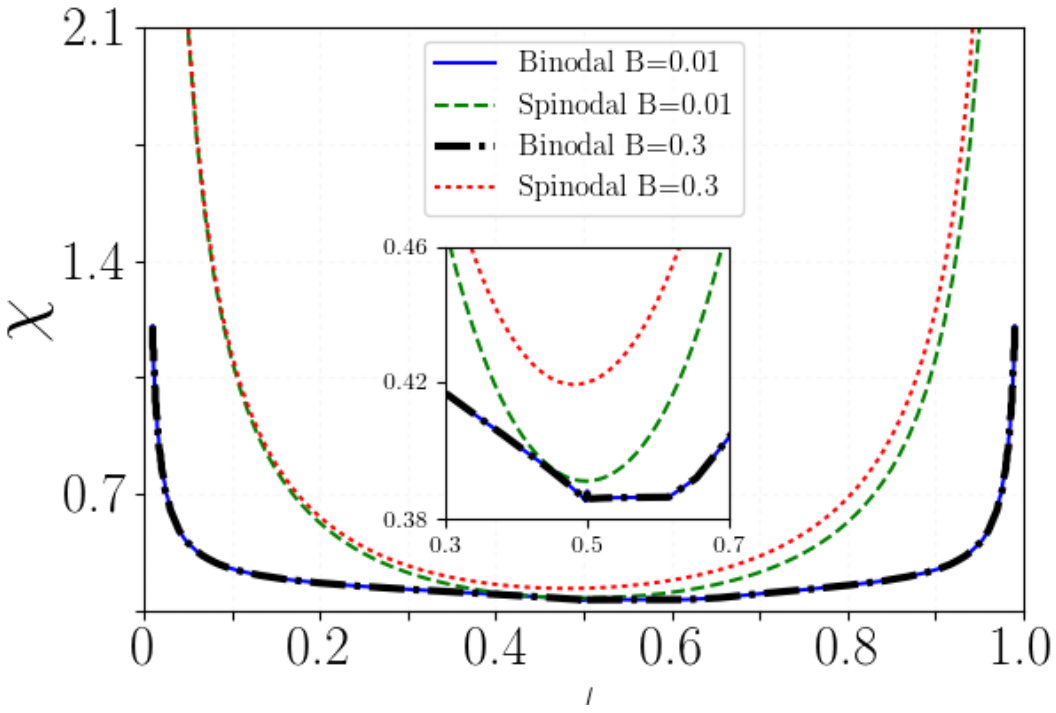

Figure 3.4: Phase diagram for the oligomer-polymer gel system with $N_a = 5$, $\phi_\infty = 0.1$. We notice that the binodal curve is not affected by the elastic modulus, but the spinodal curve is shifted upwards with increasing B. The critical point where we have the transition between mixed and unmixed system moves up and the system can remain in the mixed phase, opening up a miscibility gap (inset).

The free energy in eq.(3.1.15) can be used to draw the phase diagram of oligomer-polymer system in terms of binodal and spinodal curves demarcating regions where the homogeneous phase is metastable and unstable respectively.As in Chapter 1 we can calculate the derivatives of eq.(3.1.15) with respect to the volume fraction of the oligomer ϕ and obtain the spinodal curve by solving $\frac{\partial^2 F_{fhe}}{\partial \phi^2} = 0$ for χ and the binodal numerically, finding the minima of the free energy after common tangent construction, i.e. with equal chemical potential in the two phases. The analytical expressions are given in Appendix 1. The binodal and spinodal curves for different values of the elastic modulus are shown in fig.(3.4). In FH theory binodal and

spinodal curves touch at the critical point (χ_c,ϕ_c) but in the elastic system while the binodal curve is not affected by the presence of a non zero elastic modulus, the spinodal curve is. Beyond a critical value of $B \simeq 0.07$ the effect modifies the phase diagram opening a gap between the spinodal and binodal curves at the critical point. A similar effect is observed in a binary alloy system [93].

We calculate the critical value of the Flory parameter as a function of the elastic

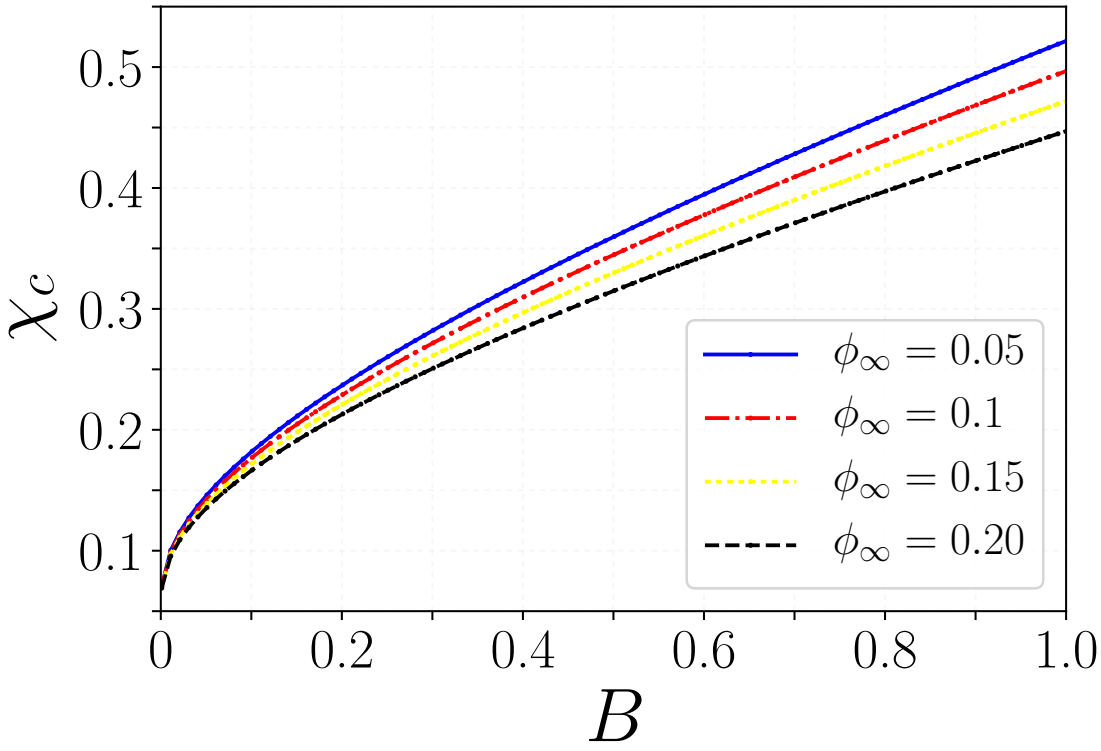

Figure 3.5: χ_c as function of the elastic modulus B for different bulk composition ϕ_∞. The parameter increases with increasing the cross linking, so the point of the phase separation moves forward, indicating that softer systems are more susceptible to phase separation.

modulus [74]. We find that χ_c increases by increasing B, therefore we increase the domain of the metastable phase by progressively moving the critical point. This effect becomes relevant especially for applications to segregation at interfaces, where it is possible to prevent the formation of wetting layers, as we will analyse in the next subsection.

3.2 Migration in a cross-linked polymer matrix

We describe the results of the elastic Schmidt-Binder theory and elastic self consistent field theory, with the profiles of polymers in fig.(3.8) and finally a Cahn construction and the surface phase diagram, to justify the absence of wetting transition in the elastic system as shown in fig.(3.6). We also discuss the nature of the wetting transition observed in this system.

In particular if we consider eq.(3.1.15) and the gradient with Random Phase Approximation (RPA) we obtain a modified theory for the surface migration in the system, the elastic Schmidt-Binder theory:

$$\frac{F[\phi]}{Ak_bT} = F_s(\phi_1) + \int_{z_{surf}}^{z_{bulk}} dz \left(\frac{F_{fhe}(\phi)}{k_bT} + k(\phi) \left(\frac{d\phi}{dz} \right)^2 - \Delta\mu\phi \right). \tag{3.2.1}$$

and solving again the Euler-Lagrange equation with natural boundary conditions built on eq.(3.2.1) we obtain an ODE which can be transformed into an integral equation. This can be solved numerically obtaining $\phi(z)$, as for the one reported in chapter 2. We report the results obtained from the SBMFT next.

3.2.1 Surface phase diagram and Wetting

In order to determine whether or not oligomeric phase wets the surface we use a geometric method pioneered by Cahn [19] and later De Gennes [43] and Jones [67]. The natural boundary conditions for the polymer systems, leads to a graphical solution of an equation involving the derivative of the surface free energy and the bulk free energy. From the boundary conditions of the SBMFT we obtain:

$$-\frac{dF_s}{d\phi_1} = \mu_1 + g\phi_1 = \pm\frac{a}{3}\sqrt{\frac{F_{mix}(\phi_1) - F_{mix}(\phi_\infty) - \Delta\mu(\phi_1 - \phi_\infty)}{\phi_1(1-\phi_1)}} \tag{3.2.2}$$

and so we can plot the left part and the right part of eq.(3.2.2). The wetting behaviour of the systems follows the schematic decribed in Chapter 1 in fig.(1.11). The area between the curves is related to the spreading coefficients, connected to the energy balance between the different phases. Increasing the matrix rigidity B, one can

raise one of the minima in the bulk energy, preventing the formation of a first order wetting transition as in fig.(3.6) [74]. Genzer has suggested elsewhere [48] that in polymer mixtures we have second order wetting transitions at the low density phase, i.e for very small values of ϕ_∞. We see an example in the schematic of fig.(3.7). In our system, as we increase the elastic modulus the minimum corresponding to the high density phase becomes unstable, so it is not possible to have wetting corresponding to the high density phase. Thus we investigated the possibility of having wetting transition at the low density phase.

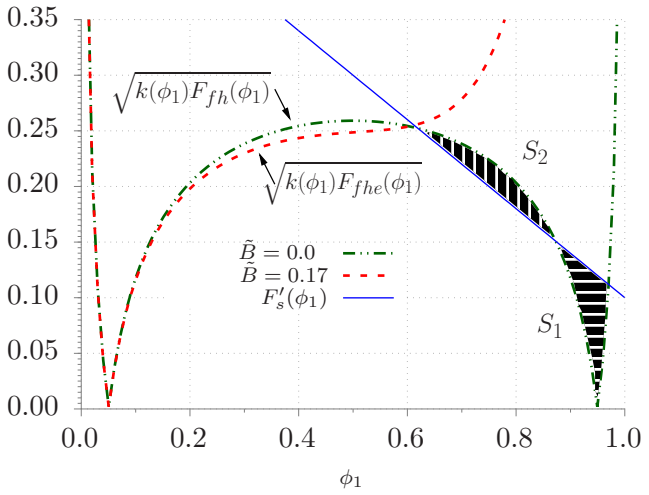

Figure 3.6: Cahn construction showing first order wetting transition for the FH free energy, F_{fh}. An intersection between $\sqrt{k(\phi_1)F_{fh}(\phi_1)}$ and $F^{'}(\phi_1)$ at three points demarcates areas S_1 and S_2, such that $S_1 > S_2$ indicates a first-order wetting transition. A similar graphical construction for the elastic FH free energy F_{fhe} with $B \sim 0.17$(over critical) shows one intersection, indicating the absence of the first order wetting transition.

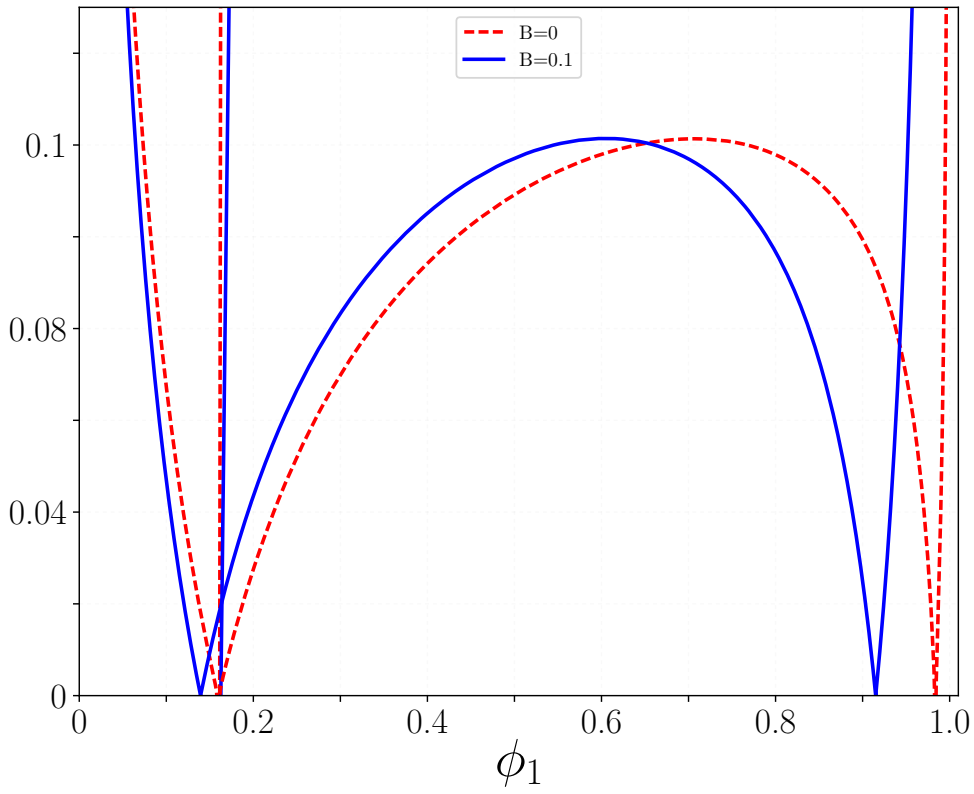

Figure 3.7: Cahn construction for second order wetting transition at the low density phase. The red curve (dashed) is for a non elastic system with $\chi = 1.7, N_a = 1, N_b = 4$ and the blue one for an elastic one with same parameters and $B = 0.1$, which is subcritical. The surface energy curves (vertical lines) are obtained with SCFT, with iterative calculations of the segregation profiles for ϕ_1. As can be seen the equilibrium corresponding to the low density polymer phase for an elastic system is shifted to lower densities in comparison to the one where elastic effects are absent.

3.2.2 Wetting profiles for SBMFT and SCFT

Solving eq.(3.2.1) via the Euler-Lagrange equation we obtain a non linear differential equation which can be converted into an integral equation like in eq.(2.1.3) with the elastic Flory-Huggins energy:

$$\frac{6z}{a} = \int_{\phi_\infty}^{\phi_s} \frac{d\phi}{\sqrt{\phi(1-\phi)[F_{fhe}(\phi,\chi) - F_{fhe}(\phi_\infty,\chi) - \Delta\mu(\phi-\phi_\infty)]}}. \tag{3.2.3}$$

Thus solution of eq.(3.2.3) is shown in fig.(3.8) with the inset showing the solutions of eq.(2.1.3). We notice a change in the concentration profiles with increasing elastic modulus and the absence of the wetting profiles, predicted in normal SBMFT (inset). In a similar way, we can include a deformation elastic energy in the SCFT model,

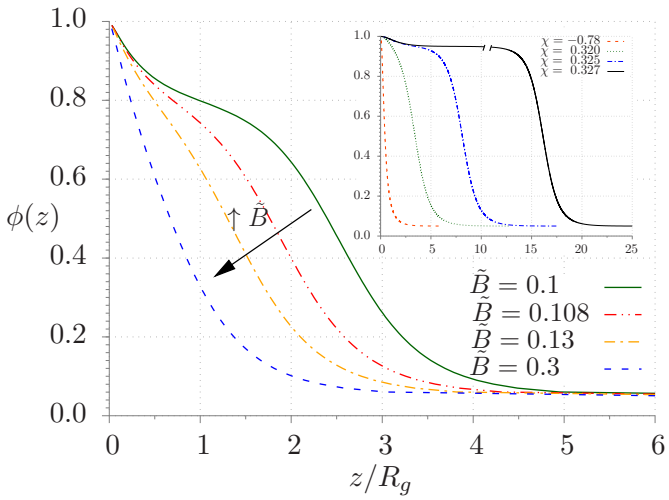

Figure 3.8: Migrant concentration profiles $\phi(z)$ for the SB model including the elasticity obtained by minimizing eq.(3.2.1) for ($\chi = 0.320$ and $N_a = 10$) and increasing B. A wetting transition is not observed in this model. Inset shows concentration profiles for the SB model without elasticity for the symmetric case $N_a = N_b = 10$ with increasing χ. The black solid line with a break indicates the formation of a macroscopic wetting layer.For $\phi_1 > 1 - \phi_\infty$, the profiles decreases from ϕ_1 to $1 - \phi_\infty$ which is a B-rich layer and then after $1 - \phi_\infty$ we find an A-rich macroscopic wetting layer, as reported by Schmidt et al.[112].

through the calculation of the chemical potential and the mean field between the oligomers and the polymer matrix, following eq.(2.1.16) and eq.(2.1.17). Nevertheless

since we do not have mixing entropy for the polymer gel, we do not compute this contribution for the mean field explicitly for corresponding b species. The equilibrium migrant concentration profiles are shown in fig.(3.9). As it is shown both the surface fraction as well as the amount of material leeched to the surface decreases with increasing elastic modulus.

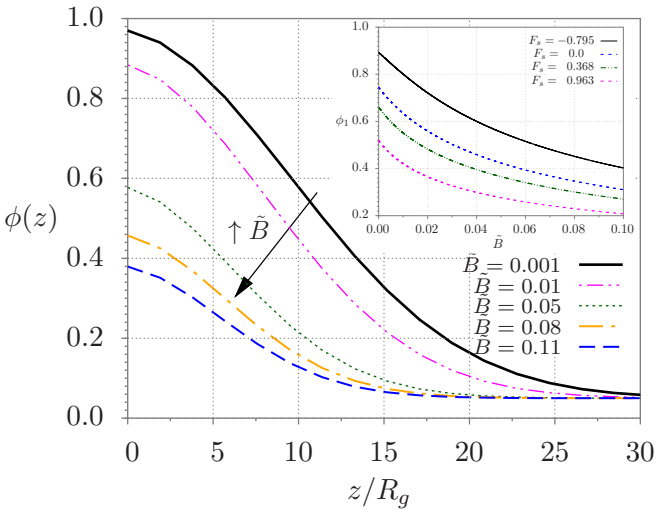

Figure 3.9: Migrant concentration profiles $\phi(z)$, calculated with SCFT, for different elastic moduli B of the polymer matrix. The amount of material flowing to the surface decreases with increasing B. The dependence of the surface fraction ϕ_1 as a function of B for different surface free energy F_s is shown in the inset. As expected, the volume fraction decreases for a system with higher F_s.

3.2.3 Surface tension

We have seen in Chapter 1 that in the framework of the SCFT we need a microscopic surface energy f_s, in units of k_bT, as a penalty for placing monomers of the oligomers on the surface. We can link the microscopic parameter to the macroscopic surface free energy, considering the total amount of oligomers on the surface with respect to the volume of the matrix. Following Budowski [16], we can link the microscopic parameter f_s to the difference of the surface energy between the polymer species ΔF_s as:

$$\Delta F_s = (A/V) f_s \tag{3.2.4}$$

where A and V are the lattice surface and volume respectively, with $b = \sqrt[3]{V}$ being the lattice parameter and ΔF_s being:

$$\Delta F_s = \int_{\phi_1}^{\phi_\infty} (\frac{dF_s}{d\phi}) d\phi. \tag{3.2.5}$$

Following Jones and Geoghegan [68, 49] this quantity represents the difference between the surface energies of the migrant and the polymer matrix and it can be calculated in SI units considering the temperature of the system and the lattice volume V, obtained with the volume of a single monomer. In particular the conversion is:

$$\Delta\gamma = \frac{k_bT}{V} \frac{dF_s}{d\phi_1} \tag{3.2.6}$$

where the derivative of the surface free energy is multiplied by the temperature and divided by the lattice volume V. We notice the results for an elastic one with different B, but same ϕ_∞. We choose a value of the lattice parameter $b = 4.64$Å and $T = 298.15K$, so $\Delta\gamma = 19.11 \times mJ/m^2 \Delta F_s$. There are different starting points for the curves, for different bulk concentration, but all of them present a saturation approaching the value which represent the highest difference between the surface energy of the two polymers $\Delta\gamma$. In particular the black dotted curve is the derivative of the surface free energy with the fitted values of μ and g. The polynomial form of the surface energy is a good representaiton for small values of ϕ_1. It does not work

for lower bulk compositions ($\phi_1 \to \phi_\infty$) and approaching the wetting transition. This limitation reflects the necessity to consider higher order corrections in the analytical approximation of F_s, including high order gradients as reported by Cohen et al.[24] at the critical wetting, and successfully measured by Bruder [13], suggesting the possibility of having entropic corrections [12].

Increasing the elastic modulus we see an effect on the curves, mainly because with B increasing ϕ_1 decreases, so we are moving the curves to the left hand side of the graph.

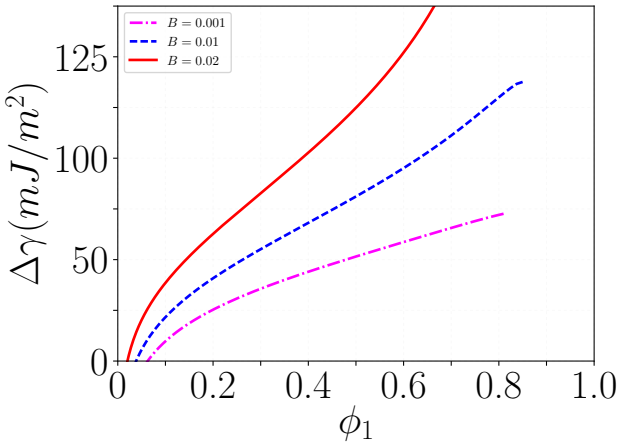

Figure 3.10: Surface free energy $\Delta\gamma$ as function of $\phi_1 - \phi_\infty$. At bulk composition the difference between surface energies is zero and then goes to saturation. Increasing the elastic modulus we increase the surface energy, meaning that becomes less convenient moving to the surface.

Calculation for a real systems

It is interesting to reproduce some experimental data reported in the literature and apply the $\Delta\gamma$ calculation to different systems. In particular we can use SCFT for PS/PVME and correctly reproduce $\Delta\gamma(M_w)$ as a function of molecular weight as in Bhatia[4].

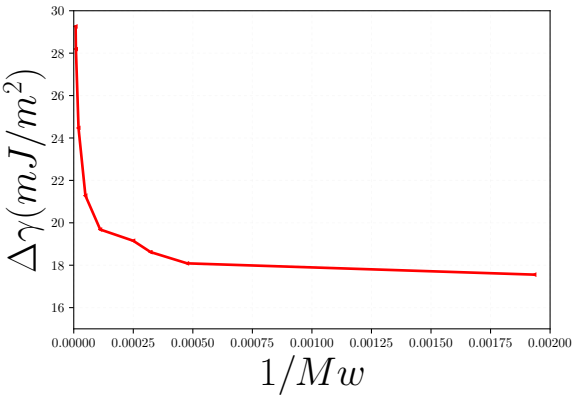

Figure 3.11: Difference in surface tension between Polystirene (PS) and Poly(vynil methyl ether) (PVME) as function of the inverse molecular weight. $\chi = 0.33 - 0.4$ as measured in [114]. We notice that the trend is similar to the one reported by previous experimental studies as in Bhatia[4].

3.3 Applications: Materials design

In the previous sections we have seen the effects of elasticity on the migration of oligomers in a polymer gel. We have seen that we can characterise nanofilms, controlling how much material goes on the surface by controlling both the bulk and the surface thermodynamics. Those models find applications in the real world in a number of different fields such as food industry, packaging [57] and consumer goods [79]. In these situations our work provides a way to tune the material properties according to the production and design needs. In particular we see how to control surface migration by means of changing the poperties of surface, the degree of polymerisation of the oligomers, and a gradient of elasticity as reported in Croce et al.[25], where they study migration in polymer gels.

3.3.1 Surface characterisation

In section 3.2.1 describing the surface phase diagram we have seen that by changing surface energy of the system one can modify the nature of the wetting transition. In particular the surface segregation depends crucially on the elastic modulus B of the material. When we increase or decrease the surface energy of the system, the same

effect arises. We have seen in Chapter 2 that f_S is an energetic cost for placing a monomer on the surface. So an increase or decrease in f_s results in a surface that is less attractive for the segregating species. We see the effect of changing f_s on the profiles in fig.(3.12), where there are both the results for a normal polymer mixture and for oligomers in a polymer gel. In both systems we alter the overall material migrated and the surface fraction ϕ_1. It may be possible to treat surfaces of polymer samples optically ([92]) or mechanically ([78]), changing f_s, for a better design of those materials, obtaining more or less oligomers, depending on the application.

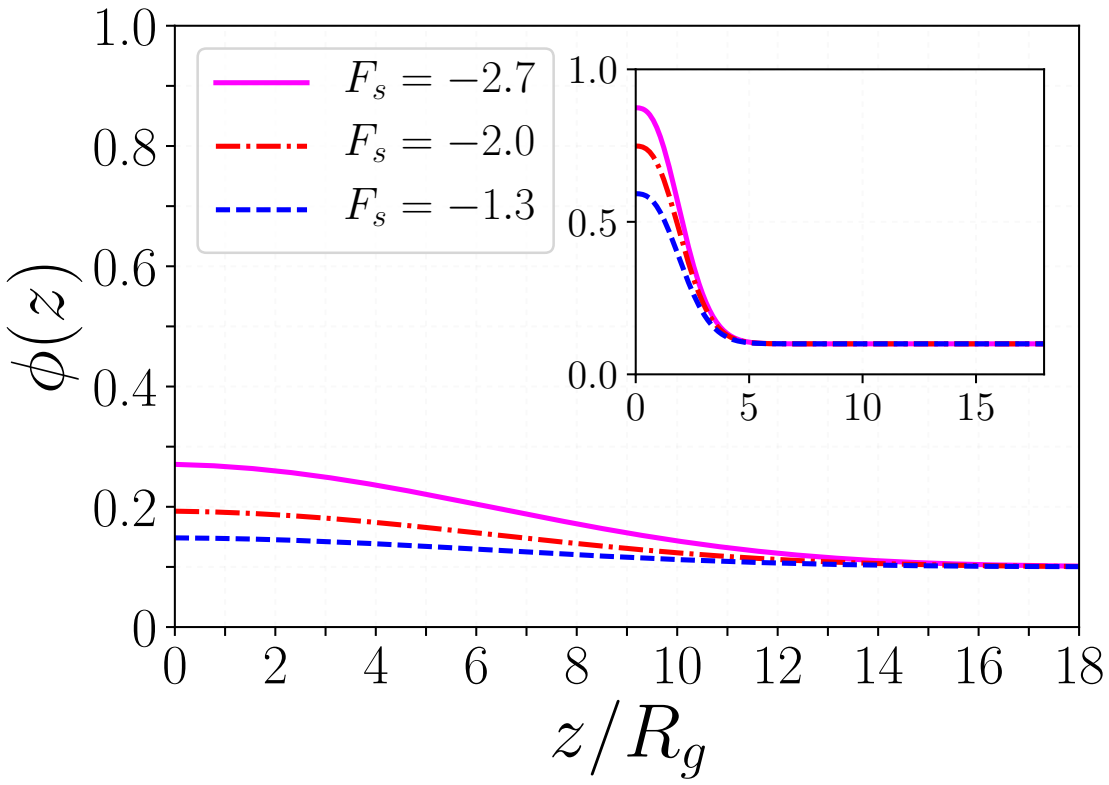

Figure 3.12: Volume fraction (SCFT) as a function of z in reduced units of R_g for $N_a = 10$,$N_b = 1000$,$\chi = 0.22$,$T = 300K$ with an increasing surface energy F_s without elasticity (inset). Volume fraction as a function of z in reduced units of R_g for $N_a = 1$,$\chi = 0.22$,$T = 300K$, $B = 0.01$ with an increasing surface energy F_s(bottom).

3.3.2 Elasticity gradient

So far we have considered the elasticity of the polymer gel as a bulk thermodynamic quantity for our system and neglecting spatial variation. To circumvent this limitation in a phenomenological way, we consider a spatially varying elastic modulus:

$$B(z) = B_0 + B_1 z. \tag{3.3.1}$$

Naturally it does not make sense to have a $B(z)$ negative, so we choose $B_1 > 0$ and for simplicity $B_0 = 0$. The concentrations profiles for migrants are shown in fig.(3.13) where we observe a more pronounced effect of elastic gradient B_1 on ϕ_1, compared to the earlier example of a system with homogeneus bulk modulus.
For systems described here not only does the surface fraction ϕ_1 depends on the elastic modulus gradient, but also the interface width ξ and the overall material on the surface z^* defined as:

$$z^* = \int (\phi(z) - \phi_\infty) dz. \tag{3.3.2}$$

In the inset in fig.(3.13) we notice a decreasing amount of the material on the surface, as function of B_1, as expected. Those effects introduce a link between the bulk and surface thermodynamics. Due to the connectivity of the gel there can arise long range elastic interaction among oligomers mediated by the gel network. Such long range interactions have been studied in the context of adhesion and seen not to play a major role in dictating the segregation behaviour [67]. However we believe that such long-rage elastic interaction might play a role in this physical situation. We will see in the next section that we can estimate the thickness ξ and compare $z^*(B_1)$ with $\xi(B_1)$.

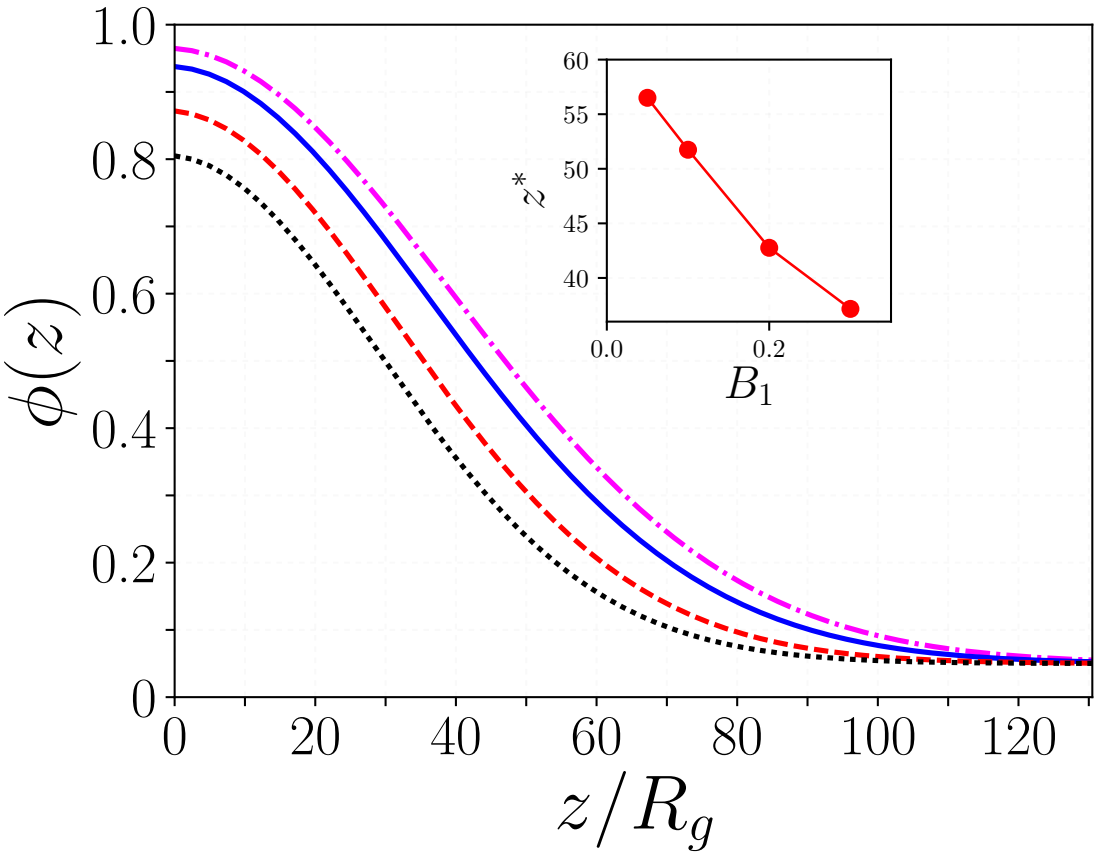

Figure 3.13: Fraction volumes (SCFT) as a function of the coordinate z/R_g with different values of B_1 as reported in Eq.(3.3.1). We notice not just the reduction of ϕ_1, but also the modulation of the shape, which may be important in the design of functional nanomaterials. The inset shows an amount of material on the surface as function of the elastic modulus.

3.3.3 Length estimation

In order to analyse our results further, we consider the effects of the elasticity gradient B_1 on the thickness. In particular we have seen that in samples with a gradient of elasticity, the width of the interface between surface and bulk phases is influenced by changing the elastic modulus. As a further step we can calculate the interface width as a function of the surface energy and also as a function the elasticity modulus. As mentioned before the SCFT equations can only be solved numerically. Nevertheless if we do not consider the time dependence in eq.(2.1.14) we obtain a second order differential equation that as reported by Jones et al.[68] can be solved analytically, obtaining an approximate solution for $q(z)$ and then $\phi(z)$ in the form of an hyperbolic tangent. We can generalise this function for fitting the numerical solution in fig.(3.14), as:

$$\phi(z) = A_1 + A_2 \tanh\left(\frac{z}{\xi}\right) \tag{3.3.3}$$

with A, B, ξ fitting parameters. The comparison is reported in Fig.(3.14) where we notice small differences, but eq.(3.3.3) is sufficiently close to the solution. We can see the result in Fig.(3.15), where it is evident that the interface width of the material decreases with increasing B. Considering the similarity with a decay exponential we can fit it to a function of the form:

$$\xi(B) = a_1 + a_2 \exp a_3 B. \tag{3.3.4}$$

3.3.4 Length of oligomers

Probably the easiest parameter someone can control experimentally is the length of the polymer segregating at the surface. Nowadays there are different techniques [56] which allow us to polymerise monomers with a desired chain length. This allows us to control the material segregating in the polymer gels, as we can see in fig.(3.17).

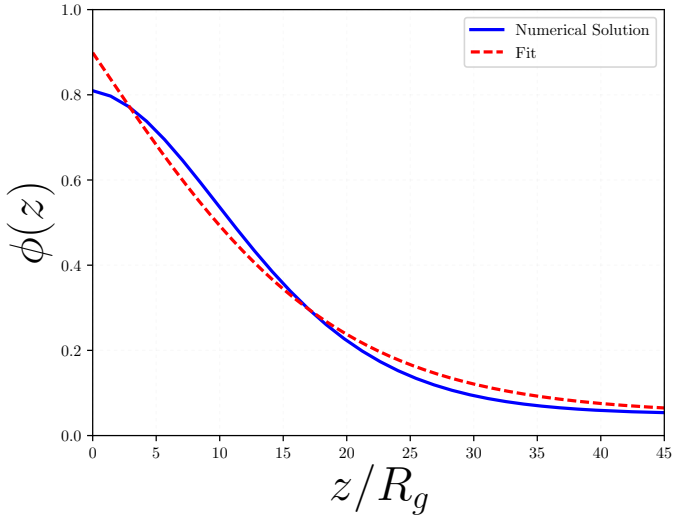

Figure 3.14: Comparison between an analytic approximation of the SCFT fitted with the exact numerical solution (inset)

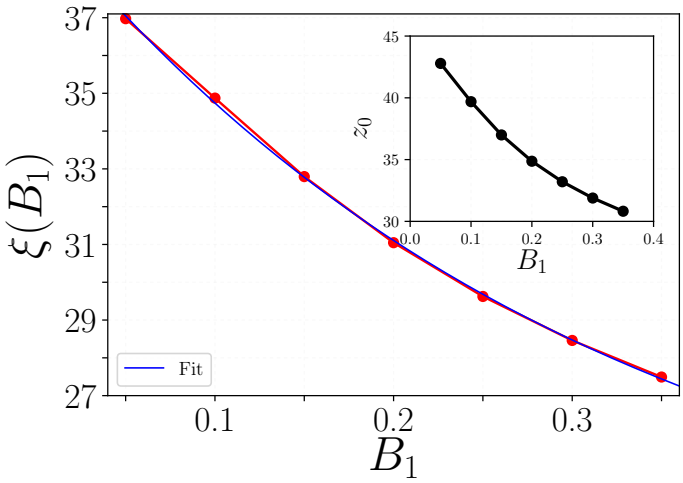

Figure 3.15: Thickness of the system as a function of the Young modulus and correspondent

Increasing the degree of polymerisation of the small molecule we modify the entropic contribution to the bulk energy, which decreases monotonically with increasing N_a. This energy contribution becomes smaller than the interaction between the polymers and the elastic deformation energy, so there is an entropic penalty for the chains segregating at the surface. This lowers ϕ_1 and the shape of the wetting profile, because as expected longer molecules migrate less.

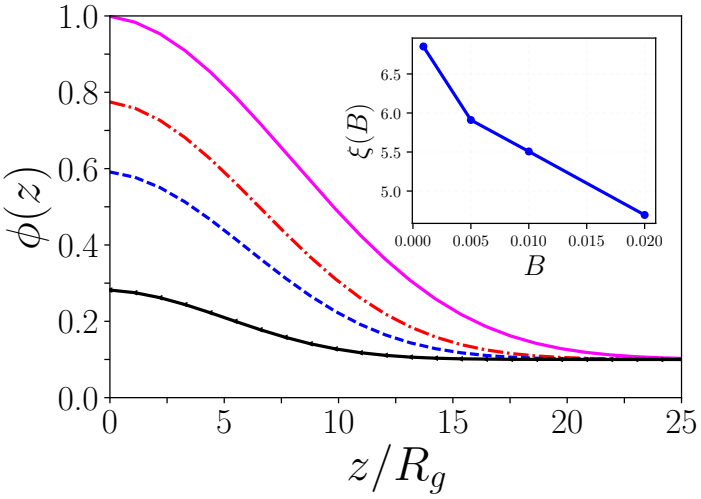

Figure 3.16: Segregation profiles for different values of B calculated with SCFT. In the inset correspondent $\xi(B)$ decreasing with B.

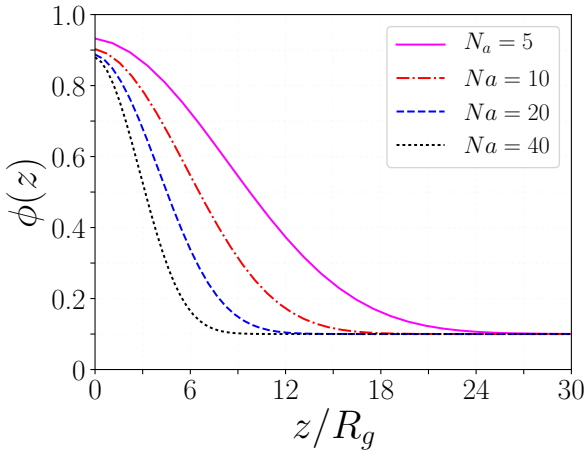

Figure 3.17: Variation of surface segregation profiles (SCFT) with increasing degree of polymerisation for the oligomer species, with $\chi = 0.22$, $\phi_\infty = 0.1$ and $F_s = -3.0$.

Conclusions: In this chapter we have studied the effects of elasticity and the application to the design of polymer materials. We shall see in the next chapter how to apply these models to experimental systems.

3.4 Appendix

3.4.1 Spinodal decomposition for elastic system

Here we introduce the equations for the spinodal curve used for the spinodal decomposition. In particular taking the second derivative of the free energy in eq.(3.1.15) and solving for χ, we obtain the spinodal curve:

$$\begin{aligned}\chi_s = \frac{1}{2}\{&\frac{1}{\phi N_a}+ \\ &+ B\frac{(1-\phi_\infty)}{9}\left[-(1-\phi)^{-\frac{4}{3}}(1-\phi_\infty)^{-\frac{2}{3}} + 2(1-\phi)^{-\frac{5}{3}}(1-\phi_\infty)^{\frac{1}{3}}\right]\}.\end{aligned} \tag{3.4.1}$$

We obtained the binodal numerically, finding the minima of eq.(3.1.15) using the common tangent construction as in Chapter 1.

3.4.2 SCFT equations for elastic system

Using eq.(3.1.15) combined with the eq.(2.1.16) and eq.(2.1.17), the chemical potential of the B polymer becomes (in $\beta = \frac{1}{k_b T}$):

$$\begin{aligned}\beta\frac{\mu_b}{N_b} = &\chi\phi^2 - \frac{1}{N_a}\phi+ \\ &+ \frac{B}{2}(1-\phi_\infty)\left[\left(\frac{1-\phi}{1-\phi_\infty}\right)^{\frac{2}{3}} + 2\left(\frac{1-\phi_\infty}{1-\phi}\right)^{\frac{1}{3}} - 3\right] + \\ &+ \frac{B}{3}\phi\left[-\left(\frac{1-\phi_\infty}{1-\phi}\right)^{\frac{4}{3}} + \left(\frac{1-\phi_\infty}{1-\phi}\right)^{\frac{1}{3}}\right]\end{aligned} \tag{3.4.2}$$

and for the mean field, considering that in the elastic approach $N_b \to \infty$, we will not have the logarithm, so $\beta w_b = \beta \frac{\mu_b}{N_b}$. The chemical potential for the a species is:

$$\begin{aligned}\beta\mu_a &= (1-\phi) + \log\phi + \chi N_a (1-\phi)^2 \\ &+ \frac{B}{2}(1-\phi_\infty) N_a \left[\left(\frac{1-\phi}{1-\phi_\infty} \right)^{\frac{2}{3}} + \left(\frac{1-\phi_\infty}{1-\phi} \right)^{\frac{1}{3}} - 3 \right] - \\ &- \frac{B}{3} N_a (1-\phi) \left[- \left(\frac{1-\phi_\infty}{1-\phi} \right)^{\frac{4}{3}} + \left(\frac{1-\phi_\infty}{1-\phi} \right)^{\frac{1}{3}} \right]\end{aligned} \tag{3.4.3}$$

and so the mean field is:

$$\begin{aligned}\beta w_a &= \frac{(1-\phi)}{N_a} + \chi (1-\phi)^2 + \\ &+ \frac{B}{2}(1-\phi_\infty) \left[\left(\frac{1-\phi}{1-\phi_\infty} \right)^{\frac{2}{3}} + \left(\frac{1-\phi_\infty}{1-\phi} \right)^{\frac{1}{3}} - 3 \right] - \\ &- \frac{B}{3} N_a (1-\phi) \left[- \left(\frac{1-\phi_\infty}{1-\phi} \right)^{\frac{4}{3}} + \left(\frac{1-\phi_\infty}{1-\phi} \right)^{\frac{1}{3}} \right]\end{aligned} \tag{3.4.4}$$

because $\beta w_a = \frac{\beta\mu - \log\phi}{N_a}$.

Chapter 4

Simulations and Experiments

In this chapter we introduce the fundamental concepts of Design of Experiments (DoE) and statistics in industrial modeling through correlation between variables. We report the results obtained by applying those statistical concepts to the optimisation and the validation of the computational model used for describing the surface segregation in the framework of self-consistent field theory (SCFT), in particular the lattice effect. We present the results of the machine learning and how to apply those concepts to compare theoretical results against experiments as a route towards model validation with a R^2 test. Finally we present some preliminary simulation results obtained with Chemistry Unified Language Interface (CULGI) package. The DoE are obtained using the softwares JMP [64] and R [101].

4.1 Design of Experiments. Latin hypercube.

In recent years, the use of statistics has become more and more important in experimental data analysis of scientific and industrial problems. For the latter some applications have been reported by Savage [110] for managing problems such as production, operation research, supply chain and more. In particular a useful technique for the analysis and ultimately the validation of computational models is the

Design of Experiments (DoE), a set of statistical tools used for simulating an experiment with all the necessary variables. DoE was first introduced by Fisher [38] as a method for addressing agricultural design and optimising parameters. However over but through the years DoE found applications in many different disciplines such as Mathematics, Chemical Engineering [77], Logistics and other industrial problems with needs of statistical tools [110] and even in experimental Particle Physics [14] for the design of hadron calorimeters and photomultipliers.

Fisher proposed several principles for setting an experimental design. In particular the three main ones are randomisation, replication and blocking, used for simple designs, while orthogonality and full factorial for more complicated DoE where one needs to evaluate the effects and possible interactions of several factors [1]. We use randomisation in an experiment each time there are factors which cannot be controlled, so by randomising the experiment we eliminate the unpredictable (white) noise. Replication entails performing the experimental steps in a random sequence, repeating the entire experiment or part of that running under different conditions. Finally blocking allows to pack some experiments in different blocks with homogeneous conditions. The aim is to eliminate an unwanted source of variability, exploring all the possible combinations of factors.

Computer models increasingly replace physical experiments in studies where there is limited knowledge about the system under study. For instance in our work, the Flory-Huggins/Self-Consistent Field Theory models have a total of seven or more parameters whose values are not known exactly. These parameters are input variables which must be treated as random variables for a successful statistical modeling of the computer simulations. Latin hypercube designs, first introduced in McKay [86] and then in Iman[63], are amongst the most popular strategies for computer experiments. We will briefly elaborate on Latin hypercube designs below.

With the growing power of computers, more techniques become available for the design and analysis of simulations, and the number of applications explodes: aerospace, bioengineering and decision under uncertainty, to name a few.

In the case of computer experiments we will analyse a particular useful design in the next section. More recently thanks to the more powerful computational tools developed, DoE finds applications also in the design and validation/development of computational models and computer experiments.

Until the work of McKay [86] and Iman and Conover [62], few statistical assumptions were made about the relationship between input variables and the output produced by a computer code. Since then methods of statistical sampling of multidimensional distributions for generating near-random samples of parameters have flourished, with different types of designs used for different problems. The words "factor", "sample", "treatment", "treatment level" and "repetition" are used generically in statistics. In our particular setting, factors are parameters, a sample is a set of values chosen, one for each parameter, a treatment is a computer run for a given sample to produce an output (for us, a segregation profile), treatment levels are different samples of the parameter values and repetition is the number of computer runs made with a fixed sample.

We use a sampling method for generating different uncorrelated combinations of the input parameters needed for calculating segregation profiles within SCFT, as these are not available in the literature or easily accessible experimentally for our system. We first fix reasonable lower and upper bounds for the parameter values relevant to our polymer system and generate random input values within these bounds for the parameters using the Latin hypercube sampling method.

The Latin hypercube design we use is a generalisation of the "completely randomized design" (CRD), which is the easiest sampling method. Indeed, CRD is appropriate in the case where the experiment depends only on one factor or parameter, call it X_1. Let this factor have L levels, that is L potential values $v_i, i = 1, .., L$ in a given interval, and let the experiment be replicated n times per level. The total size of the sample (i.e. the number of runs) is $L \times n$, and there are $\frac{(L\times n)!}{(n!)^L}$ ways to run the experiment, all equally likely to be picked by a randomization procedure. The

measured response (output) is encoded in the variables

$$Y_{kl} = \mu + \tau_k + \epsilon_{kl},\ k = 1, ..., L \qquad l = 1, ..., n \tag{4.1.1}$$

where each Y_{kl} is an observation for which the parameter X_1 takes the value v_k (i.e. X_1 is at level k) and for which l is the replication number within that level. μ is the overall mean (average over all data) and represents a recurring effect for the experiment, τ_k is the effect of having X_1 taking the value v_k, so it is estimated as the distance from the true mean μ i.e. $\tau_k = \mu_k - \mu$ where μ_k is the average of all data for which $X_1 = v_k$; ϵ_{kl} is the random error present in the l^{th} replication of the experiment where $X_1 = v_k$, and is taken to have a normal distribution with zero mean. The variables Y_{kl} are the entries of an $L \times n$ matrix, and CRD generates each entry without considering the previously generated entries, which is not ideal for uniform sampling of the space of input variables.

Experiments have nuisance factors, which may affect the measurement results but are not of primary interest. To reduce experimental errors due to nuisance factors, one uses the blocking technique, which amounts to create homogeneous blocks in which the nuisance factors are held constant and the factor of interest (X_1) is allowed to vary. In a Latin square design, one has one primary factor of interest (X_1) and two nuisance factors (blocking variables X_2, X_3). The advantage of Latin squares is that they allow to keep the nuisance factors separately, either because they cannot be combined or because this is requested by the experiment. They also allow meaningful experiments to run with a small number of runs, which is valuable in relation to CPU cost. The measured response is encoded in the variables

$$Y_{klm} = \mu + \tau_k + \nu_l + \rho_m + \epsilon_{klm} \tag{4.1.2}$$

which are observations for which the primary factor $X_1 = v_k$, while the blocking factors X_2 and X_3 are at level l and m respectively. μ and τ_k are as before, and ν_l and ρ_m denote the effects for block l and m respectively; ϵ_{klm} is a random error. Table 4.1 provides an example of Latin square for 3-level factors.

Table 4.1: Examples of Latin square design. We see all the possibilities for three factors A,B,C.

A	B	C
B	C	A
C	A	B

A Latin hypercube design can be viewed as a d-dimensional extension of the Latin square design. In this case, one deals with p points in d dimensions written as a $p \times d$ matrix $\mathbf{X}$ where each column represents the p values a given parameter can take and each row represents a sample, so that the entry X_{mn} represents the value taken by the parameter n ($1 \leq n \leq d$) within the sample m ($1 \leq m \leq p$). The design is constructed so that there is only one sample at each level. One advantage of this design is that the output is dominated by a few entries of the matrix $\mathbf{X}$. The Latin hypercube design is appropriate in the case of FH/SCFT since we have seven or more parameters to tune. An example of a (14×7) randomised input matrix $\mathbf{X}$ is given by the first seven columns in Table 4.2, while the last column tabulates the output ϕ_1. In particular we generated a latin Hypercube with 10^4 combinations and we used the file as an input for the computational C++ code, running on the Durham HPC Hamilton Cluster. We will show the results in the next section.

4.2 Machine learning for SCFT

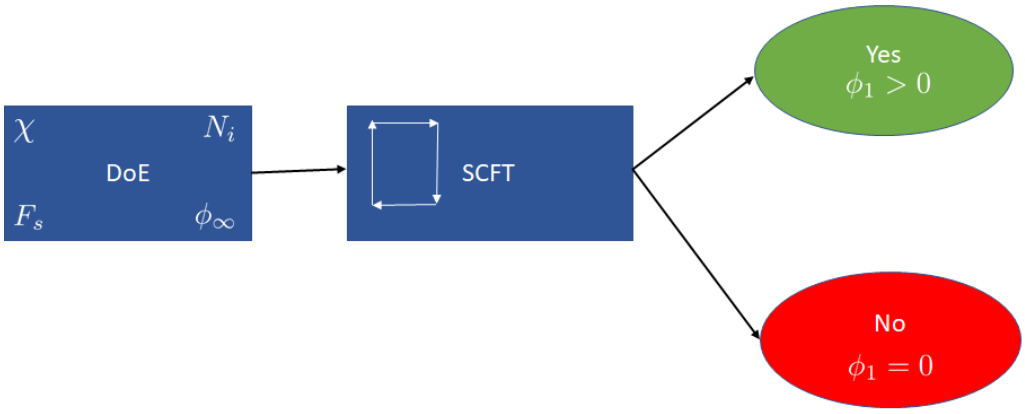

Figure 4.1: Schematic of the unsupervised machine learning for SCFT. The generated latin hypercube DoE data for the seven parameters are input for the SCFT model, which after the run produces results when $\phi_1 > 0$ (green), so the input parameters are a good design. It does not produce results when $\phi_1 = 0$ (red), meaning the the input design is not a good combination.

Table 4.2: Example of some of the values of the seven input parameters generated with Latin hypercube DoE and results of the unsupervised machine learning, with F_s surface energy, χ FH constant, $N_{a/b}$ degree of polymerisation of oligomers/polymer matrix, b lattice parameter, T temperature, ϕ_∞ bulk composition, ϕ_1 surface composition is the output.

F_s	χ	N_a	N_b	b	$T(10^{-3})$	ϕ_∞		ϕ_1
-6.752952	4.89030347	93	5541	5.10414562	0.72756917	0.18557205		0
8.59225355	2.93522828	69	8502	8.31495808	0.77676288	0.7427797		0
-6.7129505	-0.7445286	3	802	26.1982757	0.51979403	0.47487981		0.996009
-5.6959883	-2.2945883	68	5722	14.0227272	0.72376137	0.9418955		0.99851
-2.5643294	-2.4672872	74	8500	1.50409716	0.36332803	0.02007565		0.96342
7.35220585	6.16573714	5	4347	39.2615285	0.33378873	0.79501792		0
-7.9953075	4.53913612	13	7901	15.5412092	0.53390981	0.69962475		0
6.56756029	-0.2883572	54	4893	31.3229601	0.03697259	0.3408168		0.340923
6.96988346	-2.9642294	98	650	34.7630064	0.72622298	0.16902618		0.16917
-1.9258433	1.52555868	31	2537	16.0642932	0.14455258	0.67003817		0.879222
-9.6384476	1.96749875	72	3200	10.9565321	0.29863388	0.31013721		0
9.78229932	6.93192046	9	7952	10.0472891	0.01420271	0.11207673		0.11209
-2.3289357	-1.8449556	80	2819	4.96875918	0.85872675	0.91332655		0.999948
-6.2460095	-1.5149429	14	5708	20.0351159	0.59983476	0.87382752		0.997565

Using the latin hypercube, we generate a uniform sampling of the different value of the parameters we need in our code. In particular we set a maximum and a minimum for each of the parameters and, using the software JMP, we explore uniformly the

space of parameters. This sampling can be used as an input for unsupervised machine learning for the FH/SCFT code. It is particularly helpful for having an idea about the value of χ between particular polymer species with a fixed degree of polymerisation, because is quite hard to measure the FH constant . All the parameters are inputs for the C++ code, which runs multiple times, calculating segregation profiles at each run with a different combination of the parameters, which is unique being generated with a Latin Hypercube design, as in the schematic in fig.(4.1). The output, that defines the success of the calculation, is the value of ϕ_1, where $\phi_1 > 0$ means a positive output,a successful run and the calculation of a segregation profile; while $\phi_1 = 0$ an unsuccessful run. A combination of parameters, generated with JMP and the output(ϕ_1) is shown in tab.(4.2). We can see the results in fig.(4.2), where $\phi_1 = 0$ corresponds to the red colour and $\phi_1 > 0$ to the green one. We notice a strong correlation between some variables, in particular between χ and N_b, the degree of polymerisation of the polymer matrix and the interaction constant respectively in fig.(4.2). These results allow us to choose optimal combinations of parameters we need for predicting the segregation behaviour of a class of systems. Furthermore with DoE we have a window of sensibility of the model and we can understand for which combinations of parameters the SCFT converges. We can also check if these combinations of input parameters correspond to physically realistic values . Once we know the degree of polymerisation of our experimental polymers, we can look for the DoE results for the corresponding values of χ and f_s for those polymers, as in tab.(4.2) and try which one gives the best description of the experimental data, as we shall see later on.

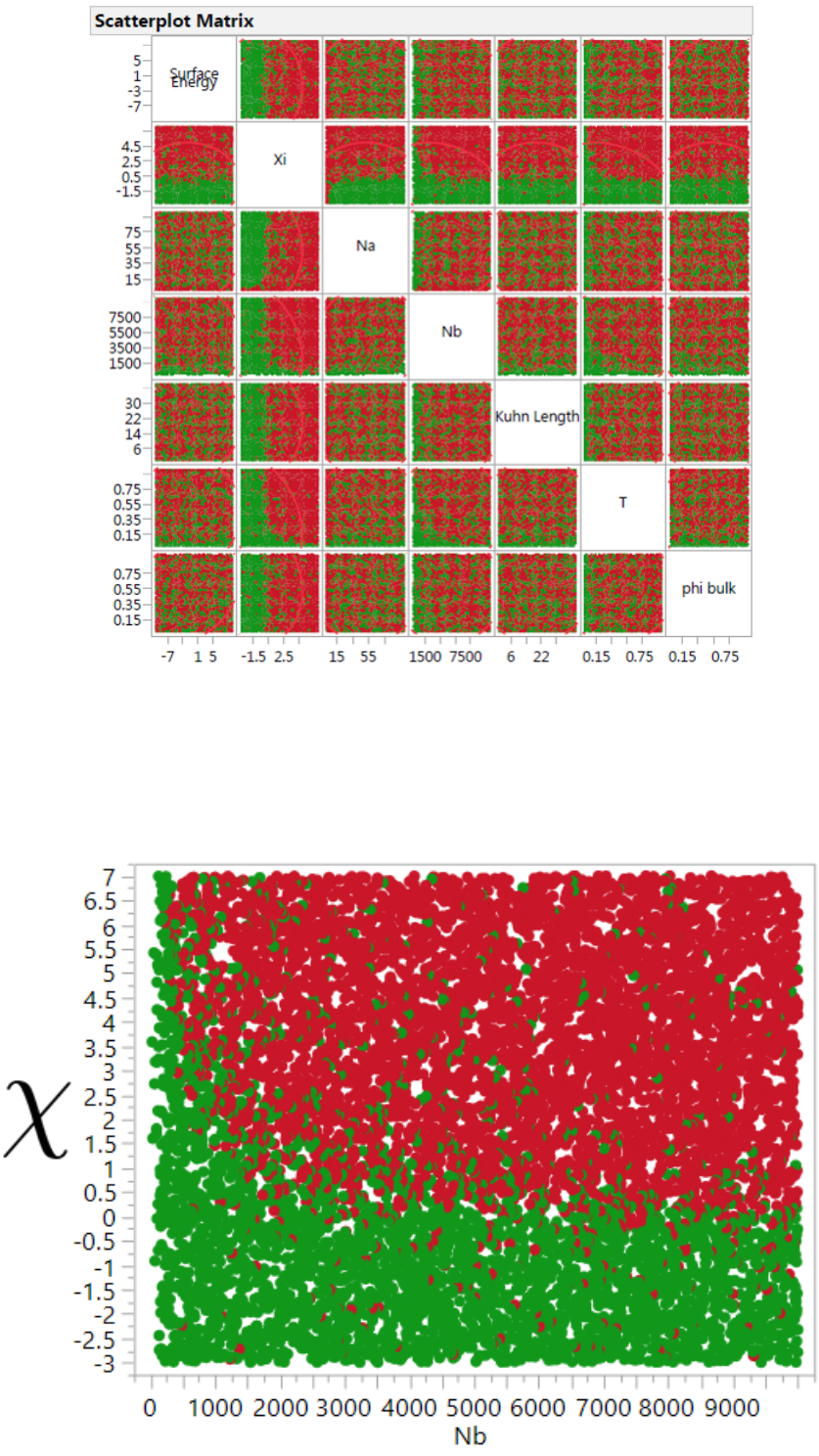

Figure 4.2: Results for DoE for the different parameters of the FH/SCFT model. Red colours corresponds to an unsuccessful run ($\phi_1 = 0$) and the green one to a successful run ($\phi_1 > 0$). We notice a strong correlation between some variables. In particular χ and N_b (below), characterising the molecular weight of the matrix and the interaction with the constant, with $\chi \sim 1/N_b$.

Lattice Dimension effect

The SCFT makes use of a discrete lattice for solving the diffusion equation with an associated lattice parameter b, to calculate the volume fractions of migrating/segregating polymers. We choose a system with fixed values of monomers for both migrants and polymer matrix and alter the lattice dimension, in order to understand its effect on the key observables. In fig.(4.3) we notice that by increasing the lattice dimension we modify the shape of the profiles, from a sharp interface to a more diffuse one. the total amount of material remains constant as can be seen in fig.(4.3). Given that longer chains will take a much longer time to relax, understanding the effect of lattice spacing is crucial when making prediction of segregation profiles of such systems. Running the code on the desktop machine and the laptop we have, there is a limitation for the RAM to a grid of $7 \times 10^3 \times 7 \times 10^3$. However we notice that for $N > 7 \times 10^3$ there are no significant variations in the interface profile on the choice of the lattice parameter. So for fitting experimental data we decided to keep this value fixed, especially since we did not analyse polymer matrices bigger than $N > 6 \times 10^3$.Bigger matrices would require a more coarse grained calculation.

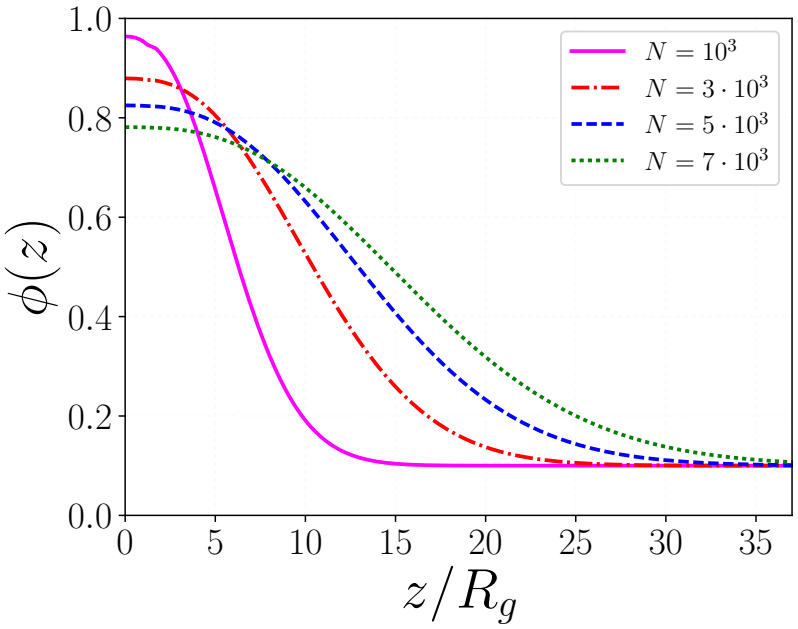

Figure 4.3: Different profiles for $N_a = 1$, $N_b = 100$, $\chi = 10^{-3}$, $\phi_\infty = 0.1$, $F_s = -3.0$ for different values of the lattice dimension, increasing from top to bottom.

4.3 Experiments

Segregating systems

Table 4.3: Values for SCFT for best fit with experimental data. Bulk values are experimental values of the mixture before measurement. After fitting raw data there are some differences with ϕ_∞ used in the sample preparation, which reflects errors of the instrument and the software.

T(K)	χ	$\Delta\gamma(mN/m)$	ϕ_∞	$a(nm)$
298	0.1	12-14	(6-70)%	0.48

We present a comparison between the wetting profiles calculated within the SCFT and neutron reflectivity data [107]. In particular we report a table with the values of all the constants referring to the system dSq/PB (deutereted Squalane in Polybutadiene), as recently studied by Sabattié et al. [108]. We have used the values reported in table (4.3). We have used the values reported in table (4.3) as they result from our previous study with the orthogonal hypercube for the SCFT model. We already knew the values of the degree of polymerisation for dSq and PB from the experiments. We looked for successful combination of χ and f_s with N_a and N_b, as in tab.(4.2) and tested those values in our code comparing the calculated profiles versus the experimental one. Values in tab.(4.3) were the most effective to produce compatible profiles, as we shall discuss later with a R^2 test. Furthermore the values are compatible with some experimental values in literature. The range of values for the surface tension is compatible with the difference between the values of PB($44mN/m$) and Sq($30mN/m$). The Kuhn length is a combination between the values for the single polymers, $a_{PB} = 5.24$å for PB and $a_{Sq} = 4.6$å for Sq, combined as in Schmidt [112], using an interpolating form:

$$a^2(\phi_\infty) = a^2_{Sq}\phi_\infty + a^2_{PB}(1 - \phi_\infty) \tag{4.3.1}$$

We notice there is a good agreement between the experimental data and the theoretical predictions at low concentrations, with error bars within the limits of validity of MFT.

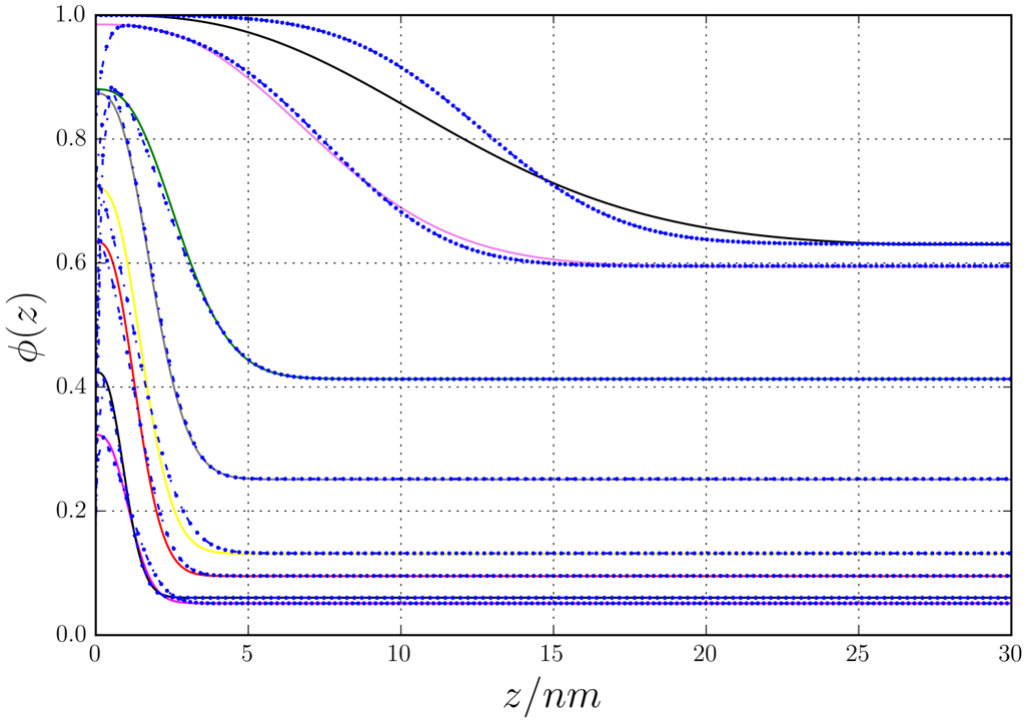

Figure 4.4: Experimental data (points) and theoretical SCFT calculation (continuous line) for the volume fraction of dSq on PB as a function of z, distance from the surface in nm. Bulk composition with $\phi_\infty = (6\%, 8\%, 10\%, 30\%, 40\%, 60\%, 70\%)$.

There is a significant discrepancy between the data and the theory for a 70% bulk concentration of migrants. We obtain the best fit for a high composition, decreasing a, with a mismatch between lattice parameter for SCFT and Kuhn length, as in Shull [116]. In this way we include the effect of entropy loss for long chains, and the end chains confined to the layers close to the surface. From eq.(1.3.24) being $N_a = 7$ and $N_b = 5185$, we would expect this behaviour at $\phi_c \simeq 0.96$. As previously reported by Norton et al. [91], MFTs are not able to capture the flattening of the profiles close to the surface for high bulk concentration. Thus stems from a limitation of mean field theory, which by definition does not take into account thermal fluctuations. In fact as reported by Sferraza et al.[113] there are capillary waves at the interface with different wave lengths depending on the quench depth of the spinodal diagram and, at high bulk compositions. In this case we are in the unstable region of the phase diagram and hence the spatial variation of $\phi(z)$ is too rapid to be captured

by an equilibrium MFT. Futhermore we might miss free volume effects as reported by White[126]. A possible solution is to scale the profiles with the bulk correlation length:

$$\xi = \frac{a}{6}\frac{1}{\sqrt{\phi_\infty(1-\phi_\infty)(\chi_{spin}-\chi)}} \tag{4.3.2}$$

as in Norton, where χ_{spin} is the value of the spinodal, as in eq.(1.3.23). We can see the results in fig.(4.5), for the high ϕ_∞. While the incorporation of this improves our fit, it is far from an exact match.

A possible explanation of this lies in the description of small oligomers as Gaussian chains, within the framework of the SCFT, and because of the mechanical effects, chain ends might present a different behaviour at high composition, with a change of radius of gyration from the ideal value to $R_g = a\sqrt{N_b/6}$ as reported by Rubinstein[105]. This might be because strongly asymmetric binary blends of long and very short chains, as in our case, leads to non Gaussian behaviour, with increasing number of monomers in the long chain, having a radius of gyration:

$$R_g = aN_b^{\frac{1}{2}}(\frac{N_b}{N_a^2})^{\nu-0.5} \tag{4.3.3}$$

with $\nu = 0.588$, where the value for the scaling is not $\frac{1}{2}$ anymore, but $\frac{3}{5}$.

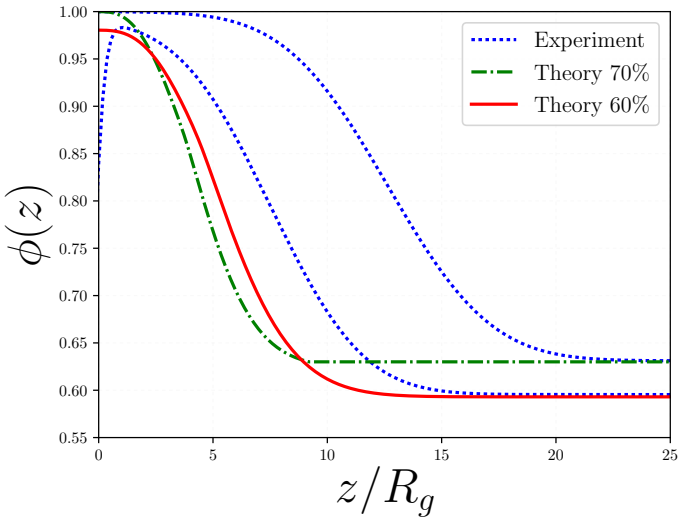

Figure 4.5: Experimental data (points) and theoretical calculation (continuous line) for the volume fraction of dSq on PB as a function of z, distance from the surface in nm. Bulk composition with $\phi_\infty = (60\%, 70\%)$ with the different scaling.

4.4 Statistical analysis

A rigorous approach to the comparison of a model with experimental data, requires a statistical test. In particular we can analyse the correlation between experimental data and theory and ultimately use the R^2 test [28].

4.4.1 R^2 test

If we consider a variable x_i, which represents our experimental data, we can define the residual sum of squares compared to another variable x_i^m, which in the case of our model is:

$$SSE = \sum (x_i - x_i^m)^2. \tag{4.4.1}$$

The R^2 measures how the correlation between different points of the model is far from the points of the experimental data [28]. If we define the total sum of squares, as the distance of the experimental data from the mean, we have:

$$SST = \sum (x_i - \overline{x_i})^2. \tag{4.4.2}$$

So as a consequence the R^2 is defined as:

$$R^2 = 1 - \frac{SSE}{SST} \tag{4.4.3}$$

When a model perfectly describes the experimental data $R^2 = 1$, which means that there is zero distance from the model and the data. On the other hand, if $R^2 \simeq 0$ the model is not good for that set of data.

We see from table 4.4 that $R^2 \sim 90\%$ for lower values of ϕ_∞, but $R^2 \simeq 0$ for the compositions where we have the wetting transition. This is a confirmation that MFT is not valid close to the critical point. Nevertheless we can still make predictions on the amount of material that blooms to the surface.

4.4.2 z^* analysis

We need to quantify how the model correctly describes the data, and the overall material that has migrated to the surface z^* is helpful. We have seen in Chapter 3 that we calculate the overall surface excess material as:

$$z^* = \int (\phi(z) - \phi_\infty) dz. \tag{4.4.4}$$

Thus having just experimental data and not analytical solutions we calculated the integral numerically with the trapezoidal rule [99]. We can see the results in table(4.4). We notice similar trends for the theory and experimental values, in particular as we see in fig.(4.6) a discontinuity at wetting, which is the indication of a wetting transition, as previously reported in experiments [49, 13] and theory[48]. There is a discrepancy in the values of z^*, probably because there is roughness at the interface and the substrate in real samples, not considered here.

Table 4.4: Different values of overall material z^* for the experimental profiles and the corresponding SCFT profiles. R^2 results showing how good the approximation with the experimental data is.

	4%	6%	8%	10%	14%	30%	40%	60%	70%
Theory	0.144	0.385	0.394	0.778	1.09	1.30	1.34	3.06	2.79
Experiments	0.127	1.01	1.48	4.09	5.78	11.9	12.1	22.9	28.5
R^2	0.996	0.933	0.956	0.916	0.906	0.953	0.982	0.0170	0.0257

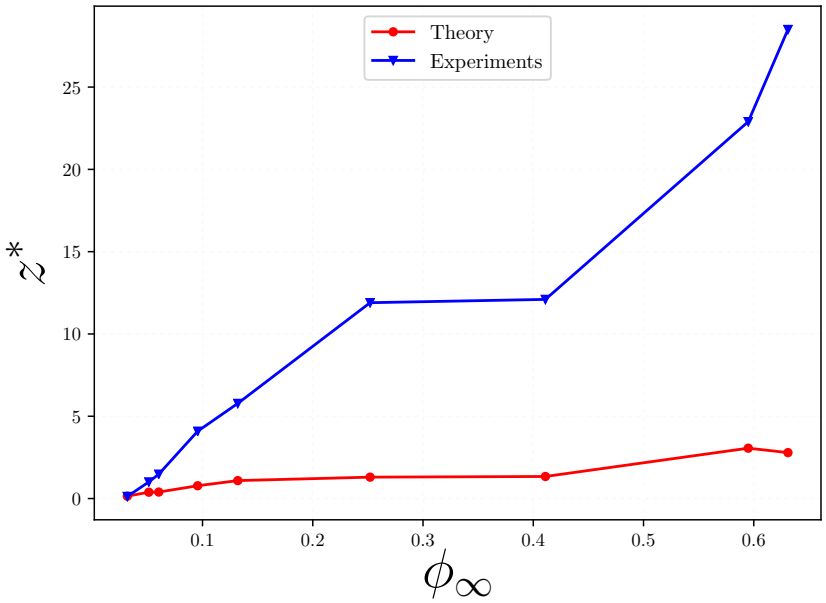

Figure 4.6: z^* as function of the bulk composition ϕ_∞ for the SCFT profiles and the experimental profiles of dSq/PB. We notice a discontinuity at composition 60%, indicating a wetting transition.

4.5 Culgi simulations

CULGI (Chemistry Unified Language Interface)[122] is a scientific program for simulations. It has been successfully used over the years for modelling different systems[120, 58]. Culgi was developed for applications and simulations of soft matter systems, molecules and in general for simulating the behaviour of chemical systems. It is a particularly useful tool for different perspectives on segregation in polymer mixtures, because it gives us a $3D$ description of a compressible system at equilibrium and with a pseudo-dynamics. The software can simulate flexible polymers by modelling them as Gaussian chains, i.e. ideal chains, as outlined in Chapter 1, but with an extension of FH theory to local equilibrium and non homogeneous phases, as we shall see later. While this is an approximation and can be a limitation for a correct description of wetting systems, we use CULGI to obtain segregation profiles for polymer mixtures.

CULGI calculates the spatial conformations of molecules, lumped together, resulting in relative density fields, and the change in the relative density field is predicted via a solution of a diffusion equation. The thermal fluctuations are modelled by adding noise to the mean field chemical potential, assuming local equilibrium. The physical conditions for the validity of the method, as reported in the CULGI manual [122], are summarised as:

- The concentration of the polymer should be over the overlap concentration;
- The polymer must be flexible;
- The coil must be large enough, to avoid inter penetrations between chains and coil volume elements;

The chemical potential field is defined as a functional derivative of the free energy as:

$$\mu_I(\mathbf{r}) = \frac{\delta F}{\delta \rho(\mathbf{r})} \tag{4.5.1}$$

in a similar manner to the SCFT, with the important difference that here we have a functional derivative.

The chemical potential can be split as:

$$\mu_I(\mathbf{r}) = -S_I(\mathbf{r}) + \mu_m(\mathbf{r}) \tag{4.5.2}$$

where S_I is the entropy field, associated with the entropy of mixing, and μ_m is the mean field chemical potential given by external contributions. In particular it has three external contributions:

$$\mu_m = \mu_P + \mu_C + \mu_E \tag{4.5.3}$$

where μ_P accounts for the pair interaction, i.e. the Flory-Huggins interaction, μ_C for the compressibility interaction and μ_E for the electrostatic interaction.

In particular we define the pair interactions between beads as [122]

$$\mu_P = \sum_J \int_V \epsilon_J(\mathbf{r} - \mathbf{r}^{'})\rho_J d\mathbf{r}^{'} \tag{4.5.4}$$

where $\epsilon_J(\mathbf{r} - \mathbf{r}^{'})$ is a Gaussian function as in eq.(1.1.4) multiplied by ϵ_J^0, the pair interaction parameter. In CULGI one can input a dimensionless χ, as in FH theory as:

$$\chi_J = \frac{\epsilon_J^0}{k_b T \nu} \tag{4.5.5}$$

that coincides with the standard FH parameter, if the density is equal to unity in eq.(4.5.4). It is also possible to use a local interaction parameter, where we do not consider the space dependence in eq.(4.5.4).

CULGI makes use of a free energy which is a generalisation of FH. In particular the energy is defined as:

$$F_T = F_{ideal} + F_{non-ideal} \tag{4.5.6}$$

where ideal and non-ideal contributions are given by:

$$\beta F_{ideal} = -\sum_i n_i(1 + \log \tfrac{\phi_i}{n_i}) - \int_V \sum_k \tfrac{\rho_k}{\nu} S_k \tag{4.5.7}$$

$$\beta F_{non-ideal} = \tfrac{1}{2} \int_V d\mathbf{r}^{'} \sum_{j,k} \tfrac{\rho_j}{\nu} \chi_{j,k}^{local} \rho_k + \tfrac{1}{2} \int_V d\mathbf{r}^{'} \sum_{j,k} \tfrac{\rho_j}{\nu} \chi_{j,k} \Omega[\rho_k] \tag{4.5.8}$$

where S_k is the entropic contribution as in eq.(4.5.2) and $\Omega[\rho_k]$ is an integral with a Gaussian kernel as in eq.(4.5.4).

As previously pointed out the evolution of this system is predicted by a diffusion equation, adapted to the different kind of solvers. So as opposed to a FH approach, we can include an electrostatic interaction (not considered here) and compressibility effects. Running the simulation with conditions set by FH, we obtain concentrations profiles shown in fig.(4.7). We choose directly χ while N_a, N_b are chosen inverting the relation between the molecular weight and the radius of gyration for an ideal chain, as $N_i = \frac{6}{a^2} R_g^2$ for Gaussian chains defined in a box. We use dynamic density functional theory and equilibrium SCFT to obtain our results, as a complementary description to the SCFT results.

Density dynamics

The basic equation for the density dynamics is derived from the collective Rouse equation[122]

$$\frac{\partial \rho_I}{\partial t} = D_I \nabla^2 (\rho_I - F_T) \tag{4.5.9}$$

where F_T is the density obtained from the free energy as in eq.(4.5.6), calculated with the mean field and it may also be zero locally. We can derive the equation following the Rouse dynamic equation[84], calculating correlation functions with the De Gennes' Random Phase Approximation. The DDFT method allows us to

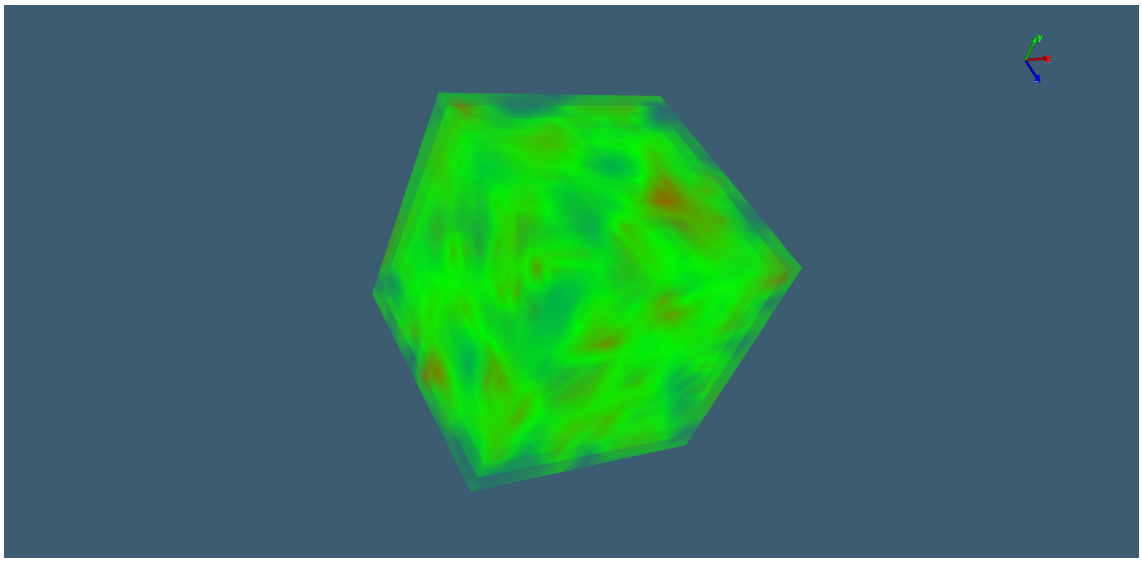

Figure 4.7: Density Dynamics calculation for $\chi = 0.22$, $N_b/N_a = 10$, $\phi_\infty = 0.05$. Green lines refer to the polymer matrix and red ones to the migrating polymers.

simulate the system in a $3D$ box, analysing the behaviour of the molecules along different spatial directions. We notice the formation of the layer is not homogeneous and there are islands of oligomers along the surface, as reported in recent publications with AFM measurements[108]. We notice that the 3D simulation allows to visualise effects of lateral migration (red points) not present in the 1D model. 3D solutions are obtained with Crank-Nicolson [122].

Equilibrium: SCFT

The self consistent field theory in Culgi is an equilibrium version of eq.(4.5.9). In particular it is possible to use the equilibrium condition:

$$\mu_I = 0 \tag{4.5.10}$$

Hence $\mu = S_I$, that defines a local equilibrium, is suitable for describing a fully relaxed monomeric configuration. In the case of strong interacting polymers or far from equilibrium it is possible to use the Picard method, with the Picard equation[31]:

$$\frac{\partial \rho_I}{\partial t} = -D_I \mu_I \tag{4.5.11}$$

that is an effective method, since it avoids the computation of a Laplacian operator. Picard's model is a fast self-consistent field solver for equilibrium, where mass can be transferred non locally. We see the results in fig.(4.8) and fig.(4.9), respectively for

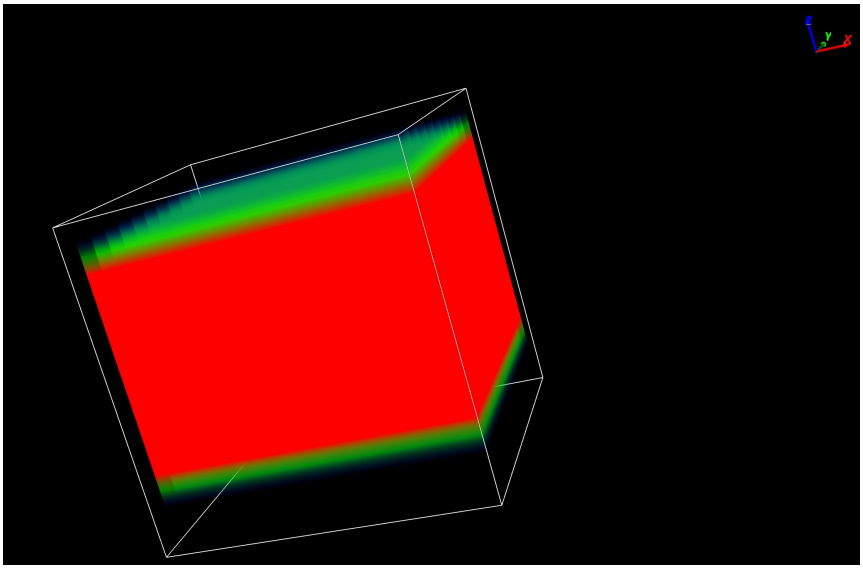

Figure 4.8: Polymer matrix(green) at equilibrium for $\chi = 0.22$, $N_b/N_a = 10$, $\phi_\infty = 0.05$.

the segregating species at the surface and substrate (red), and the polymer matrix (green). We have chosen χ to have a value which is $\chi > \chi_c$, i.e. point on the phase diagram where there is phase separation. We notice a high segregation at interfaces with air and substrate , not present in SCFT, which confirms the results

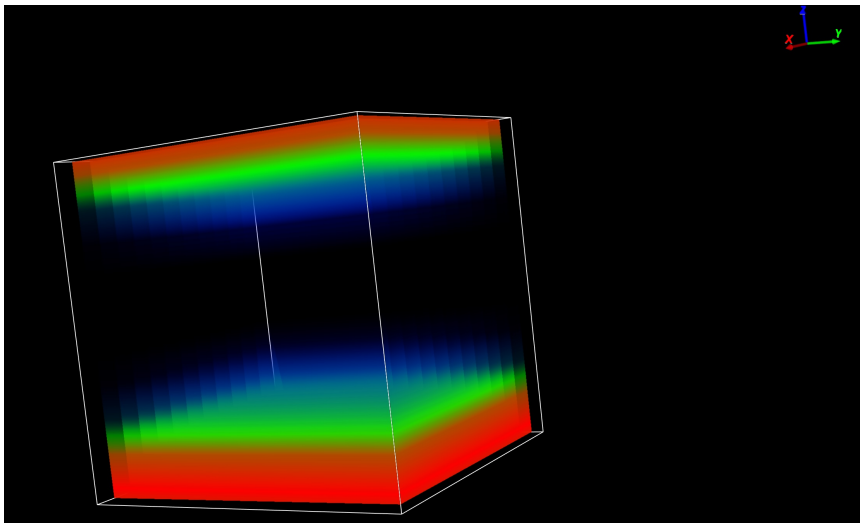

Figure 4.9: Oligomers segregation at air interface and with the substrate of the sammple for $\chi = 0.22$, $N_b/N_a = 10$, $\phi_\infty = 0.05$. The equivalent 1D profile would be obtained cutting the $z-x$ plane and reporting the number of red points as a density of states.

of the $1D$ SCFT in fig(4.4). Furthermore we also notice a diffusive interface with a compenetration of surfaces, between the wetting interfaces and the matrix, which is more realistic than a sharp one, a result non present in the 1D SCFT results. There is an equivalent schematic in fig.(4.10) for a 1D profile for oligomers segregating at surface and substrate and the polymer matrix in the middle.

Table 4.5: Analogies and differences between SCFT theory and CULGI simulations.

Properties	Free energy	Solution method	Dimension	Lateral migration
SCFT	FH/FHE	Lattice method	1D	no
CULGI	FH enhanced	Rouse/Crank-Nicolson	3D	yes

Conclusions: In this chapter we have seen some statistical and computational tools for comparing the MFT theories with the experimental data. Varying the parameters, we get a good agreement between theory and experimental profiles for low bulk composition. For higher ϕ_∞ the agreement between theory and experiment is not good, probably due to non Gaussian effects. It will be interesting to consider going beyond a mean field description in an attempt to match theoretical results with

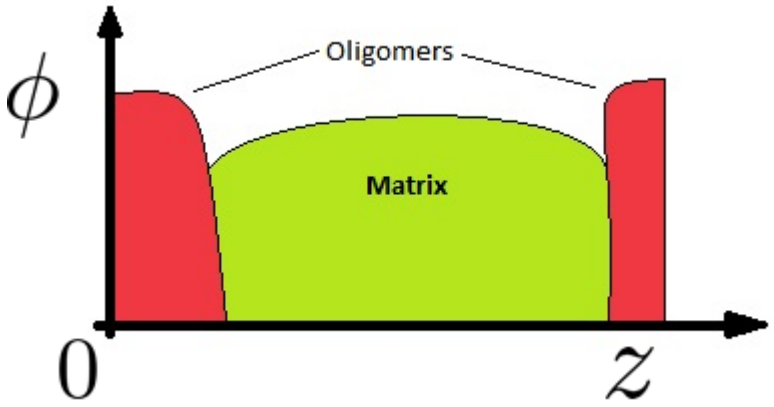

Figure 4.10: Equivalent SCFT 1D profiles to CULGI results, with polymer matrix(green) and the segregation for oligomers (red) at surface and substrate.

experimental data. We have seen that we can obtain some missing effects , such as lateral migration and substrate segregation, using the software CULGI, which allows us to obtain $3D$ profiles and an equilibration dynamics. It is not really suitable for a direct comparison with experiments, especially because we did not have access to the source code, but just to the GUI and in this way it was harder to control parameters. We have also quantified MFT limitations with the R^2 test. Nevertheless it can give us insights on the properties of the system. In the next chapter we will present the Locally Correlated Lattice (LCL) theory developed to describe oligomers in polymer matrices, combined with MFT theory for describing the properties of the polymer mixtures with a richer thermodynamics, closer to the real behaviour.

Chapter 5

Locally Correlated Lattice theory to model Surface segregation

We present the Locally Correlated Lattice (LCL) theory as derived by White et al.[125] and their description of a free energy to understand thermodynamics behaviour of some bulk phases of small molecules in polymer mixtures [81]. We use the LCL functional form of free energy in combination with mean field models of surface migration in polymer mixtures to compute equilibrium migrant concentration profiles. In particular we successful combine the LCL functional with SCFT that can be used for real polymer mixtures.

5.1 Locally correlated lattice theory

The Locally Correlated Lattice theory, LCL, has been introduced recently by White et al.[125] based on a previous work by Gugghenheim [54] for correctly describing the behaviour of real polymer mixtures incorporating effects not captured within FH theory. FH theory suffers from some limitations, such as the incompressibility approximation and it cannot really describe the thermodynamics of all systems including those having Upper Critical Solution Temperature (UCST) and Lower Critical Solution Temperature (LCST). On the contrary LCL can describe UCST

and LCST systems, interactions between polymers, account for excluded volume effects and can be applied to real polymers.

Gugghenheim considered the statistics of N_i molecules occupying r_i sites on a lattice for a chain molecule (polymer) and a solvent; the number of neighbouring sites of a molecule i occupying r_i sites with coordination z is smaller and given by $q_i z = r_i z - 2z + 2$, excluding the ring polymers, studied just more recently[71]. The frequency of occupation is given by $\xi_i = n_i q_i/(n_a q_a + n_b q_b + n_h)$. The interactions among different species have a Boltzmann form given by:

$$\exp \frac{\mu_a - \mu_{a,0}}{k_b T} = \frac{\lambda_a}{\lambda_{a,0}} = \frac{P_a}{P_{a,0}} = N_a \frac{(N_a + N_b/r)^{\frac{r(q-1)}{r-q}}}{(N_a + N_b/q)^{\frac{q(r-1)}{r-q}}} \tag{5.1.1}$$

$$\exp \frac{\mu_b - \mu_{b,0}}{k_b T} = \frac{\lambda_b}{\lambda_{b,0}} = \frac{P_b}{P_{b,0}} = N_b \frac{(rN_a + N_b)^{\frac{(q-1)}{r-q}}}{(qN_a + N_b)^{\frac{(r-1)}{r-q}}} \tag{5.1.2}$$

where (a, b) refers to the polymer species and the index 0 is for the activity λ (fugacity for partial pressure) or pressure p, before mixing. The activity is proportional to the partition function Z and therefore, taking the logarithm of Z, we have the free energy of the system.

Gugghenheim's model did not consider compressible binary mixtures of polymers and the major improvement made by White and Lipatov introduces holes and an explicit volume dependence in the theory, arriving at a functional form of the Helmoltz free energy that can easily be used to understand segregation behaviour in real polymers[128, 59].

Following Lipatov the LCL free energy for a binary mixture is:

$$\begin{aligned} \frac{F_{LCL}}{k_b T} &= n_a \log \phi_a + n_b \log \phi_b + n_h \log \phi_h \\ &+ \frac{n_a q_a z}{2} \log \left(\frac{\xi_a}{\phi_a} \right) + \frac{n_b q_b z}{2} \log \left(\frac{\xi_b}{\phi_b} \right) + \frac{n_h z}{2} \log \left(\frac{\xi_h}{\phi_h} \right) \\ &- \frac{n_a q_a z}{2} \log \left[\xi_a \exp \frac{-\epsilon_{aa}}{k_b T} + \xi_b \exp \frac{-\epsilon_{ab}}{k_b T} + \xi_h \right] \\ &- \frac{n_b q_b z}{2} \log \left[\xi_a \exp \frac{-\epsilon_{ab}}{k_b T} + \xi_b \exp \frac{-\epsilon_{bb}}{k_b T} + \xi_h \right] \end{aligned} \tag{5.1.3}$$

where $n_h = (V/\nu) - n_a N_a - n_b N_b$, $\phi_i = n_i N_i \nu / V$, $\xi_i = n_i q_i / (n_a q_a + n_b q_b + n_h)$ and $q_i z = N_a z - 2N_i + 2$ with $i = a, b, h$, but $q_h = n_h = 1$. The free energy is a function of the independent variables (n_a, n_b, V, T), different from the variables we have used in the previous chapters, in particular Flory Huggins theory. We notice immediately the absence of a mean field (χ), because the interaction between chains has been split in three different contributions, ϵ_{aa}, ϵ_{bb} and ϵ_{ab}, defined by $\epsilon_{ab} = g\sqrt{\epsilon_{aa}\epsilon_{bb}}$ as a geometric mean of the self interactions. This approach allows one to derive the thermodynamics properties of mixtures by fitting Pressure, Volume and Temperature (PVT) data diagrams for single components (as in the next section), with the exception of g which has different values for the UCST and LCST systems. It has to be fitted for the mixtures in question [128]. The LCL theory introduces a model which has the microscopic ingredients seen in the experimental systems, such as the interaction between single polymers, degree of polymerisation, coordination number of monomers in the lattice, microscopic volume. At the same time it allows to include macroscopic variables, such as pressure, volume and temperature which can be more easily measured to obtain the microscopic behaviour of real polymers. In order to study migration, it is convenient to rewrite the free energy as a main function of the volume fraction of the polymers a and b, thus the volume fraction for holes ϕ_h and n_h are:

$$\phi_h = n_h = V/\nu(1 - \phi_a - \phi_b) \tag{5.1.4}$$

Substituting eq.(5.1.4) in eq.(5.1.3) the Helmholtz free energy is given by:

$$\begin{aligned}\frac{F_{LCL}}{k_bT} =&\frac{V}{\nu}\frac{\phi_a}{N_a}\log\phi_a + \frac{\phi_b}{N_b}\log\phi_b] + (\frac{V}{\nu}(1-\phi_a-\phi_b))\log(\frac{V}{\nu}(1-\phi_a-\phi_b))+\\ &+\frac{\phi_a q_a z}{2N_a}\log(\frac{q_a}{\frac{V}{\nu}(1-\phi_a-\phi_b)}) + \frac{\phi_b q_b z}{2N_b}\log(\frac{q_b}{\frac{V}{\nu}(1-\phi_a-\phi_b)})-\\ &-\frac{\frac{V}{\nu}(1-\phi_a-\phi_b)z\log\frac{V}{\nu}(1-\phi_a-\phi_b)}{(2(\frac{V}{\nu}(1-\phi_a-\phi_b))} - \phi_a q_a z(\frac{q_a\phi_a}{(N_a(\frac{V}{\nu}(1-\phi_a-\phi_b))})e^{-\epsilon_{aa}/k_bT}\\ &+(\frac{1}{2N_a})\frac{q_b\phi_b}{(N_b(\frac{V}{\nu}(1-\phi_a-\phi_b))e^{-\epsilon_{ab}/T}+\frac{V}{\nu})}\\ &-\phi_b q_b z(\frac{q_b\phi_b}{(N_a(\frac{V}{\nu}(1-\phi_a-\phi_b))}e^{-\epsilon_{ab}/k_bT}+\\ &+(\frac{1}{2N_b})\frac{q_b\phi_b}{(N_b(\frac{V}{\nu}(1-\phi_a-\phi_b))e^{-\epsilon_{bb}/T}+\frac{V}{\nu})}.\end{aligned} \tag{5.1.5}$$

From eq.(5.1.3) we can derive some of the fundamental thermodynamics properties of the system, a described in the next section.

5.1.1 Bulk phase diagrams

We can compute all the relevant thermodynamic quantities from eq.(5.1.3), such as Gibbs free energy, pressure, chemical potential and isothermal compressibility. In particular the latter allows us to compute the phase diagram of the system. In particular following[127] for the a polymer, we obtain the chemical potential as $\mu_a = \frac{\partial F}{\partial \phi_a}$:

$$\begin{aligned}\frac{\mu_a}{k_bT} =&\log\phi_a - N_a\log(V/\nu(1-\phi_a-\phi_b)) + 1 - N_a\\ &+\frac{q_a z}{2}\log\left(\frac{q_a}{N_a(V/\nu(1-\phi_a-\phi_b))}\right) + \frac{N_a z}{2}\log(V/\nu(1-\phi_a-\phi_b)) + \frac{z}{2}(N_a-q_a)\\ &-\frac{q_a z}{2}\log\left(\frac{q_a\phi_a}{N_a(V/\nu(1-\phi_a-\phi_b))}e^{-\epsilon_{aa}/k_bT} + \frac{q_b\phi_b}{N_b(V/\nu(1-\phi_a-\phi_b))}e^{-\epsilon_{ab}/k_bT} + \frac{V}{\nu}\right)\\ &-\frac{z\xi_a}{2}\left[N_a - q_a + \frac{q_a e^{-\frac{\epsilon_{aa}}{k_bT}} - N_a}{\xi_a e^{-\frac{\epsilon_{aa}}{k_bT}} + \xi_b e^{-\frac{\epsilon_{ab}}{k_bT}} + \frac{V}{\nu}}\right]\\ &-\frac{z\xi_b}{2}\left[N_a - q_a + \frac{q_a e^{-\frac{\epsilon_{ab}}{k_bT}} - N_a}{\xi_a e^{-\frac{\epsilon_{ab}}{k_bT}} + \xi_b e^{-\frac{\epsilon_{bb}}{k_bT}} + \frac{V}{\nu}}\right]\end{aligned} \tag{5.1.6}$$

where ξ_i with $i = a, b$ as in Section 1 and we obtain the chemical potential for the b polymer *mutatis mutandis* (the a index replaced with the b one). The chemical potential for PS/PB is given in fig.(5.1) using the parameter values given in [128], where we notice that it is monotonically decreasing function of ϕ_a and ϕ_b.

As mentioned in the context of Flory Huggins theory we calculate the bulk phase diagram from the chemical potential. Equating the chemical potential at two different phases a and b, for both species, we obtain the binodal line. This expression is equivalent to:

$$\chi_{bin} \Rightarrow \mu_a - \mu_b = 0. \tag{5.1.7}$$

We can see the binodal curve in fig.(5.2) for PS/PB and fig.(5.3) for PS/PVME, which are UCST and LCST systems respectively. The binodal curve separates the region of the phase diagram where a single phase is stable, as opposed to being metastable.

We calculate the spinodal line of the phase diagram taking the derivatives of the chemical potential with respect to the volume fraction for the different phases as:

$$\begin{aligned} \chi_{spin} =& (\frac{\partial(\mu_a - \mu_b)}{\partial \phi_i})_{T,P} \\ =& (\frac{\partial(\mu_a - \mu_b)}{\partial \phi_i})_{T,V} - (\frac{\partial(\mu_a - \mu_b)}{\partial V})_{T,\phi_i} \frac{\frac{\partial P}{\partial \phi_i}}{\frac{\partial P}{\partial V}} \end{aligned} \tag{5.1.8}$$

where for an incompressible system the second term is zero and we have an FH like expression. We see two different diagrams in fig.(5.4) and fig.(5.5). for different UCST and LCST behaviours for experimental systems[109]

5.2 LCL and surface segregation

The knowledge of the chemical potential is crucial for the SCFT (discussed in chapter 3) to obtain segregation profiles. Using eq.(5.1.3) and eq.(5.1.6) we can incorporate the expression of chemical potential and free energy obtained with LCL theory into the migration models SBMFT and SCFT. In this way we can study the wetting properties of more complex systems[27], using chemical potentials for real

experimental systems.

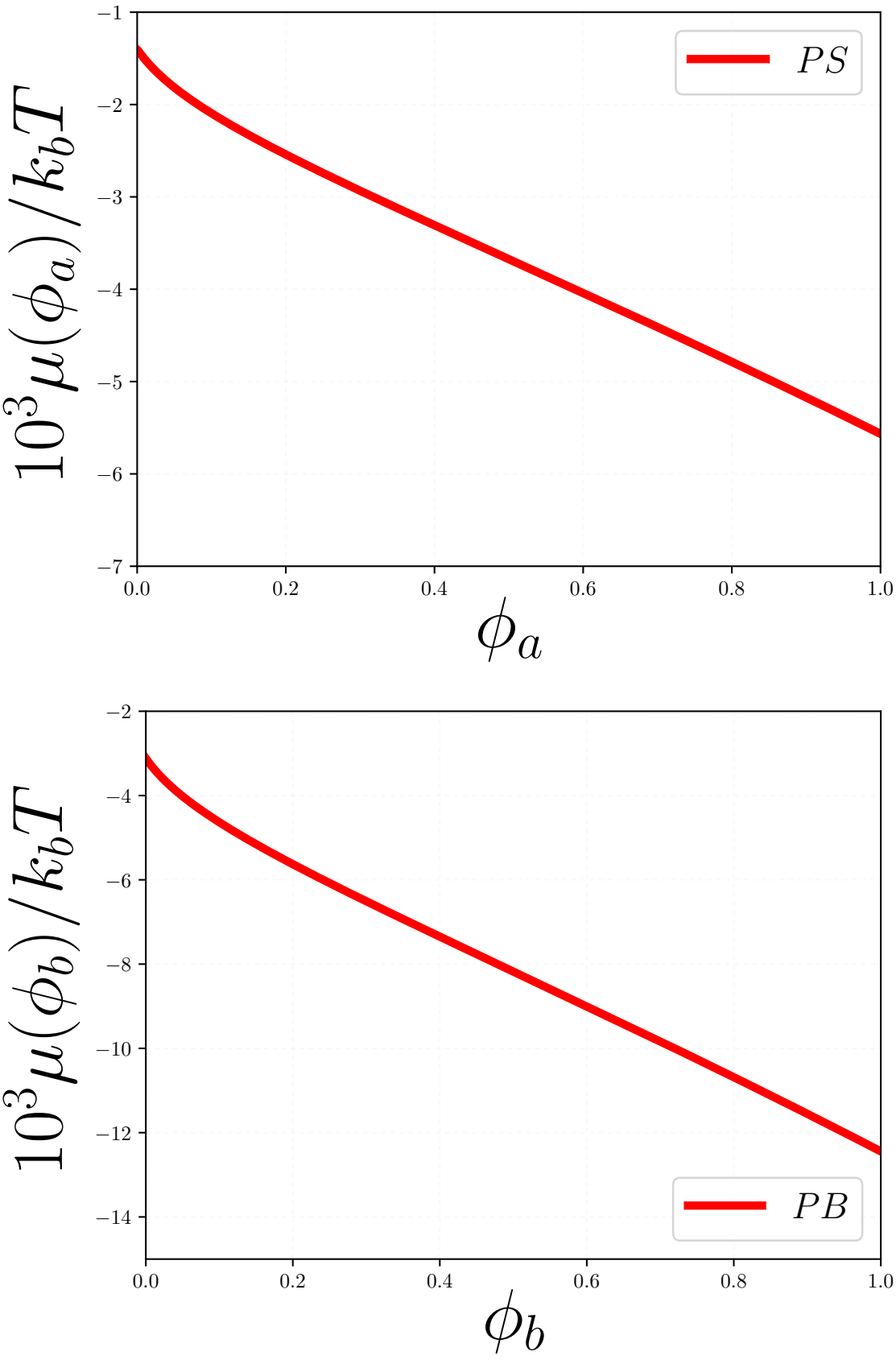

Figure 5.1: Chemical potential for a mixture of Polistyrene in Polibutadiene as function of ϕ_a and ϕ_b, for $\phi_{b/a}$ fixed at 0.01, and with values of the interaction constants taken from White *et al.* [128].

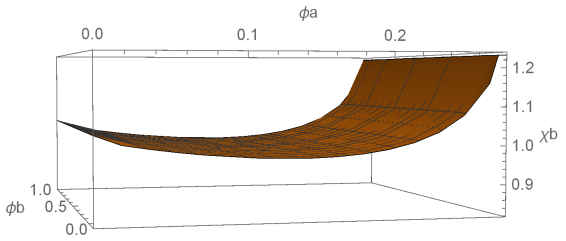

Figure 5.2: 3D representation of the binodal surface for PS/PB as function of ϕ_a and ϕ_b. We notice phase separation just for $\phi_a < 0.3$.

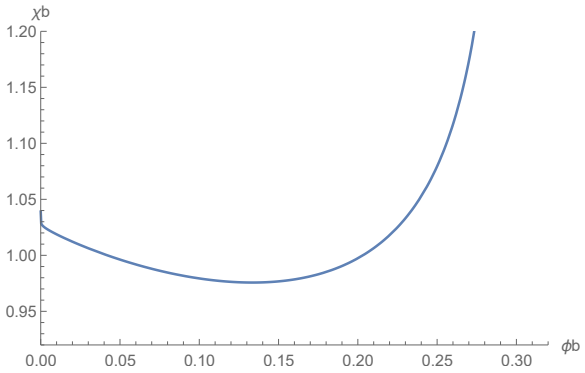

Figure 5.3: Binodal diagram for PS/PB with $\phi_b = 0.4$. We notice that the system is UCST.

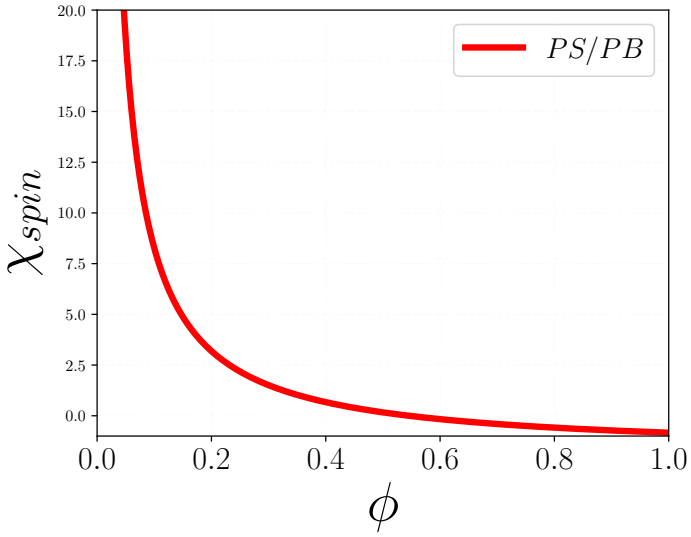

Figure 5.4: Spinodal diagram as function of the volume fraction at $T = 360K$ for a binary mixture of PS/PB of the UCST type. Data from Lipson et al.[81].

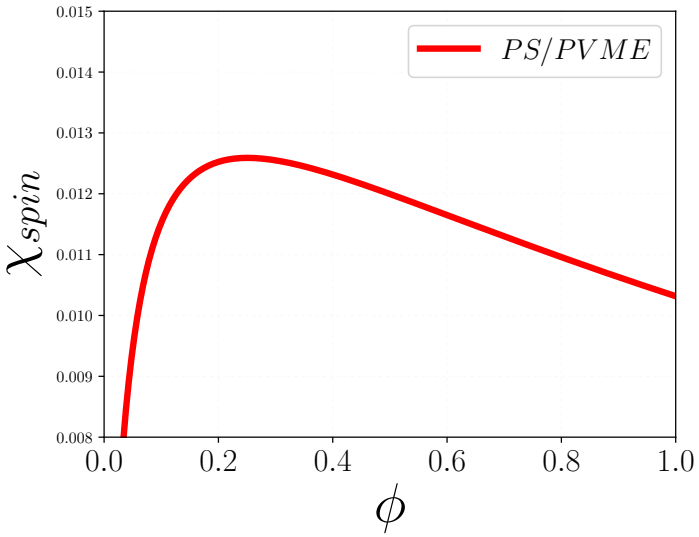

Figure 5.5: Spinodal diagram as function of the volume fraction at $T = 394K$ for a binary mixture of PS/PVME of the LCST type. Data from Lipson et al.[81].

5.2.1 SB theory

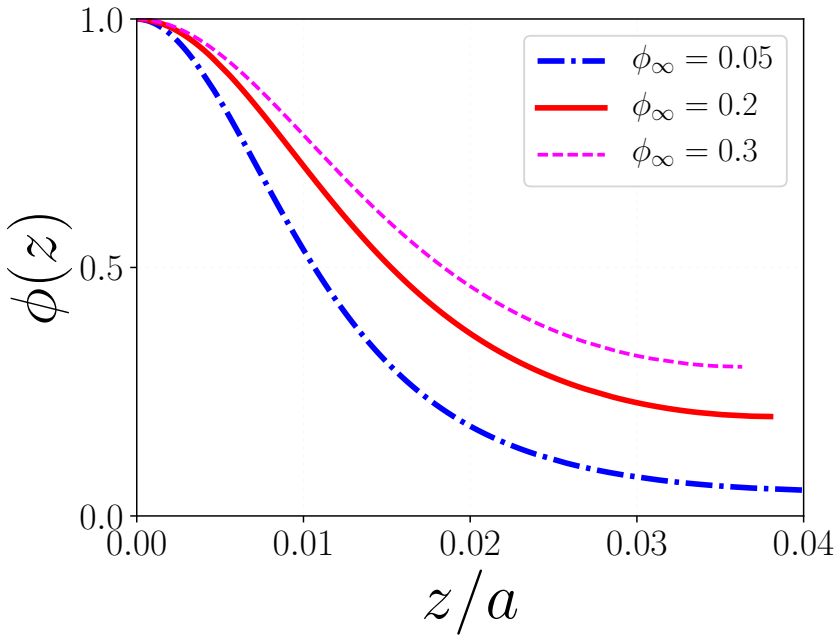

Figure 5.6: Different profiles for the PS/PB systems for different values of ϕ_∞ calculated with experimental data from White et al. [128].

We thus use eq.(5.1.3) in place of eq.(2.1.3) to combine LCL free energy functional with SBMFT. In particular, if we use the LCL theory we can obtain migrant concentration profiles as shown in fig.(5.6) i.e. the volume fraction as function of depth z/a for a fixed polymer matrix concentration. In particular we combine eq.(5.1.3) into the eq.(2.1.2), fixing one of the volume fractions ϕ_a or ϕ_b and calculating the distance from the surface z as function of the other volume fraction ϕ_b or ϕ_a, as in eq.(2.1.3). With a reverse engineering process we obtain $\phi_{a/b}(z)$ and we use the experimental parameters as in White et al. [128] to compute the final profile in fig.(5.6). We choose ϕ_1 as graphical solution of a Cahn construction as in Chapter 2, with eq.(5.3.4) being the bulk energy.

Considering compatibility for the system PS/PB as expected we observe very low segregation, as shown in fig.(5.6) as expected for both low and high values of the bulk concentration.

5.2.2 SCFT theory

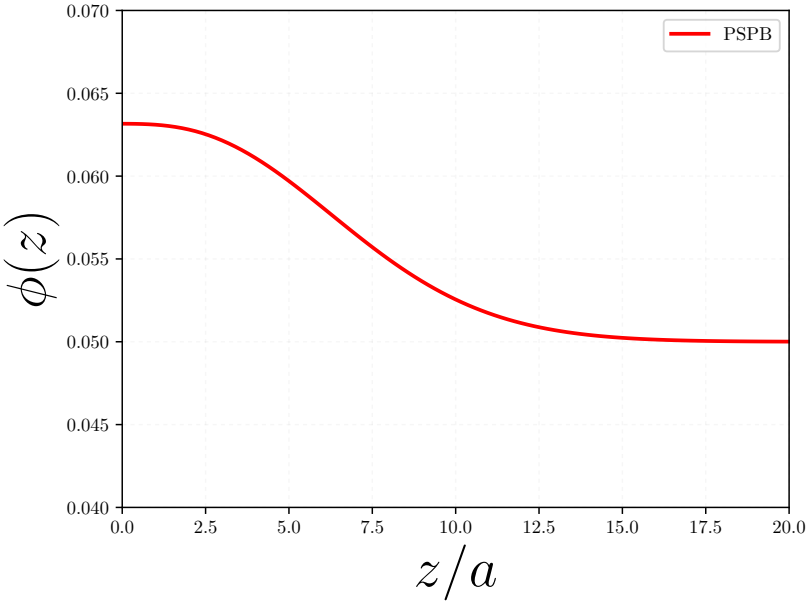

Figure 5.7: Profiles (SCFT) for PS/PB system for different values of F_s.

The SCFT can be combined with the LCL, in a manner similar to SBMFT. In particular we have the advantage of being able to calculate chemical potentials directly with an explicit dependence of the volume fraction for real polymers. Following the outline of SCFT in chapter 2, we use eq.(5.1.3) as the free energy of the system and eq.(5.1.6) as the chemical potential, respectively as $\mu(\phi_a)$ for the A polymer and $\mu(\phi_b)$ for the B polymer. Hence we use two distributions for describing the LCL-SCFT, q_a and q_b for the A and B species and two mean fields w_a and w_b, which we calculate from the chemical potentials as in eq.(2.1.16). We start the self consistent calculation solving eq.(2.1.15) twice for each distribution and calculating the two volume fractions using eq.(2.1.18) with (μ_a, w_a) and (μ_b, w_b). As a consequence we update the values of the chemical potentials and the mean fields with the new volume fractions. Despite the SCFT FH based, with the LCL SCFT becomes crucial to maintain incompressibility in the system, because this condition becomes linked to the precence of holes in the lattice, so we include ΔW as in eq.(2.1.16). We eventually obtain the final profiles $\phi_a(z)$ after ground state dominance in the self

consistent calculation.

The results are shown in fig.(5.7), where again there is a very small segregation at the free interface for PS/PB. The physical scenario is more realistic, since the presence of holes allows for relaxation of constituent molecules to their equilibrium state.

5.3 Compressibility

We can calculate the pressure of the system once we know the free energy, as:

$$P = -\left(\frac{\partial F_{LCL}}{\partial V}\right)_T \tag{5.3.1}$$

and so for a single component, keeping the V dependence and with a finite molecular volume, we obtain:

$$\begin{aligned}\frac{P}{k_bT} = -\frac{1}{\nu}\log\left(\frac{V}{\nu}(1-\phi)\right) + \frac{z}{2\nu}\log\left(1+\frac{\phi q}{N}-\phi\right) - \\ -\frac{z}{2\nu}\left(\frac{\phi q}{1-\phi+\frac{\phi q}{N}}\right)\left[\frac{(\frac{\phi q}{N})(e^{\epsilon_{aa}/k_bT}-1)-1-\phi}{(\frac{\phi q}{N})e^{\epsilon_{aa}/k_bT}+1-\phi}\right]\end{aligned} \tag{5.3.2}$$

where we made the same simplifications as in eq.(5.1.4). We can see an example in fig.(5.8) where we have different pressures as function of volume (PV diagram) and temperature (PT diagram).

This expression is really helpful for testing some of the assumptions we made in Chapter 3, especially the incompressibility. In the framework of the LCL we can calculate the isothermal compressibility of the system as:

$$K = -\frac{1}{V}\left(\frac{\partial P}{\partial V}\right)^{-1} \tag{5.3.3}$$

where after some algebra we obtain, for PS/PB:

$$K(T,V) = \frac{1}{k_bTV\left(-\frac{0.340337\left(e^{235.897/T}-1\right)}{V^2\left(0.336817e^{235.897/k_bT}+\frac{\nu}{V}\right)^2}-\frac{V}{0.875}\right)}. \tag{5.3.4}$$

We can see the bulk modulus in fig.(5.9) as a function of T.

Conclusions: In this chapter we have seen that the LCL theory, which is a useful theory for a correct thermodynamic description of small molecules in polymer mixtures can be applied to study segregation phenomena in polymer mixtures. We presented some of the results of SB-LCL and SCFT-LCL, going beyond the limitations of FH theory. Finally we calculated some PVT profiles useful for deducing polymer properties from PVT diagrams and bulk modulus for applications to gels.

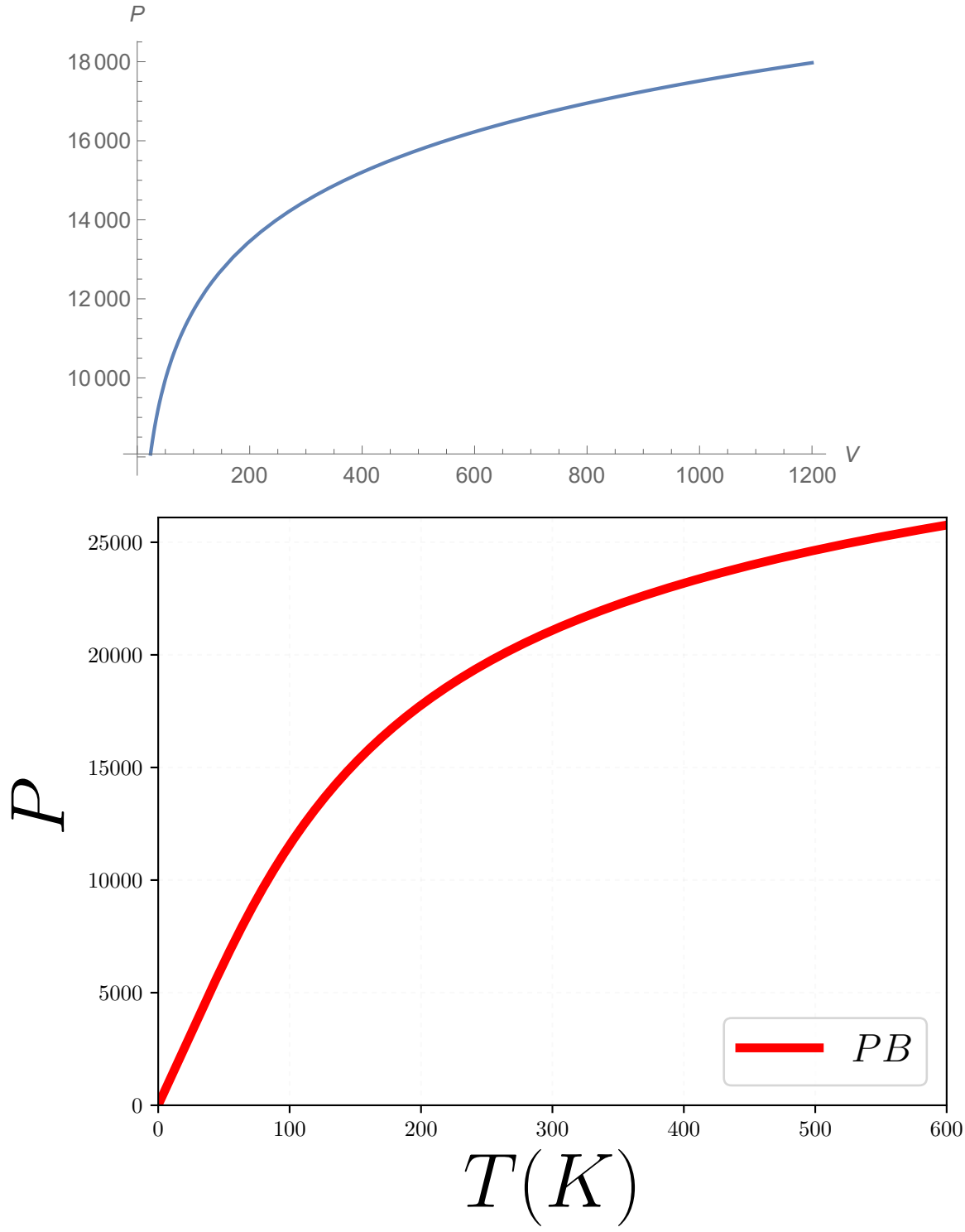

Figure 5.8: PV on the top with $T = 360K$. PT on the bottom with $V = 100\text{Å}^3$

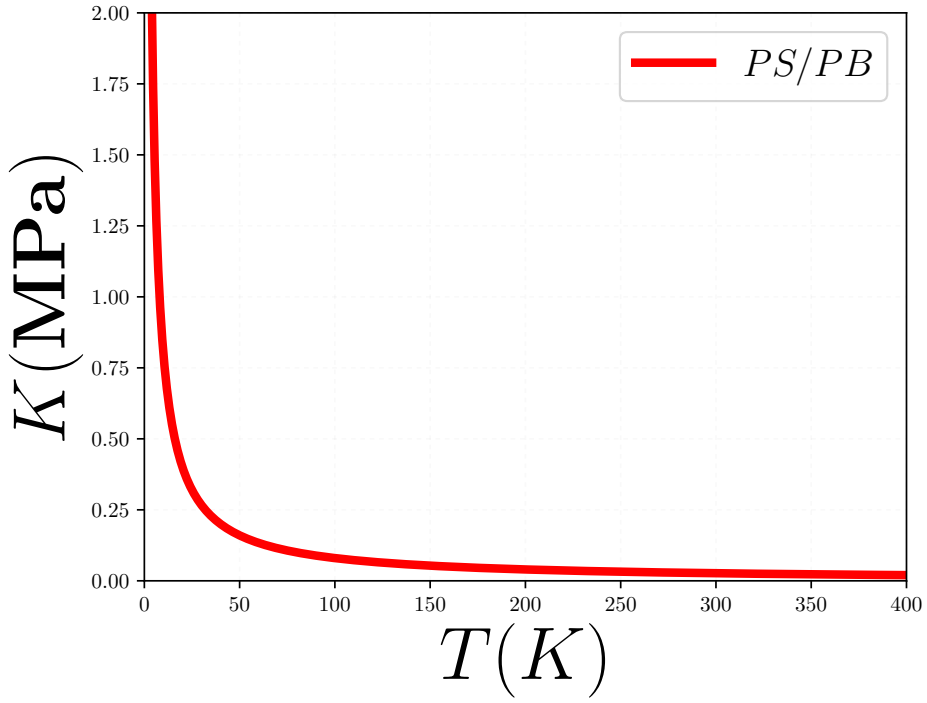

Figure 5.9: Bulk modulus as a function of the volume fraction and the temperature, from eq.(5.3.4).

Chapter 6

Conclusions

In this thesis we have analysed the phenomenon of migration of small molecules to an interface open to atmosphere in polymer mixtures. In particular, in the first chapter we presented the basic theory of polymers as random Gaussian chains. Then we saw how to analyse the bulk thermodynamic behaviour of such mixtures, by means of Flory Huggins theory (FH), which tells us about the compatibility of different polymers as a balance of entropy and enthalpy. We also discuss Cahn's theory of wetting.

We reviewed a method to combine these models to quantitatively describe surface migration in polymer mixtures. We outlined a method for going beyond the phenomenological description with the help of a Self Consistent Field Theory (SCFT). Both theories are suitable for describing migration.

The research of methodologies for controlling migration has brought us to the description of surface segregation in gels. In Chapter 3 we saw how elasticity of a gel network can control migration and the thermodynamics of bulk and surface. That is a fascinating problem, which opens new perspectives, as we shall elaborate upon below.

We have also compared the FH theory with experimental data for a validation of SCFT. The application of Design of Experiments (DoE) allowed us to make the comparison and with statistical tests we quantified the validity of a mean field theory,

such as SCFT, close to the wetting transition.

Finally in order to go beyond the limitation of FH theory, we implemented a combination of the Locally Correlated Lattice (LCL) theory with the Mean Field Theory (MFT) for migration, enabling us to predict the segregation behaviour of some polymer mixtures having UCST and LCST phase diagrams. Hence we would like to compare our theoretical predictions to experiments, especially the LCL SCFT profiles. It would be important to measure the experimental parameters of real polymers via PVT diagrams and then the corresponding segregation profiles. We hope that our theoretical models validated by experiments will aid to the development of a predictive toolkit to control small migration in industrial formulation. Our work [74] on controlling segregation of small molecules in polymer mixtures by tuning bulk rigidity of the sample might form the basis of future experimental studies by combining the LCL theory with the gel theory for migration. Further we can parametrise a gel to obtain its bulk modulus as a function of molecular scale parameters. That would allow to test the theory directly on experimental systems relevant for technological applications. In that case the elastic contribution to the free energy should allow volume changes, similar to a linear spring "elastic energy. Furthermore we might want to consider gel swelling with the osmotic pressure proportional to the volume fraction. The swelling of a gel and a polymer mixture is particularly relevant for all those applications involving adsorbing polymers and its implication on migration might be easily tested using out theoretical framework. Last but not least one could explore the dynamics of segregation in gels, which is an interesting area worth of exploration in its own right.

Combining different types of free energies with MFT theories, we can address and introduce different effects in the study of a variety of systems. In particular a very interesting problem not considered here, is crystallisation. Crystallisation for molecules studied in soft matter research might sound unexpected, but there has been evidence of this phenomenon since the late 50's [34]. Eppe et al. showed an electron micrograph of polyethylene, with a structure characterized by the presence

of crystals. Polymer crystallisation has been reviewed for theory and experiments by Strobl [119]. In some polymer mixtures there are islands of crystals in the matrix and they may affect the segregation behavior. We should expect the crystals to act as a barrier to the migrating molecules, approaching the critical temperature. A very interesting future direction might be the combination of such a free energy with the SCFT and SBMFT.

Finally I hope this work will help the scientific community to move a little step forward in understanding those phenomena and that it will stimulate further studies in this direction in order to fill in the gaps in this work, but also to encourage experimental studies of such systems and stimulate also new theoretical research.

Maybe at some point in future it would be nice to see this tiny piece of science applied to real products used by people in some countries of the world.

Chapter 7

Standard Operating Procedure(SOP)-Procter&Gamble gmbh confidential

7.1 Guide to the thesis

In this chapter there are all the codes I wrote during my PhD project. They are divided in section, relative to the main model implemented and subsections withe the specific problem solved.
For all the C++ codes someone can compile the source code as:

```
g++ name.cpp -o name
```

and run the program from a bash terminal as:

```
./name
```

in case of heavy computation is possible to uncomment the OMP commands for the loop and choose the numer of threads. Using SCOREP (developed by TU DRESDEN and JÜLICH FORSCHUNG ZENTRUM) the optimal number is between 4 and 16. In this case someone has to compile as:

```
g++ name.cpp -o name -fopenmp
```

I have used the python codes with the Anaconda framework and the editor Spyder. I have used Python for generating the majority of the figures in the thesis. Opening a source code and running it in a Python console someone can obtain the figures. I have used the mathematica notebook for the LCL theory. The functions for the free energy, the chemical potential, the phase diagrams and the pressure and compressibility are defined in the file. Using the $P(V,T)$ function is possible to fit PVT diagrams for obtaining the parameters of single polymers of a mixture. Using those parameters, guessing g with DoE is it possible to calculate the phase diagrams and with the LCL C++ code the wetting profiles relative to those systems.

7.2 Square Gradient theory codes

This code can be used for generating figures from Chapter 2:

7.2.1 Flory-Huggins

```
/*
 *  simpson.cpp
 *
 *
 *  Created by Salvatore Croce on 01/11/14.
 *  Copyright 2014 __Durham university-Procter&Gamble__. All rights reserved.
 *
 */
#include <stdio.h>
#include <math.h>
#include <stdlib.h>
#include <iostream>
#include <fstream>
#include <omp.h>
```

```
double florhug (double phi0, double Na,
double Nb, double chi){
double florhug=(phi0*log(phi0)/Na+((double)1-phi0)*log((double)1-phi0)/Nb
+chi*phi0*((double)1-phi0));
return florhug;
}
int i,j,k;
double phi0,phi1,dphi,chi;
double mu,N,Na,Nb,z1,z0,z,a,k1,k2,k3,k4,G,phinf,T;
using namespace std;
main(){
/*_____________________________________*/
/*Variables*/
mu=0.0; //chemical potential
dphi=1e-3;//integration step
a=4.6; //lattice constant
/*_____________________________________*/
Na=7;
Nb=5185;
phi0=0.999; //phi1 on graphics
phinf=0.63; //bulk concentration
T=300; //Temperature in Kelvin
//chi=(Na*(log(1-phinf)+1)-Nb*(log(phinf)+1)+Na*Nb*mu)/(Na*Nb*((double)1-(double)2*phinf));/
//cout<<chi<<endl;
chi=0.001;
/*-------------------------------------*/
fstream f("test.dat",ios::out);
Na=1;
Nb=10;
phi0=0.999;//phi1 in figures
phinf=0.1; //bulk concentration-phi infinity
//z0=(double)a/(double)6*dphi/sqrtl(phinf*((double)1-phinf)*(florhug( phinf, Na, Nb, chi)-fl
for(i=1;i<=1;i++){ \\loop for testing variables
z0=0.31;//initial step guess
```

```
j=1;
phi1=phi0;
while(phi1>phinf){
z=(double)a/(double)6*dphi/sqrtl(phi1*((double)1-phi1)*(florhug(phi1, Na, Nb, chi)-florhug(p
if(j%2==0){
z*=(double)2/(double)3;
}
else{
z*=(double)4/(double)3;
}
z0=z0+z;
j+=1;
f<<z0<<" "<<phi1<<endl;
phi1=phi1-dphi;
}
//mu=mu+i*0.05;
//f<<endl;
//f<<endl;
}//loop for testing bulk,mu, chi etc.
//cout<<z0<<endl;
//z1=z0+(double)a/(double)6*dphi/sqrtl(phi0*((double)1-phi0)*(florhug(phi0,Na,Nb,chi)-florhu
//f<<z0-z1/(double)3<<" "<<phi0<<endl;
return 0;
}
```

7.2.2 Elasticity

This code generates figures from Chapter 3. It is the same of the previous one, but with F_{fhe} instead of F_{fh}.

7.3 Self Consistent field theory codes

This code generates figures from Chapter 2 and Chapter 4

7.3.1 Flory-Huggins

```
//Self consistent Field theory by Salvatore Croce
//Copyright 2015-Durham University/Procter&Gamble
#include <stdio.h>
#include <math.h>
#include <stdlib.h>
#include <iostream>
#include <fstream>
#include <omp.h>
int i,j,k,l,N,Nint;
double wb[7000],wa[7000],qa[7000][7000],qb2[7000][7000];
double qb1[7000][7000],chis,chib,phia[7000],phib[7000];
double chiab,Na,Nb,mub[7000];
mua[7000],dw[7000],M,T,csi,Rg,a,surface,
massimo1,eps,massimo2,eps2,V,kb;
using namespace std;
main(){
//Initial values
N=2000; //lattice dimension
kb=1.38*1e-23; //Joule\Kelvin
V=1;//1e-28;//100 Cubic Angstrom
chis=-4; //surface interaction
chib=0.0; //bulk interaction
Na=10; //Degree of polymerization PS Ma=104.15
Nb=100; //Degree of polymerization PVME Ma=58
csi=1/12; //inverse compressibility per unit surface
a=1; //lattice constant
dw[0]=csi;
M=10; //number of iterations
T=(1e-3); //Temperature
Rg=a*sqrt(Na/(double)6);
phib[0]=0.6;
phia[0]=1-phib[0];
chiab=0.01; //Flory-Huggins parameter 0.33 at 30%, 0.4 at 80%
massimo1=1;
```

```
massimo2=1;
eps=1e-6;
Nint=1;
eps2=1e-2;
/*------------------------------*/ //Files
//fstream f("gamma_PS_Na5_PVME.dat",ios::out);
fstream fb2("test.dat",ios::out); //output profiles
srand((unsigned)time(0));
/*--------------------------------*/  //initial conditions
//f<<"#Parameters Na,Nb,chi,phinf,T="<<Na<<" "<<Nb<<" "<<chiab<<" "<<phib[0]<<" "<<T<<endl;
//#pragma omp parallel //remove comment for parallelization
//{                    //remove comment for parallelization
for(l=1;l<=Nint;l++){ //cycle for increasing the interaction
for(j=1;j<=N;j++){ //length of repeated unit
qa[0][j]=0;
qb1[0][j]=0;
qb2[0][j]=0;
}
qb1[1][0]=exp(-chis); //distance from surface
#pragma omp parallel for
for(i=1;i<=N;i++){
qa[i][0]=1;
//rand()/(RAND_MAX+(double)1)-0.5;
qb2[i][0]=1;
//rand()/(RAND_MAX+(double)1)-0.5;
qb1[i+1][0]=0; //exp(-chib);
}
//qb1[N][0]=exp(-chib);
 //Conditions for chemical potential and field
#pragma omp parallel for
for(j=1;j<=N;j++){
#pragma omp parallel for
for(i=1;i<=N;i++){
phia[i]=phia[i-1]+rand()/(RAND_MAX+(double)1);
phib[i]=phib[i-1]+rand()/(RAND_MAX+(double)1);
```

```
//cout<<phia[i]<<" "<<phib[i]<<endl; //check
dw[i]=csi*(1-phia[i]-phib[i]);
//Fields for B polymer
mub[i]=T*(log(phib[i])+phia[i]*((Na-Nb)/Na)+chiab*Nb*pow(phia[i],2));
wb[i]=T*(phia[i]*(1/Nb)-1/Na+chiab*pow(phia[i],2))-dw[i];
//Fields for A polymer
mua[i]=T*(log(phia[i])+phib[i]*((Nb-Na)/Nb)+chiab*Na*pow(phib[i],2));
wa[i]=T*(phib[i]*(1/Na)-1/Nb+chiab*pow(phib[i],2))-dw[i];
//cout<<w[i]<<" "<<mu[i]<<" "<<dw[i]<<endl; //check
}
}
/*--------------------------------*/ //Recursive relations
for(k=1;k<=M;k++){
//surface=0;
#pragma omp parallel for
for(j=1;j<=N;j++){
#pragma omp parallel for
for(i=1;i<=N;i++){
qa[i][j]=(qa[i-1][j-1]+qa[i+1][j-1]
+4*qa[i][j-1])*exp(-wa[i])/(double)6;
//f<<i<<" "<<j<<" "<<qa[i-1][j-1]<<endl; //check
qb1[i][j]=(qb1[i-1][j-1]+qb1[i+1][j-1]
+4*qb1[i][j-1])*exp(-wb[i])/(double)6;
qb2[i][j]=(qb2[i-1][j-1]+qb2[i+1][j-1]
+4*qb2[i][j-1])*exp(-wb[i])/(double)6;
//cout<<qa[i][j]<<" "<<qb1[i][j]<<endl; //check
/*-----------------------*/
phia[i]=phia[i-1]+qa[i][j]*qa[N-i][j-1]
*exp(mua[i]+T*chis*V);
phib[i]=phib[i-1]+qb1[i][j]*qb2[N-i][j-1]
*exp(mub[i]+T*chis*V);
if(phia[i]>1){phia[i]=1;}
if(phib[i]>1){phib[i]=1;}
//surface+=phib[i]*i;
/*-------------------------*/
```

```
dw[i]=csi*(1-phia[i]-phib[i]);
//Fields for B polymer
mub[i]=(log(phib[i])+phia[i]*(1-Nb/Na)+chiab*Nb*pow(phia[i],2))*T;
wb[i]=T*(phia[i]*(1/Nb-1/Na)
+chiab*pow(phia[i],2))-dw[i];
//Fields for A polymer
mua[i]=T*(log(phia[i])+phib[i]*((Nb-Na)/Nb)+chiab*Na*pow(phib[i],2));
wa[i]=T*(phib[i]*(1/Na-1/Nb)
+chiab*pow(phib[i],2))-dw[i];
//cout<<w[i]<<" "<<mu[i]<<" "<<dw[i]<<endl;
/*-------------------------*/
if(fabs(phia[i]-phia[i-1])<=eps){
massimo1=phia[i];
}
if(fabs(phib[i]-phib[i-1])<=eps){
massimo2=phib[i];
}
}
}
}
//}                    //remove comment for parallelization
//#pragma end parallel //remove comment for parallelization
//cout<<phib[0]<<" "<<phia[0]<<endl;
//fb2<<"#Degree of polymerization="<<Nb<<" "<<Na<<endl;
for(i=0;i<=N;i++){
//f<<j<<" "<<i<<" "<<phia[i-1]<<" "<<qb1[i][j]<<endl;
//if((1+phib[0]-(phib[i]/massimo2))<1){
//cout<<chis<<" "<<1+phib[0]-(phib[1]/massimo2)<<endl;
/*---------------------------------*/ //calculation of surface energies
//if((1+phib[0]-(phib[1]/massimo2))<1){
//f<<chis<<" "<<1+phib[0]-(phib[1]/massimo2)<<endl;}
//else{f<<chiab<<" "<<1<<endl;}
/*-------------------------------------------*/
fb2<<i/Rg<<" "<<1+phib[0]-(phib[i])<<endl;
} //loop for writiing
```

```
//}
//}
chis+=0.1; //increase surface interaction
//Na*=2;
//Nb*=5;
//fb2<<endl;
//fb2<<endl;
}
}
```

7.3.2 Elasticity

This code can be used for generating figures from Chapter 3

```
*
 *  scft_elast.cpp
 *
 *
 *  Created by Salvatore Croce on 23/12/14.
 *  Copyright 2014 __Durham university-P&G__. All rights reserved.
 *
 */
#include <stdio.h>
#include <math.h>
#include <stdlib.h>
#include <iostream>
#include <fstream>
#include <omp.h>
/*-----------------------------------------------------*/
double florhug (double phi0, double Na,double phinf, double chi, double B){
double florhug=(phi0*log(phi0)/Na
+chi*phi0*((double)1-phi0))+B*((double)1-phinf)*(pow(((double)1-phi0)/((double)1-phinf),2/3)-
return florhug;
}
/*-----------------------------------------------------*/
//double kinda (int i,int j,)
```

```
int i,j,k,l,N,Na,Nb,Nint;
double wb[1000],wa[1000],qa[1000][1000];
double qb2[1000][1000],qb1[1000][1000],chis,chib;
double phia[1000],phib[1000],chiab,mub[1000],mua[1000];
double dw[1000],M,T,csi,Rg,a,surface,B,eps,massimo,B1,B0,B2;
using namespace std;
main(){
//Initial values
phia[0]=0.99; //Surface concentration
phib[0]=0.01; //Bulk concentration
N=500; //lattice dimension
chis=-5.9; //surface energy
//chib=5.75; //bulk interaction
//-2*chis-log(phib[0]); //surface interaction
chiab=2.48; //Flory-huggins parameter
Na=1; //Degree of polymerization
Nb=1; //Degree of polymerization
csi=1/12; //inverse compressibility per unit surface
a=1; //lattice constant
//dw[0]=csi;
M=10; //number of iterations
T=1e-3; //Temperature
Rg=a*sqrt(Na/(double)6);
B0=140;
B1=0;
B2=0.0;
B=B0+B1*i;//phib[i]+B2*phib[i]*phib[i];
eps=1e-6;
massimo=1;
Nint=250;
/*------------------------------*/ //Files
//fstream f("surf_chis_na5_bulk005_B1.dat",ios::out);
fstream fb2("surf_chis_na1_bulk001_B140_bis.dat",ios::out); //output profiles
srand((unsigned)time(0));
fb2<<"#parameter Na,phi_nf,Fs,chi,a,B: "<<" "<<Na<<" "<<phib[0]<<" "<<chis<<" "<<chiab<<" "<
```

```
/*--------------------------------*/  //initial conditions

//#pragma omp parallel //remove comment for parallelization
//{                    //remove comment for parallelization

for(l=1;l<=Nint;l++){ //cycle for increasing the interaction
for(j=1;j<=N;j++){ //length of repeated unit
qa[0][j]=0;
qb1[0][j]=0;
qb2[0][j]=0;
}
qb1[1][0]=exp(-chis); //distance from surface
#pragma omp parallel for
for(i=1;i<=N;i++){
qa[i][0]=1;
//rand()/(RAND_MAX+(double)1)-0.5;
qb2[i][0]=1;
//rand()/(RAND_MAX+(double)1)-0.5;
qb1[i+1][0]=0;
//exp(-chib);
}
//Conditions for chemical potential and field
#pragma omp parallel for
for(j=1;j<=N;j++){
#pragma omp parallel for
for(i=1;i<=N;i++){
//
//if(i<200){B=T*(B0+B1*i);}//phib[i]+B2*phib[i]*phib[i];
//
phia[i]=phia[i-1]+rand()/(RAND_MAX+(double)1);
phib[i]=phib[i-1]+rand()/(RAND_MAX+(double)1);
//cout<<phia[i]<<" "<<phib[i]<<endl; //check
dw[i]=csi*(1-phia[i]-phib[i]);
//Fields for B polymer
mub[i]=T*Nb*(chiab*pow(phia[i],2)-phia[i]/Na+B*phib[0]*(pow(phib[i]/phib[0],2/3)+2*pow(phib[
```

```
wb[i]=T*(chiab*pow(phia[i],2)-phia[i]/Na+B*phib[0]*(pow(phib[i]/phib[0],2/3)+2*pow(phib[0]/pl
//Fields for A polymer
mua[i]=T*(log(phia[i])+phib[i]+chiab*Na*pow(phib[i],2)+B*phib[0]*Na*(pow(phib[i]/phib[0],2/3
wa[i]=T*(phib[i]/Na+chiab*pow(phib[i],2)+B*phib[0]*(pow(phib[i]/phib[0],2/3)+pow(phib[i]/phil
//cout<<w[i]<<" "<<mu[i]<<" "<<dw[i]<<endl; //check
}
}
/*---------------------------------
for(i=0;i<=N;i++){
//f<<i<<" "<<phia[i-1]<<endl;
//if((1+phib[0]-phib[i]/massimo)<=1){
fb2<<i/(M*Rg)<<" "<<1+phib[0]-phib[i]/massimo<<" "<<1+phia[0]-phia[i]/phia[N]<<" "<<mub[i]<<
}

fb2<<endl;
fb2<<endl;
---------------------------------*/ //Recursive relations
for(k=1;k<=M;k++){
//while(fabs(phib[i]-phib[i-1])>0.1){
//surface=0;
#pragma omp parallel for
for(j=1;j<=N;j++){
#pragma omp parallel for
for(i=1;i<=N;i++){
//if(i<200){B=T*(B0+B1*i);}
//B=B0+B1*i+B2*phib[i]*phib[i];
qa[i][j]=(qa[i-1][j-1]+qa[i+1][j-1]+4*qa[i][j-1])*exp(-wa[i])/(double)6;
//f<<i<<" "<<j<<" "<<qa[i-1][j-1]<<endl; //check
qb1[i][j]=(qb1[i-1][j-1]+qb1[i+1][j-1]+4*qb1[i][j-1])*exp(-wb[i])/(double)6;
qb2[i][j]=(qb2[i-1][j-1]+qb2[i+1][j-1]+4*qb2[i][j-1])*exp(-wb[i])/(double)6;
//cout<<qa[i][j]<<" "<<qb1[i][j]<<endl; //check
/*-----------------------*/
phia[i]=phia[i-1]+qa[i][j]*qa[i][N-j]*exp(mua[i]+chis*T);
phib[i]=phib[i-1]+qb1[i][j]*qb2[i][N-j]*exp(mub[i]+chis*T);
//surface+=phib[i]*i;
```

```
/*-------------------------*/
dw[i]=csi*(1-phia[i]-phib[i]);
//Fields for B polymer
mub[i]=T*Nb*(chiab*pow(phia[i],2)-phia[i]/Na
+B*phib[0]*(pow(phib[i]/phib[0],2/3)+2*pow(phib[0]/phib[i],1/3)-3)/2
+B*phia[i]*(-pow(phib[0]/phib[i],4/3)+pow(phib[0]/phib[i],1/3))/3);
wb[i]=T*(chiab*pow(phia[i],2)-phia[i]/Na
+B*phib[0]*(pow(phib[i]/phib[0],2/3)+2*pow(phib[0]/phib[i],1/3)-3)/2+B*phia[i]*(-pow(phib[0]/
//Fields for A polymer
mua[i]=T*(log(phia[i])+phib[i]+chiab*Na*pow(phib[i],2)+B*phib[0]*Na*(pow(phib[i]/phib[0],2/3
wa[i]=T*(phib[i]/Na+chiab*pow(phib[i],2)+B*phib[0]*(pow(phib[i]/phib[0],2/3)+pow(phib[i]/phi
//cout<<w[i]<<" "<<mu[i]<<" "<<dw[i]<<endl;
if(phib[i]>1){phib[i]=1;}
if(phia[i]>1){phia[i]=1;}
if(abs(phib[i]-phib[i-1])<=eps){
massimo=phib[i];
}
/*-------------------------*/

}
}
}

//}                    //remove comment for parallelization
//#pragma end parallel //remove comment for parallelization
//fb2<<"#B="<<B*T<<endl;
//for(i=0;i<=N;i++){
//f<<i<<" "<<phia[i-1]<<endl;
//if((1+phib[0]-phib[i]/massimo)<=1){
//fb2<<i/Rg<<" "<<1+phib[0]-phib[i]/massimo<<" "<<1+phia[0]-phia[i]/phia[N]<<" "<<mub[i]<<"
//fb2<<i/Rg<<" "<<1+phib[0]-phib[i]/massimo<<" "<<florhug(phib[i],Na,phib[0], chiab,B*T)<<en
//cout<<"Surface="<<surface/(M*2*M*pow(N,2))<<endl;
//if((1+phib[0]-phib[1]/massimo)<1){
fb2<<chis<<" "<<1+phib[0]-phib[1]/massimo<<" "<<0.05/(phib[0]/massimo)<<endl;//}
//else{f<<chis<<" "<<1<<endl;}
```

```
chis+=0.05;
//B0+=0.01;//increase elastic modulus
//fb2<<endl;
//fb2<<endl;
}
}
```

7.3.3 Lattice correlated theory

This code generates figures from Chapter 5

```
//Self consistent Field theory by Salvatore Croce
//Copyright Durham University
#include <stdio.h>
#include <math.h>
#include <stdlib.h>
#include <iostream>
#include <fstream>
#include <omp.h>
#include <new>
/*-------------------------------------------------------*/
/*-------------------------------------------------------*/
//Lipatov-White-Higgins free energy kb=1
double LWH (double Na, double Nb, double phia, double phib, double qa, double qb, double z,
double LWH=T*(phia*log(phia)/Na+phib*log(phib)/Nb+((double)1-phia/Na-phib/Nb)*log(1-phia/Na-
return LWH;
}
/*-------------------------------------------------------*/
//Lipatov-White-Higgins chemical potential
double LWH_chem (double T, double phia, double phib, double Na, double Nb, double qa, double
double LWH_chem=T*(log(phia)-Na*log((double)1-phia/Na-phib/Nb)+(double)1-Na+qa*z*log(qa/(Na*

return LWH_chem;
```

```
}
/*-------------------------------------------------------*/
//Mean field of interaction
double meanfield(double mua, double phia, double Na, double T){
double meanfield=(mua-T*log(phia))/Na;
return meanfield;
}
/*-------------------------------------------------------*/
int i,j,k,l,N,Nint,q1,q2,v;
double wb[7000],wa[7000],qa[7000][7000],qb2[7000][7000],qb1[7000][7000],chis,chib,phia[7000]
mua[7000],M,T,Rg,a,massimo1,eps,massimo2,eps2,F1,F2,mu1,mu2;
double nu,z,epsa,epsb,epsba,g,kb,x[1001][5];
using namespace std;
FILE*f1;
main(){
//Initial values
N=5000; //lattice dimension
chis=-12; //surface interaction
chib=5.75; //bulk interaction
chiab=-4.6e-2; //-2.6e-3 0.00341; //Flory-Huggins parameter \\-3.5e-5;
Na=151; //Degree of polymerization PS with nu=8
Nb=335; //Degree of polymerization PB
//csi=1/12; //inverse compressibility per unit surface
//dw[0]=csi;
M=10; //number of iterations
kb=8.31*(1e-4);
T=1.2e-3;//360; //Temperature
a=1;//phia[0]*10.5+phib[0]*1.6; //lattice constant
Rg=a*sqrt(Na/(double)6);
phib[0]=0.1;
phia[0]=1-phib[0];
massimo1=1;
massimo2=1;
eps=1e-6;
Nint=1;
```

```
eps2=1e-2;
//Parameters for chemical species PS/PB
g=0.996415;
epsa=2042.5/8.31;
epsb=1960.3/8.31;
epsba=g*sqrt(epsa*epsb);
z=6; //coordination number always fixed
/*------------------------------*/ //Files
//fstream f("PS_PB.dat",ios::out);
fstream fb2("test3.dat",ios::out); //output profiles
//fstream phi("phi1_simple_fluid_ter.csv",ios::out); //output phi1
srand((unsigned)time(0));
/*-----------------------------------------------------------
f1=fopen("DoE_LCL_20000_bis_100.csv","r");
fscanf(f1,"\n");
for(v=1;v<=500;v++){//Number of lines
fscanf(f1,"%lf,%lf,%lf,%lf,%lf,%lf\n",&x[v][0],&x[v][1],&x[v][2],&x[v][3],&x[v][4],&x[v][5])
fscanf(f1,"\n");
} //end of reading file
for(v=1;v<=500;v++){//Number of lines
Na=int(x[v][0]);//1000); //Degree of polymerization
Nb=int(x[v][1]);//1000); //Degree of polymerization
ra=x[v][2]/10;
rb=(x[v][3]);
epsa=x[v][4];
epsb=x[v][5];
}
--------------------------------*/  //initial conditions
fb2<<"#Parameters Na,Nb,ra,rb,epsa,epsb="<<Na<<" "<<Nb<<" "<<epsa<<" "<<epsb<<endl;
/*-------------------------------------------------------------*/
nu=8; //mL/mol
//epsa=2042/10; //J/mol//Course grained scaling
//epsb=1960/10; //J/mol
epsba=g*sqrt(epsa*epsb); //J/mol
q1=Na-2*Na/z+2;
```

```
q2=Nb-2*Nb/z+2;
/*--------------------------------*/  //initial conditions
//f<<"#Parameters Na,Nb,chi,phinf,T="<<Na<<" "<<Nb<<" "<<chiab<<" "<<phib[0]<<" "<<T<<endl;
//#pragma omp parallel //remove comment for parallelization
//{                    //remove comment for parallelization
for(l=1;l<=Nint;l++){ //cycle for increasing the interaction
for(j=1;j<=N;j++){ //length of repeated unit
qa[0][j]=0;
qb1[0][j]=0;
qb2[0][j]=0;
}
qb1[1][0]=exp(-chis); //distance from surface
//#pragma omp parallel for
for(i=1;i<=N;i++){
qa[i][0]=1;
//rand()/(RAND_MAX+(double)1)-0.5;
qb2[i][0]=1;
//rand()/(RAND_MAX+(double)1)-0.5;
qb1[i+1][0]=0; //exp(-chib);
}
 //Conditions for chemical potential and field
//#pragma omp parallel for
for(j=1;j<=N;j++){
//#pragma omp parallel for
for(i=1;i<=N;i++){
//phia[i]=phia[i-1]+rand()/(RAND_MAX+(double)1)+phia[0];
//phib[i]=phib[i-1]+rand()/(RAND_MAX+(double)1)+phib[0];
phia[i]=rand()/(RAND_MAX+(double)1);
phib[i]=rand()/(RAND_MAX+(double)1);
if(phia[i]>1){phia[i]=1;}
if(phib[i]>1){phib[i]=1;}
if(phia[i]<phia[0]){phia[i]=phia[0];}
if(phib[i]<phib[0]){phib[i]=phib[0];}
//Free energy LCL
F1=LWH(Na,Nb,phia[i],phib[i],q1,q2,z,epsa,epsba,epsb,T);
```

```
F2=LWH(Na,Nb,phia[i-1],phib[i-1],q1,q2,z,epsa,epsba,epsb,T);
//dw[i]=csi*(1-phia[i]-phib[i]);
//Fields for B polymer
mu1=LWH_chem(T,phib[i],phia[i],Na,Na,q2,q1,z,epsa,epsba,epsa);//(F1-F2)/(phib[i]-phib[i-1]);
mub[i]=mu1;
wb[i]=meanfield(mu1,phib[i],Nb,T);
//Fields for A polymer
mu2=LWH_chem(T,phia[i],phib[i],Na,Nb,q1,q2,z,epsa,epsba,epsb);//(F1-F2)/(phia[i]-phia[i-1]);
mua[i]=mu2;
wa[i]=meanfield(mu2,phia[i],Na,T);
//cout<<w[i]<<" "<<mu[i]<<" "<<dw[i]<<endl; //check
}
}
/*---------------------------------
for(i=0;i<=N;i++){
fb2<<i/Rg<<" "<<1+phib[0]-(phib[i]/massimo2)<<" "<<1+phia[0]-(phia[i]/massimo1)<<endl;
}
fb2<<endl;
fb2<<endl;
---------------------------------*/ //Recursive relations
for(k=1;k<=M;k++){
//surface=0;
//#pragma omp parallel for
for(j=1;j<=N;j++){
//#pragma omp parallel for
for(i=1;i<=N;i++){
qa[i][j]=(qa[i-1][j-1]+qa[i+1][j-1]+4*qa[i][j-1])*exp(-wa[i])/(double)6;
//f<<i<<" "<<j<<" "<<qa[i-1][j-1]<<endl; //check
qb1[i][j]=(qb1[i-1][j-1]+qb1[i+1][j-1]+4*qb1[i][j-1])*exp(-wb[i])/(double)6;
qb2[i][j]=(qb2[i-1][j-1]+qb2[i+1][j-1]+4*qb2[i][j-1])*exp(-wb[i])/(double)6;
//cout<<qa[i][j]<<" "<<qb1[i][j]<<endl; //check
/*-----------------------*/
phia[i]=phia[i-1]+qa[i][j]*qa[N-i][j-1]*exp(mua[i]+T*chis);
phib[i]=phib[i-1]+qb1[i][j]*qb2[N-i][j-1]*exp(mub[i]+T*chis);
if(phia[i]>1){phia[i]=1;}
```

```
if(phib[i]>1){phib[i]=1;}
//surface+=phib[i]*i;
/*-------------------------*/
//Free energy LCL
F1=LWH(Na,Nb,phia[i],phib[i],q1,q2,z,epsa,epsba,epsb,T);
F2=LWH(Na,Nb,phia[i-1],phib[i-1],q1,q2,z,epsa,epsba,epsb,T);
//dw[i]=csi*(1-phia[i]-phib[i]);
//Fields for B polymer
mu1=LWH_chem(T,phib[i],phia[i],Na,Na,q2,q1,z,epsa,epsba,epsa);//(F1-F2)/(phib[i]-phib[i-1]);
mub[i]=mu1;
wb[i]=meanfield(mu1,phib[i],Nb,T);
//Fields for A polymer
mu2=LWH_chem(T,phia[i],phib[i],Na,Nb,q1,q2,z,epsa,epsba,epsb);//(F1-F2)/(phia[i]-phia[i-1]);
mua[i]=mu2;
wa[i]=meanfield(mu2,phia[i],Na,T);
//cout<<w[i]<<" "<<mu[i]<<" "<<dw[i]<<endl;
/*-------------------------*/
if(fabs(phia[i]-phia[i-1])<=eps){
massimo1=phia[i];
}
if(fabs(phib[i]-phib[i-1])<=eps){
massimo2=phib[i];
}
}
}
}
//}                    //remove comment for parallelization
//#pragma end parallel //remove comment for parallelization
//cout<<phib[0]<<" "<<phia[0]<<endl;
//fb2<<"#Degree of polymerization="<<Nb<<" "<<Na<<endl;
for(i=0;i<=N;i++){
//f<<j<<" "<<i<<" "<<phia[i-1]<<" "<<qb1[i][j]<<endl;
//if((1+phib[0]-(phib[i]/massimo2))<1){
//cout<<chis<<" "<<1+phib[0]-(phib[1]/massimo2)<<endl;
/*---------------------------------*///calculation of surface energies
```

```
//if((1+phib[0]-(phib[1]/massimo2))<1){
//f<<chis<<" "<<1+phib[0]-(phib[1]/massimo2)<<endl;}
//else{f<<chiab<<" "<<1<<endl;}
/*-----------------------------------------------*/
fb2<<i/Rg<<" "<<1+phib[0]-(phib[i]/massimo2)<<" "<<1+phia[0]-(phia[i]/massimo1)<<endl;}
//phi<<1+phib[0]-(phib[1]/massimo2)<<endl;
//else{
//fb2<<i/(a*Rg)<<" "<<1<<" "<<1<<" "<<mub[i]<<" "<<mua[i]<<" "<<wb[i]*N<<" "<<dw[i]<<endl;

//}
//}
//cout<<"Surface="<<surface/(M*2*M*pow(N,2))<<endl;
//chis+=1e-1; //increase surface interaction
//B+=1e-3; //increase elasticity
//temp+=1e-1;
//fb2<<endl;
// fb2<<endl;
}
}
```

7.4 Python codes for figures

```
""
Created on Mon Sep 04 17:16:14 2017

@author: Salvatore Croce
"""
import numpy as np
import matplotlib.pyplot as plt
#
#x = np.arange(-0.1, 30.0 + 0.0001, 0.0001) #if you need to plot functions
plt.rc('text', usetex=True) #latex fonts
plt.rc('font', family='serif')
#
#
```

```
plt.xlabel(r'\textbf{$z/a$}',fontsize=30)
plt.ylabel(r'\textit{$\phi(z)$}',fontsize=30)
#
plt.ylim(0.0,1.0)
plt.xlim(0.0,270.0)
#
data = np.loadtxt('test.dat') #load data file
plt.plot(data[:,0],(data[:,1]), color='red',linestyle='-',label= '$test$',linewidth=2)
#
legend = plt.legend(loc=3, shadow=False, fontsize=10)
plt.grid(True,color='grey',alpha=0.07,linestyle=':')
plt.savefig('test.pdf', bbox_inches='tight', dpi=500)
plt.show()
```

7.5 Mathematica notebook

This file generates figures from Chapter 5.

```
(*Chemical Potential per unit temperature mu/KbT for a single polymer*)


mu[phia_, phib_, Na_, Nb_, qa_, qb_, z_, epsa_, epsb_, epsab_, T_,
  nu_, V_] :=
 Log[phia] - Na*Log[nu/V - phia/Na - phib/Nb] + (Na - 1) +
  qa*z*Log[qa/(Na*(nu/V - phia/Na - phib/Nb))]/2 +
  Na*z*Log[(nu/V - phia/Na - phib/Nb)] +
  z*(Na - qa)/2 - (qa*z)*
   Log[qa*phia*Exp[-epsa/T]/(Na*(nu/V - phia/Na - phib/Nb)) +
      qb*phib*Exp[-epsab/T]/(Nb*(nu/V - phia/Na - phib/Nb)) + 1]/
    2 - (z*qa*
     phia/(Na*(nu/V - phia/Na - phib/Nb)))*(Na -
      qa + (qa*Exp[-epsa/T] -
         Na)/(qa*phia*Exp[-epsa/T]/(Na*(nu/V - phia/Na - phib/Nb)) +
         qb*phib*Exp[-epsab/T]/(Nb*(nu/V - phia/Na - phib/Nb)) + 1))/
    2 - (z*qb*
     phib/(Nb*(nu/V - phia/Na - phib/Nb)))*(Na -
```

```
      qa + (qa*Exp[-epsab/T] -
         Na)/(qa*phia*Exp[-epsab/T]/(Na*(nu/V - phia/Na - phib/Nb)) +
         qb*phib*Exp[-epsb/T]/(Nb*(nu/V - phia/Na - phib/Nb)) + 1))/2


q[r_, za_] := r - 2*r/za + 2
(*PS for PS/PB*)
qa = q[151.31, 6];
qb = q[335.42, 6];
Plot3D[mu[phia, phib, 151.31, 335.42, qa, qb,
  6, -2042.5/8.31, -1993.6/8.31, -1960.3/8.31, 360, 8, 50], {phia,
  0.01, 1}, {phib, 0.01, 1}, AxesLabel -> {\[Phi]a, \[Phi]b}]
Plot[mu[phia, 0.01, 151.31, 335.42, qa, qb,
   6, -2042.5/8.31, -1993.6/8.31, -1960.3/8.31, 360, 8, 200]/
  1000, {phia, 0.01, 1}, AxesLabel -> {\[Phi]a, \[Mu]}]
test = MatrixForm[
   Table[mu[phia, 0.01, 151.31, 335.42, qa, qb,
      6, -2042.5/8.31, -1993.6/8.31, -1960.3/8.31, 360, 8, 200]/
     1000, {phia, 0.00001, 1, 0.001}]];
Export["muPS.dat", test];
(*PB for PS/PB a and b index inverted*)
qa = q[151.31, 6];
qb = q[335.42, 6];
Plot3D[mu[phib, phia, 335.42, 151.31, qb, qa,
  6, -1993.6/8.31, -2042.5/8.31, -1960.3/8.31, 360, 8, 50], {phia,
  0.01, 1}, {phib, 0.01, 1}, AxesLabel -> {\[Phi]a, \[Phi]b}]
Plot[mu[0.01, phib, 335.42, 151.31, qb, qa,
   6, -1993.6/8.31, -2042.5/8.31, -1960.3/8.31, 360, 8, 200]/
  1000, {phib, 0.01, 1}, AxesLabel -> {\[Phi]b, \[Mu]}]
test = MatrixForm[
   Table[mu[0.01, phib, 335.42, 151.31, qb, qa,
      6, -1993.6/8.31, -2042.5/8.31, -1960.3/8.31, 360, 8, 200]/
     1000, {phib, 0.00001, 1, 0.001}]];
Export["muPB.dat", test];
(*PVME for PS/PVME*)
qa = q[13652.0, 6];
```

```
qb = q[11419.0, 6];
Plot3D[mu[phia, phib, 13652.0, 11419.0, qa, qb,
  6, -2144.3/8.31, -1946/8.31, -2045.6/8.31, 394, 7.667, 120], {phia,
  0.01, 1}, {phib, 0.01, 1}, AxesLabel -> {\[Phi]a, \[Phi]b}]
Plot[mu[0.01, phib, 13652.0, 11419.0, qa, qb,
   6, -2144.3/8.31, -1946/8.31, -2045.6/8.31, 394, 7.667, 200]/
  1000, {phib, 0.01, 1}, AxesLabel -> {\[Phi]b, \[Mu]}]
test = MatrixForm[
   Table[mu[0.01, phib, 13652.0, 11419.0, qa, qb,
      6, -2144.3/8.31, -1946/8.31, -2045.6/8.31, 394, 7.667, 200]/
     1000, {phib, 0.00001, 1, 0.001}]];
Export["muPVME.dat", test];
```

Spinodal diagram:

```
(*Spinodal decomposition at fixed Volume*)
(*BINODAL*)
ClearAll
mu[phia_, phib_, Na_, Nb_, qa_, qb_, z_, epsa_, epsb_, epsab_, T_,
  nu_, V_] :=
 Log[phia] - Na*Log[nu/V - phia/Na - phib/Nb] + (Na - 1) +
  qa*z*Log[qa/(Na*(nu/V - phia/Na - phib/Nb))]/2 +
  Na*z*Log[(nu/V - phia/Na - phib/Nb)] +
  z*(Na - qa)/2 - (qa*z)*
   Log[qa*phia*Exp[-epsa/T]/(Na*(nu/V - phia/Na - phib/Nb)) +
      qb*phib*Exp[-epsab/T]/(Nb*(nu/V - phia/Na - phib/Nb)) + 1]/
    2 - (z*qa*
     phia/(Na*(nu/V - phia/Na - phib/Nb)))*(Na -
      qa + (qa*Exp[-epsa/T] -
         Na)/(qa*phia*Exp[-epsa/T]/(Na*(nu/V - phia/Na - phib/Nb)) +
         qb*phib*Exp[-epsab/T]/(Nb*(nu/V - phia/Na - phib/Nb)) + 1))/
    2 - (z*qb*
     phib/(Nb*(nu/V - phia/Na - phib/Nb)))*(Na -
      qa + (qa*Exp[-epsab/T] -
         Na)/(qa*phia*Exp[-epsab/T]/(Na*(nu/V - phia/Na - phib/Nb)) +
         qb*phib*Exp[-epsb/T]/(Nb*(nu/V - phia/Na - phib/Nb)) + 1))/2
```

```
q[r_, za_] := r - 2*r/za + 2
(*PS for PS/PB*)
qa = q[151.31, 6];
qb = q[335.42, 6];
Bin[phia_, phib_] =
 mu[phia, phib, 151.31, 335.42, qa, qb,
   6, -2042.5/8.31, -1993.6/8.31, -1960.3/8.31, 360, 8, 10] -
  mu[phib, phia, 335.42, 151.31, qb, qa,
   6, -1993.6/8.31, -2042.5/8.31, -1960.3/8.31, 360, 8, 10]
(*K=Solve[Bin[phia,phib]\[Equal]0,T]
Plot3D[K,{phia,0,1},{phib,0,1}]
Plot3D[Bin[phia,phib],{phia,0,1},{phib,0,1}]*)
p1 = Plot[-Bin[phia, 0.1], {phia, 0, 1}];
p2 = Plot[Bin[phia, 0.1], {phia, 0, 1}];
p3 = Plot[Bin[0.1, phib], {phib, 0, 1}];
p4 = Plot[Bin[0.3, phib], {phib, 0, 1}];
Show[p2, p1]

(*SPINODAL PS/PB UCTS*)
ClearAll@phib
D1 = D[mu[phia, phib, 151.31, 335.42, qa, qb,
    6, -2042.5/8.31, -1993.6/8.31, -1960.3/8.31, 360, 8, 10], phia];
D2 = D[mu[phia, phib, 151.31, 335.42, qa, qb,
    6, -2042.5/8.31, -1993.6/8.31, -1960.3/8.31, 360, 8, 10], phib];
D3 = D[mu[phib, phia, 335.42, 151.31, qb, qa,
    6, -1993.6/8.31, -2042.5/8.31, -1960.3/8.31, 360, 8, 10], phia];
D4 = D[mu[phib, phia, 335.42, 151.31, qb, qa,
    6, -1993.6/8.31, -2042.5/8.31, -1960.3/8.31, 360, 8, 10], phib];
Plot3D[D1 - D2 + D3 - D4, {phia, 0, 1}, {phib, 0, 1},
 AxesLabel -> {\[Phi]a, \[Phi]b}]
phib = 0.55
Plot[-1/(D1 - D2 + D3 - D4), {phia, 0, 1},
 AxesLabel -> {\[Phi]a, \[Chi]s}]
data = Table[x, {x, 0, 1, 0.001}];
```

```
PSPBspin = Table[1/(D1 - D2 + D3 - D4), {phia, 0.00001, 1, 0.001}];
test = MatrixForm[
   Table[(D1 - D2 + D3 - D4), {phia, 0.00001, 1, 0.001}]];
Export["PSPBspin_LCL.dat", test];
(*SPINODAL PS/PVME LCTS*)
ClearAll@phib
D1 = D[mu[phia, phib, 13652.0, 11419.0, qa, qb,
    6, -2144.3/8.31, -1946/8.31, -2045.6/8.31, 394, 8, 7.5], phia];
D2 = D[mu[phia, phib, 13652.0, 11419.0, qa, qb,
    6, -2144.3/8.31, -1946/8.31, -2045.6/8.31, 394, 8, 7.5], phib];
D3 = D[mu[phia, phib, 11419.0, 13652.0, qa, qb,
    6, -1946/8.31, -2144.3/8.31, -2045.6/8.31, 394, 8, 7.5], phia];
D4 = D[mu[phia, phib, 11419.0, 13652.0, qa, qb,
    6, -1946/8.31, -2144.3/8.31, -2045.6/8.31, 394, 8, 7.5], phib];
(*spinod[T_,phia_,phib_]:=Solve[D1-D2+D3-D4\[Equal]0,T]
Plot[spinod[T,0.4,0.6]]*)
Plot3D[1/(D1 - D2 + D3 - D4), {phia, 0, 1}, {phib, 0, 1},
 AxesLabel -> {\[Phi]a, \[Phi]b}]
phib = 0.7
Plot[1/(D1 - D2 + D3 - D4 + 0.2), {phia, 0, 1},
 AxesLabel -> {\[Phi]a, \[Chi]s}]
Export["PSPVMEspin_LCL.dat",
  MatrixForm[
   Table[1/(D1 - D2 + D3 - D4), {phia, 0.00001, 1, 0.001}]]];
```

Pressure and compressibility:

```
(*Pressure function*)
ClearAll
P[phi_, z_, N_, eps_, T_, V_, nu_,
  q_] := -T*(Log[nu*(1 - phi/N)/V]/nu +
    z/(2*nu)*Log[(nu^2)*(1 - phi/N)/(V^2)] -
    z*(phi*q/(N - phi))/(2*
        nu)*((phi*
         q/(N - phi)*(Exp[eps/T] - 1))/(phi*q/(N - phi)*Exp[eps/T] +
         nu/V)))
```

```
q[r_, za_] := r - 2*r/za + 2
P[phia, z, Na, epsa, T, nu, qc]
(*PB polymer in PS*)
qpb = q[335.42, 6];
PV1 = P[0.3, 6, 335.42, 1960.3/8.31, 360, V, 8, qpb];
PV2 = P[0.3, 6, 335.42, 1960.3/8.31, T, 100, 8, qpb];
Plot[PV1, {V, 0.001, 120}, AxesLabel -> {V, P}]
Plot[PV2, {T, 0, 600}, AxesLabel -> {T, P}]
Export["Pressure_V_LCL.dat",
 MatrixForm[Table[PV1, {V, 0.001, 120, 0.1}]]]
Export["Pressure_T_LCL.dat", MatrixForm[Table[PV2, {T, 0, 600, 0.1}]]]
ClearAll@V
ClearAll@T
(*Compressibility*)
P[phia, z, Na, epsa, T, nu, qc]
test = -1/D[P[phia, z, Na, epsa, T, nu, qc], V]/V
TeXForm[test]
B = (-1/D[P[phi, 6, 335.42, 1960.3/8.31, T, V, 8, qpb], V])/V;
V = 120;
phi = 0.5;
Plot3D[1000*B, {phi, 0, 1}, {T, 1, 500}]
Plot[1000*B, {T, 0.01, 500}, AxesLabel -> {T[K], Modulus[MPa]}]
Export["elastic_modulus_LCL.dat",
  MatrixForm[Table[1000*B, {T, 0.01, 500, 0.1}]]];
```

7.6 Common tangent construction

C++ Code for the common tangent construction:

```
#include <stdio.h>
#include <math.h>
#include <stdlib.h>
#include <iostream>
#include <fstream>
#include <omp.h>
```

```
/*------------------------------------------------------ //If you want to use normal FH you ca
//Free energy of the system
double florhug (double phia, double phib, double Na,double Nb, double chi){
double florhug=phia*log(phia)/Na+chi*phia*phib+phib*log(phib)/Nb;
return florhug;
}
------------------------------------------------------*/
//Inflection points
double inflectionA (double Na, double Nb, double chi){
 double inflectionA=0.5+1/(4*Na*chi)-1/(4*Nb*chi);
return inflectionA;
}
/*------------------------------------------------------*/
double inflectionB (double Na, double Nb, double chi){
 double inflectionB=sqrt(pow((Nb-Na+2*Na*Nb*chi),2)-8*Na*pow(Nb,2)*chi)/(4*Na*Nb*chi);
return inflectionB;
}
/*------------------------------------------------------*/
double florhug (double phi0, double Na,double phinf, double chi, double B){
double florhug=(phi0*log(phi0)/Na+chi*phi0*((double)1-phi0))+B*((double)1-phinf)*(pow(((doub
return florhug;
}

/*------------------------------------------------------*/
int i,j,k;
double phia,phib,chi,Na,eps,B,minima[3],phinf,Nb,inflection1,inflection2,slop[100000],locati
using namespace std;
main(){
fstream fb("common_tangent_elast_comparison.dat",ios::out); //output energy
/*------------------------------------------------------*/
//Vairables
chi=1.7; //Flory-Huggins parameter
Na=1; //Degree of polymerization
Nb=4;
phinf=0.05; //phi infinity
```

```
B=0.1; //elastic modulus
eps=1e-5; //lattice parameter. Change for better calculation
/*-------------------------------------------------*/
//Initialization
phia=1e-12;
//Inflection points
inflection1=0.296337;//chi=1.7//0.187653;//0.189832;//chi=2.7 //0.24741;//chi=2.1//0.202342;
//-------------------------------------------------------------------------
//Free energy local slop and zeros
j=0;
test1=1;
for(i=1;i<=1e+5;i++){
//test1=florhug(phia,Na,phinf,chi,B);
slop[i]=(florhug(phia+eps,Na,phinf,chi,B)-florhug(phia,Na,phinf,chi,B))/eps; //numerical che
if(fabs(slop[i]/fabs(slop[i])-slop[i-1]/fabs(slop[i-1]))==2){
minima[j]=phia;
locationminima[j]=i;
j=j+1;
cout<<phia<<endl;
}
if((florhug(phia,Na,phinf,chi,B)<test1)&&(phia>0.6)){
test2=phia;
test1=florhug(phia+eps,Na,phinf,chi,B);
}
phia=phia+eps;
//end for loop1
}
//cout<<test2<<endl;//" "<<j<<endl;
//minima[2]=0.92;
phia=minima[0];//left minimum
phib=minima[2];//right minimum
cout<<phia<<" "<<phib<<" "<<inflection1<<endl;
while(phia<=inflection1){
i=0;
phib=minima[2];//0.87;
```

```
//cout<<phib<<endl;
while(phib<=1){
slopetan[i]=(florhug(phia,Na,phinf,chi,B)-florhug(phib,Na,phinf,chi,B))/(phia-phib);
test1=fabs(slopetan[i]-(florhug(phia+eps,Na,phinf,chi,B)-florhug(phia,Na,phinf,chi,B))/eps);
test2=fabs(slopetan[i]-(florhug(phib+eps,Na,phinf,chi,B)-florhug(phib,Na,phinf,chi,B))/eps);
if((test1<=1e-4)&&(test2<=1e-4)){
angular[0]=phia;
angular[1]=phib;
angular[2]=slopetan[i];
cout<<phia<<" "<<phib<<endl;
}
//end second while loop
phib=phib+eps;
i++;
}
//end first while loop
phia=phia+eps;
//cout<<i<<endl;
}
//angular[2]=0.1794;
//angular[0]=0.037;
//angular[1]=0.906368;
cout<<"tangent1:y="<<angular[2]<<"x"<<florhug(angular[0],Na,phinf,chi,B)-angular[2]*angular[
cout<<"tangent2:y="<<angular[2]<<"x"<<florhug(angular[1],Na,phinf,chi,B)-angular[2]*angular[
cout<<florhug(angular[0],Na,phinf,chi,B)<<" "<<florhug(angular[1],Na,phinf,chi,B)<<endl;
phia=1e-12;
for(i=1;i<=1e+5;i++){
test1=florhug(phia,Na,phinf,chi,B)-florhug(angular[0],Na,phinf,chi,B)+angular[2]*angular[0]-
fb<<phia<<" "<<test1<<" "<<florhug(phia,Na,phinf,chi,B)<<endl;
phia=phia+eps;
}

//end program
}
```

Bibliography

[1] J. Antony. *Design of Experiments for Engineers and Scientists*. Elsevier Science, 2003.
https://books.google.co.uk/books?id=Lg2iyehYXroC.

[2] Pedro F. Arce and Martín Aznar. 'Modeling of thermodynamic behavior of {PVT} properties and cloud point temperatures of polymer blends and polymer blend + carbon dioxide systems using non-cubic equations of state'. In: *Fluid Phase Equilibria* 286.1 (2009), pp. 17 –27.
http://www.sciencedirect.com/science/article/pii/S0378381209003008
doi:https://doi.org/10.1016/j.fluid.2009.08.002.

[3] V.I. Arnol'd and V.I. ArnolÊ¹d. *Dynamical systems III*. Encyclopaedia of mathematical sciences. Springer, 1988.
https://books.google.co.uk/books?id=PVTvAAAAMAAJ.

[4] Qamardeep S. Bhatia, David H. Pan and Jeffrey T. Koberstein. 'Preferential surface adsorption in miscible blends of polystyrene and poly(vinyl methyl ether)'. In: *Macromolecules* 21.7 (1988), pp. 2166–2175.
http://dx.doi.org/10.1021/ma00185a049
doi:10.1021/ma00185a049.
arXiv:http://dx.doi.org/10.1021/ma00185a049.

[5] Qamardeep S. Bhatia, David H. Pan and Jeffrey T. Koberstein. 'Preferential surface adsorption in miscible blends of polystyrene and poly(vinyl methyl ether)'. In: *Macromolecules* 21.7 (1988), pp. 2166–2175.

http://dx.doi.org/10.1021/ma00185a049

doi:10.1021/ma00185a049.

arXiv:http://dx.doi.org/10.1021/ma00185a049.

[6] Kanishka Bhunia, Shyam S. Sablani, Juming Tang and Barbara Rasco. 'Migration of Chemical Compounds from Packaging Polymers during Microwave, Conventional Heat Treatment, and Storage'. In: *Comprehensive Reviews in Food Science and Food Safety* 12.5 (2013), pp. 523–545.

http://dx.doi.org/10.1111/1541-4337.12028

doi:10.1111/1541-4337.12028.

[7] K. Binder. 'Collective diffusion, nucleation, and spinodal decomposition in polymer mixtures'. In: *The Journal of Chemical Physics* 79.12 (1983), pp. 6387–6409.

http:

//scitation.aip.org/content/aip/journal/jcp/79/12/10.1063/1.445747

doi:http://dx.doi.org/10.1063/1.445747.

[8] K. Binder. 'Nucleation barriers, spinodals, and the Ginzburg criterion'. In: *Phys. Rev. A* 29 (1 1984), pp. 341–349.

http://link.aps.org/doi/10.1103/PhysRevA.29.341

doi:10.1103/PhysRevA.29.341.

[9] Daniel Bonn, Jens Eggers, Joseph Indekeu, Jacques Meunier and Etienne Rolley. 'Wetting and spreading'. In: *Rev. Mod. Phys.* 81 (2 2009), pp. 739–805.

http://link.aps.org/doi/10.1103/RevModPhys.81.739

doi:10.1103/RevModPhys.81.739.

[10] W. L. Bragg and E. J. Williams. 'The Effect of Thermal Agitation on Atomic Arrangement in Alloys'. In: *Proceedings of the Royal Society of London A: Mathematical, Physical and Engineering Sciences* 145.855 (1934), pp. 699–730.

http://rspa.royalsocietypublishing.org/content/145/855/699
doi:10.1098/rspa.1934.0132.
arXiv:http:
//rspa.royalsocietypublishing.org/content/145/855/699.full.pdf.

[11] A.J. Bray. 'Theory of phase-ordering kinetics'. In: *Advances In Physics* 43 (3 1994).
doi:10.1080/00018739400101505.

[12] Pavel K. Brazhnik, Karl F. Freed and Hai Tang. 'Polymer melt near a solid wall'. In: *The Journal of Chemical Physics* 101.10 (1994), pp. 9143–9154.
http:
//scitation.aip.org/content/aip/journal/jcp/101/10/10.1063/1.468044
doi:http://dx.doi.org/10.1063/1.468044.

[13] F. Bruder and R. Brenn. 'Surface Phase Transition in a Polymer Blend'. In: *EPL (Europhysics Letters)* 22.9 (1993), p. 707.
http://stacks.iop.org/0295-5075/22/i=9/a=012.

[14] Rene Brun and Fons Rademakers. 'ROOT — An object oriented data analysis framework'. In: *Nuclear Instruments and Methods in Physics Research Section A: Accelerators, Spectrometers, Detectors and Associated Equipment* 389.1 (1997). New Computing Techniques in Physics Research V, pp. 81 –86.
http://www.sciencedirect.com/science/article/pii/S016890029700048X
doi:http://dx.doi.org/10.1016/S0168-9002(97)00048-X.

[15] A. Budkowski, J. Rysz, F. Scheffold and J. Klein. 'Surface enrichment-depletion duality in a binary polymer blend'. In: *EPL (Europhysics Letters)* 43.4 (1998), p. 404.
http://stacks.iop.org/0295-5075/43/i=4/a=404.

[16] Andrzej Budkowski. 'Interfacial Phenomena in Thin Polymer Films: Phase Coexistence and Segregation'. In: *Interfaces Crystallization Viscoelasticity.*

Berlin, Heidelberg: Springer Berlin Heidelberg, 1999, pp. 1–111.
https://doi.org/10.1007/3-540-48836-7_1
doi:10.1007/3-540-48836-7_1.

[17] Andrzej Budkowski. 'Interfacial Phenomena in Thin Polymer Films: Phase Coexistence and Segregation'. In: *Interfaces Crystallization Viscoelasticity*. Berlin, Heidelberg: Springer Berlin Heidelberg, 1999, pp. 1–111.
https://doi.org/10.1007/3-540-48836-7_1
doi:10.1007/3-540-48836-7_1.

[18] Andrzej Budkowski, Ullrich Steiner and Jacob Klein. 'The effects of confinement and surface interactions on coexistence in a binary polymer mixture'. In: *The Journal of Chemical Physics* 97.7 (1992), pp. 5229–5238.
http://dx.doi.org/10.1063/1.463821
doi:10.1063/1.463821.
arXiv:http://dx.doi.org/10.1063/1.463821.

[19] J. Cahn. 'Critical point wetting.' In: *J. Chem. Phys.* 66 (1977), p. 3667.

[20] P.M. Chaikin and T.C. Lubensky. *Principles of Condensed Matter Physics*. Cambridge University Press, 2000.
http://books.google.nl/books?id=P9YjNjzr9OIC.

[21] Kan Chen, C. Jayaprakash, Rahul Pandit and Wolfgang Wenzel. 'Microemulsions: A Landau-Ginzburg theory'. In: *Phys. Rev. Lett.* 65 (21 1990), pp. 2736–2739.
http://link.aps.org/doi/10.1103/PhysRevLett.65.2736
doi:10.1103/PhysRevLett.65.2736.

[22] Zheng Yu Chen and Jaan Noolandi. 'Wetting transitions of asymmetric binary polymer mixtures'. In: *Macromolecular Theory and Simulations* 1.1 (1992), pp. 31–35.
http://dx.doi.org/10.1002/mats.1992.040010104
doi:10.1002/mats.1992.040010104.

[23] C. J. Clarke, R. A. L. Jones, J. L. Edwards, K. R. Shull and J. Penfold. 'The Structure of Grafted Polystyrene Layers in a Range of Matrix Polymers'. In: *Macromolecules* 28.6 (1995), pp. 2042–2049.
http://dx.doi.org/10.1021/ma00110a043
doi:10.1021/ma00110a043.
arXiv:http://dx.doi.org/10.1021/ma00110a043.

[24] Scott M. Cohen and M. Muthukumar. 'Critical wetting in two-component polymer blends'. In: *The Journal of Chemical Physics* 90.10 (1989), pp. 5749–5755.
http:
//scitation.aip.org/content/aip/journal/jcp/90/10/10.1063/1.456383
doi:http://dx.doi.org/10.1063/1.456383.

[25] Salvatore Croce, Jarosław Krawczyk, Gabriel Schäfer, Torsten Lindner and Buddhapriya Chakrabarti. 'Surface segregation and wetting in binary polymeric gels'. In: *manuscript in preparation* (2018).

[26] G D'Agostini. 'Bayesian inference in processing experimental data: principles and basic applications'. In: *Reports on Progress in Physics* 66.9 (2003), p. 1383.
http://stacks.iop.org/0034-4885/66/i=9/a=201.

[27] Jeffrey DeFelice, Julia S. Higgins and Jane E.G. Lipson. 'The effects of branching and deuterium labeling on blend miscibility'. In: *Polymer* 114 (2017), pp. 149 –160.
http://www.sciencedirect.com/science/article/pii/S0032386117302306
doi:https://doi.org/10.1016/j.polymer.2017.02.089.

[28] J.L. Devore. *Probability and Statistics for Engineering and the Sciences*. Cengage Learning, 2011.
https://books.google.co.uk/books?id=3qoP7dlO4BUC.

[29] M. Doi. *Introduction to Polymer Physics*. Oxford science publications. Clarendon Press, 1996.
http://books.google.co.uk/books?id=mYkAngEACAAJ.

[30] M. Doi and S.F. Edwards. *The theory of polymer dynamics*. International series of monographs on physics. Clarendon Press, 1986.
http://books.google.co.uk/books?id=h-PvAAAAMAAJ.

[31] Fran çois Drolet and Glenn H. Fredrickson. 'Combinatorial Screening of Complex Block Copolymer Assembly with Self-Consistent Field Theory'. In: *Phys. Rev. Lett.* 83 (21 1999), pp. 4317–4320.
https://link.aps.org/doi/10.1103/PhysRevLett.83.4317
doi:10.1103/PhysRevLett.83.4317.

[32] S F Edwards. 'The statistical mechanics of polymers with excluded volume'. In: *Proceedings of the Physical Society* 85.4 (1965), p. 613.
http://stacks.iop.org/0370-1328/85/i=4/a=301.

[33] J. F. Elman, B. D. Johs, T. E. Long and J. T. Koberstein. 'A Neutron Reflectivity Investigation of Surface and Interface Segregation of Polymer Functional End Groups'. In: *Macromolecules* 27.19 (1994), pp. 5341–5349.
http://dx.doi.org/10.1021/ma00097a013
doi:10.1021/ma00097a013.
arXiv:http://dx.doi.org/10.1021/ma00097a013.

[34] R. Eppe, E. W. Fischer and H. A. Stuart. 'Morphologische strukturen in polyäthylenen, polyamiden und anderen kristallisierenden hochpolymeren'. In: *Journal of Polymer Science* 34.127 (1959), pp. 721–740.
http://dx.doi.org/10.1002/pol.1959.1203412748
doi:10.1002/pol.1959.1203412748.

[35] R. Esposito. *Appunti dalle lezioni di meccanica razionale*. Aracne, 1999.
https://books.google.co.uk/books?id=8pxsPQAACAAJ.

[36] Richard P. Feynman. 'There's Plenty of Room at the Bottom'. In: 1959.

[37] R.P. Feynman and A.R. Hibbs. *Quantum mechanics and path integrals*. International series in pure and applied physics. McGraw-Hill, 1965. https://books.google.it/books?id=14ApAQAAMAAJ.

[38] R.A. Fisher. *The design of experiments*. Hafner Pub. Co., 1966. https://books.google.co.uk/books?id=909qAAAAMAAJ.

[39] P. Flory. 'Thermodynamics of high polymer solutions.' In: *J. Chem. Phys* 9 (1941), p. 660.

[40] Johannes G. E. M. Fraaije, Shyamal K. Nath, Klaas Remerie and Jan Groenewold. 'Phase Evolution Theory for Polymer Blends with Extreme Chemical Dispersity: Parameterization of DDFT Simulations and Application to Poly(propylene) Impact Copolymers'. In: *Macromolecular Theory and Simulations* 20.2 (2011), pp. 133–145. http://dx.doi.org/10.1002/mats.201000056 doi:10.1002/mats.201000056.

[41] Glenn H. Fredrickson. *The Equilibrium Theory of Inhomogeneous Polymers*. The International Series Of Monograohs On Physics. Oxford university press, 2006.

[42] K.F. Freed. *Renormalization Group Theory of Macromolecules*. A Wiley-Interscience publication. Wiley, 1987. http://books.google.co.uk/books?id=Hgt2QgAACAAJ.

[43] P. G. de Gennes. 'Wetting: statics and dynamics'. In: *Rev. Mod. Phys.* 57 (3 1985), pp. 827–863. http://link.aps.org/doi/10.1103/RevModPhys.57.827 doi:10.1103/RevModPhys.57.827.

[44] P.G. de Gennes. *Scaling Concepts in Polymer Physics*. Cornell University Press, 1979.

[45] J. Genzer and R. J. Composto. 'Surface segregation amplification in miscible polymer blends near criticality'. In: *EPL (Europhysics Letters)* 38.3 (1997), p. 171.
http://stacks.iop.org/0295-5075/38/i=3/a=171.

[46] J. Genzer, A. Faldi and R. J. Composto. 'Self-consistent mean-field calculation of surface segregation in a binary polymer blend'. In: *Phys. Rev. E* 50 (3 1994), pp. 2373–2376.
http://link.aps.org/doi/10.1103/PhysRevE.50.2373
doi:10.1103/PhysRevE.50.2373.

[47] J. Genzer, A. Faldi, R. Oslanec and R. J. Composto. 'Surface Enrichment in a Miscible Polymer Blend: An Experimental Test of Self-Consistent Field and Long-Wavelength Approximation Models'. In: *Macromolecules* 29.16 (1996), pp. 5438–5445.
http://dx.doi.org/10.1021/ma951108f
doi:10.1021/ma951108f.
arXiv:http://dx.doi.org/10.1021/ma951108f.

[48] Jan Genzer and Russell J. Composto. 'A self-consistent field study of the wetting transition in binary polymer blends'. In: *The Journal of Chemical Physics* 106.3 (1997), pp. 1257–1263.
http:
//scitation.aip.org/content/aip/journal/jcp/106/3/10.1063/1.473222
doi:http://dx.doi.org/10.1063/1.473222.

[49] Mark Geoghegan and Georg Krausch. 'Wetting at polymer surfaces and interfaces'. In: *Progress in Polymer Science* 28.2 (2003), pp. 261 –302.
http://www.sciencedirect.com/science/article/pii/S0079670002000801
doi:http://dx.doi.org/10.1016/S0079-6700(02)00080-1.

[50] H. Goldstein. *Classical Mechanics*. Pearson Education, 2002.
https://books.google.co.uk/books?id=Spy6xHWFJIEC.

[51] Gerhard Gompper and Michael Schick. 'An Introduction to Soft Matter'. In: *Soft Matter*. Wiley-VCH Verlag GmbH Co. KGaA, 2007, pp. 1–16. http://dx.doi.org/10.1002/9783527617050.ch doi:10.1002/9783527617050.ch.

[52] Martin J. Greenall, D. Martin A. Buzza and Thomas C. B. McLeish. 'Micelle Formation in Block Copolymer/Homopolymer Blends: Comparison of Self-Consistent Field Theory with Experiment and Scaling Theory'. In: *Macromolecules* 42.15 (2009), pp. 5873–5880. http://dx.doi.org/10.1021/ma9000594 doi:10.1021/ma9000594. arXiv:http://dx.doi.org/10.1021/ma9000594.

[53] G. Grosso and G.P. Parravicini. *Solid State Physics*. Elsevier Science, 2013. https://books.google.co.uk/books?id=ZJzmUAp0hMcC.

[54] E. A. Guggenheim. 'Statistical Thermodynamics of Mixtures with Zero Energies of Mixing'. In: *Proceedings of the Royal Society of London A: Mathematical, Physical and Engineering Sciences* 183.993 (1944), pp. 203–212. http://rspa.royalsocietypublishing.org/content/183/993/203 doi:10.1098/rspa.1944.0032. arXiv:http: //rspa.royalsocietypublishing.org/content/183/993/203.full.pdf.

[55] A. Halperin, M. Tirrell and T. P. Lodge. 'Tethered chains in polymer microstructures'. In: *Macromolecules: Synthesis, Order and Advanced Properties*. Berlin, Heidelberg: Springer Berlin Heidelberg, 1992, pp. 31–71. http://dx.doi.org/10.1007/BFb0051635 doi:10.1007/BFb0051635.

[56] Archie E. Hamielec and Hidetaka Tobita. *Polymerization Processes*. Wiley-VCH Verlag GmbH & Co. KGaA, 2000.

http://dx.doi.org/10.1002/14356007.a21_305

doi:10.1002/14356007.a21_305.

[57] J. Han. *Innovations in Food Packaging, 2nd Edition*. Elsevier, 2013.

[58] Jan-Willem Handgraaf, Ruben Serral Gracia, Shyamal K. Nath, Zhong Chen, Shih-Hung Chou, Richard B. Ross, Nate E. Schultz and Johannes G. E. M. Fraaije. 'A Multiscale Modeling Protocol To Generate Realistic Polymer Surfaces'. In: *Macromolecules* 44.4 (2011), pp. 1053–1061.

http://dx.doi.org/10.1021/ma1022567

doi:10.1021/ma1022567.

arXiv:http://dx.doi.org/10.1021/ma1022567.

[59] Julia S. Higgins, Jane E. G. Lipson and Ronald P. White. 'A simple approach to polymer mixture miscibility'. In: *Philosophical Transactions of the Royal Society of London A: Mathematical, Physical and Engineering Sciences* 368.1914 (2010), pp. 1009–1025.

http://rsta.royalsocietypublishing.org/content/368/1914/1009

doi:10.1098/rsta.2009.0215.

arXiv:http:

//rsta.royalsocietypublishing.org/content/368/1914/1009.full.pdf.

[60] P. C. Hohenberg and B. I. Halperin. 'Theory of dynamic critical phenomena'. In: *Rev. Mod. Phys.* 49 (3 1977), pp. 435–479.

http://link.aps.org/doi/10.1103/RevModPhys.49.435

doi:10.1103/RevModPhys.49.435.

[61] T. Idema, J. M. J. van Leeuwen and C. Storm. 'Phase coexistence and line tension in ternary lipid systems'. In: *Phys. Rev. E* 80 (4 2009), p. 041924.

http://link.aps.org/doi/10.1103/PhysRevE.80.041924

doi:10.1103/PhysRevE.80.041924.

[62] Ronald L. Iman and W. J. Conover. 'A distribution-free approach to inducing rank correlation among input variables'. In: *Communications in*

Statistics - Simulation and Computation 11.3 (1982), pp. 311–334.
https://doi.org/10.1080/03610918208812265
doi:10.1080/03610918208812265.
arXiv:https://doi.org/10.1080/03610918208812265.

[63] Ronald L. Iman and W.J. Conover. 'Small sample sensitivity analysis techniques for computer models.with an application to risk assessment'. In: *Communications in Statistics - Theory and Methods* 9.17 (1980), pp. 1749–1842.
https://doi.org/10.1080/03610928008827996
doi:10.1080/03610928008827996.
arXiv:https://doi.org/10.1080/03610928008827996.

[64] SAS Institute Inc. *Using JMP® 13*. SAS Institute Inc. Cary, NC, USA, 2016.

[65] R. A. L. Jones. 'Effect of long-range forces on surface enrichment in polymer blends'. In: *Phys. Rev. E* 47 (2 1993), pp. 1437–1440.
http://link.aps.org/doi/10.1103/PhysRevE.47.1437
doi:10.1103/PhysRevE.47.1437.

[66] R. A. L. Jones et al. 'The Form of the Enriched Surface Layer in Polymer Blends'. In: *EPL (Europhysics Letters)* 12.1 (1990), p. 41.
http://stacks.iop.org/0295-5075/12/i=1/a=008
doi:10.1209/0295-5075/12/1/008.

[67] R.A.L. Jones. 'The wetting transition for polymer mixtures'. In: *Polymer* 35.10 (1994), pp. 2160 –2166.
http://www.sciencedirect.com/science/article/pii/0032386194902445
doi:http://dx.doi.org/10.1016/0032-3861(94)90244-5.

[68] R.A.L. Jones and R.W. Richards. *Polymers at Surfaces and Interfaces*. Cambridge University Press, 1999.
http://books.google.co.uk/books?id=WUFLcLS4ZzkC.

[69] Richard A. L. Jones, Laura J. Norton, Edward J. Kramer, Frank S. Bates and Pierre Wiltzius. 'Surface-directed spinodal decomposition'. In: *Phys. Rev. Lett.* 66 (10 1991), pp. 1326–1329.
http://link.aps.org/doi/10.1103/PhysRevLett.66.1326
doi:10.1103/PhysRevLett.66.1326.

[70] Richard A. L. Jones, Edward J. Kramer, Miriam H. Rafailovich, Jonathon Sokolov and Steven A. Schwarz. 'Surface Enrichment in an Isotopic Polymer Blend'. In: *Phys. Rev. Lett.* 62 (3 1989), pp. 280–283.
http://link.aps.org/doi/10.1103/PhysRevLett.62.280
doi:10.1103/PhysRevLett.62.280.

[71] M. Kapnistos, M. Lang, D. Vlassopoulos, W. Pyckhout-Hintzen, D. Richter, D. Cho, T. Chang and M. Rubinstein. 'Unexpected power-law stress relaxation of entangled ring polymers'. In: *Nature materials* 7 (2008), pp. 997 –1002.
doi:10.1038/nmat2292.

[72] Solomon M. Kimani, Sarah J. Hardman, Lian R. Hutchings, Nigel Clarke and Richard L. Thompson. 'Synthesis and surface activity of high and low surface energy multi-end functional polybutadiene additives'. In: *Soft Matter* 8 (12 2012), pp. 3487–3496.
http://dx.doi.org/10.1039/C2SM07361G
doi:10.1039/C2SM07361G.

[73] S. Komura, H. Shirotori, P. D. Olmsted and D. Andelman. 'Lateral phase separation in mixtures of lipids and cholesterol'. In: *EPL (Europhysics Letters)* 67.2 (2004), p. 321.
http://stacks.iop.org/0295-5075/67/i=2/a=321.

[74] Jarosław Krawczyk, Salvatore Croce, T. C. B. McLeish and Buddhapriya Chakrabarti. 'Elasticity Dominated Surface Segregation of Small Molecules in Polymer Mixtures'. In: *Phys. Rev. Lett.* 116 (20 2016),

p. 208301.
http://link.aps.org/doi/10.1103/PhysRevLett.116.208301
doi:10.1103/PhysRevLett.116.208301.

[75] Sanat K. Kumar, Arun Yethiraj, Kenneth S. Schweizer and Frans A. M. Leermakers. 'The effects of local stiffness disparity on the surface segregation from binary polymer blends'. In: *The Journal of Chemical Physics* 103.23 (1995), pp. 10332–10346.
http:
//scitation.aip.org/content/aip/journal/jcp/103/23/10.1063/1.469871
doi:http://dx.doi.org/10.1063/1.469871.

[76] L.D. Landau and E.M. Lifshitz. *Statistical Physics*. v. 5. Elsevier Science, 2013.
https://books.google.com/books?id=VzgJN-XPTRsC.

[77] Z.R. Lazic. *Design of Experiments in Chemical Engineering: A Practical Guide*. Wiley, 2006.
https://books.google.co.uk/books?id=QwxvTUjlW-IC.

[78] Woo Lee, Mi-Kyoung Jin, Won-Cheol Yoo and Jin-Kyu Lee. 'Nanostructuring of a Polymeric Substrate with Well-Defined Nanometer-Scale Topography and Tailored Surface Wettability'. In: *Langmuir* 20.18 (2004). PMID: 15323517, pp. 7665–7669.
http://dx.doi.org/10.1021/la049411+
doi:10.1021/la049411+.
arXiv:http://dx.doi.org/10.1021/la049411+.

[79] T. Lindner. 'Adhesive technologies'. In: *P&G R&D department* (2016).

[80] J. E. G. Lipson and S. S. Andrews. 'A Born–Green–Yvon integral equation treatment of a compressible fluid'. In: *The Journal of Chemical Physics* 96.2 (1992), pp. 1426–1434.
http://dx.doi.org/10.1063/1.462178

doi:10.1063/1.462178.

arXiv:http://dx.doi.org/10.1063/1.462178.

[81] Jane E. G. Lipson and Ronald P. White. 'Connecting Theory and Experiment To Understand Miscibility in Polymer and Small Molecule Mixtures'. In: *Journal of Chemical & Engineering Data* 59.10 (2014), pp. 3289–3300.

http://dx.doi.org/10.1021/je5002818

doi:10.1021/je5002818.

arXiv:http://dx.doi.org/10.1021/je5002818.

[82] Pierre Lonchampt and Richard W. Hartel. 'Fat bloom in chocolate and compound coatings'. In: *European Journal of Lipid Science and Technology* 106.4 (2004), pp. 241–274.

http://dx.doi.org/10.1002/ejlt.200400938

doi:10.1002/ejlt.200400938.

[83] J. E. Mark. 'The use of model polymer networks to elucidate molecular aspects of rubberlike elasticity'. In: *Polymer Networks*. Ed. by Karel Dušek. Berlin, Heidelberg: Springer Berlin Heidelberg, 1982, pp. 1–26.

http://dx.doi.org/10.1007/3-540-11471-8_1

doi:10.1007/3-540-11471-8_1.

[84] N. M. Maurits and J. G. E. M. Fraaije. 'Mesoscopic dynamics of copolymer melts: From density dynamics to external potential dynamics using nonlocal kinetic coupling'. In: *The Journal of Chemical Physics* 107.15 (1997), pp. 5879–5889.

http://dx.doi.org/10.1063/1.474313

doi:10.1063/1.474313.

arXiv:http://dx.doi.org/10.1063/1.474313.

[85] J. C. Maxwell. 'On the Dynamical Evidence of the Molecular Constitution of Bodies'. In: *Nature* 11 (1875), pp. 357–359. doi:10.1038/011357a0.

[86] M. D. McKay, R. J. Beckman and W. J. Conover. 'A Comparison of Three Methods for Selecting Values of Input Variables in the Analysis of Output from a Computer Code'. In: *Technometrics* 21.2 (1979), pp. 239–245. http://www.jstor.org/stable/1268522.

[87] S. T. Milner. 'Polymer Brushes'. In: *Science* 251 (4996 1991). doi:10.1126/science.251.4996.905.

[88] S. T. Milner, T. A. Witten and M. E. Cates. 'Theory of the grafted polymer brush'. In: *Macromolecules* 21.8 (1988), pp. 2610–2619. http://dx.doi.org/10.1021/ma00186a051 doi:10.1021/ma00186a051. arXiv:http://dx.doi.org/10.1021/ma00186a051.

[89] Mithun K. Mitra and M. Muthukumar. 'Theory of spinodal decomposition assisted crystallization in binary mixtures'. In: *The Journal of Chemical Physics* 132.18, 184908 (2010). http: //scitation.aip.org/content/aip/journal/jcp/132/18/10.1063/1.3425774 doi:http://dx.doi.org/10.1063/1.3425774.

[90] M. Muthukumar. 'Nucleation in Polymer Crystallization'. In: *Advances in Chemical Physics*. John Wiley & Sons, Inc., 2004, pp. 1–63. http://dx.doi.org/10.1002/0471484237.ch1 doi:10.1002/0471484237.ch1.

[91] L. J. Norton, E. J. Kramer, F. S. Bates, M. D. Gehlsen, R. A. L. Jones, A. Karim, G. P. Felcher and R. Kleb. 'Neutron Reflectometry Study of Surface Segregation in an Isotopic Poly(ethylenepropylene) Blend: Deviation from Mean-Field Theory'. In: *Macromolecules* 28.25 (1995), pp. 8621–8628.

http://dx.doi.org/10.1021/ma00129a022

doi:10.1021/ma00129a022.

arXiv:http://dx.doi.org/10.1021/ma00129a022.

[92] E. Kumacheva N.Zhihong. 'Patterning surfaces with functional polymers'. In: *Nature Materials* 7.4 (2008/04//print), pp. 277–290.

http://dx.doi.org/10.1038/nmat2109

doi:10.1038/nmat2109.

arXiv:http://dx.doi.org/10.1038/nmat2109.

[93] H. Okamoto and T. B. Massalski. 'The AuPt (Gold-Platinum) system'. In: *Bulletin of Alloy Phase Diagrams* 6.1 (1985), pp. 46–56.

http://dx.doi.org/10.1007/BF02871187

doi:10.1007/BF02871187.

[94] P. D. Olmsted, W. C. K. Poon, T. C. B. McLeish, N. J. Terrill and A. J. Ryan. 'Spinodal-Assisted Crystallization in Polymer Melts'. In: *Phys. Rev. Lett.* 81 (2 1998), pp. 373–376.

http://link.aps.org/doi/10.1103/PhysRevLett.81.373

doi:10.1103/PhysRevLett.81.373.

[95] D.H.-K. Pan and W. M. Prest. 'Surfaces of polymer blends: X-ray photoelectron spectroscopy studies of polystyrene/poly(vinyl methyl ether) blends'. In: *Journal of Applied Physics* 58.8 (1985), pp. 2861–2870.

http:

//scitation.aip.org/content/aip/journal/jap/58/8/10.1063/1.335858

doi:http://dx.doi.org/10.1063/1.335858.

[96] Rahul Pandit and Michael E. Fisher. 'Wetting Transitions near Bulk Triple Points'. In: *Phys. Rev. Lett.* 51 (19 1983), pp. 1772–1775.

http://link.aps.org/doi/10.1103/PhysRevLett.51.1772

doi:10.1103/PhysRevLett.51.1772.

[97] Rahul Pandit, M. Schick and Michael Wortis. 'Systematics of multilayer adsorption phenomena on attractive substrates'. In: *Phys. Rev. B* 26 (9 1982), pp. 5112–5140.
http://link.aps.org/doi/10.1103/PhysRevB.26.5112
doi:10.1103/PhysRevB.26.5112.

[98] Sergei Panyukov and Yitzhak Rabin. 'Statistical physics of polymer gels'. In: *Physics Reports* 269.1 2 (1996), pp. 1–131.
http://www.sciencedirect.com/science/article/pii/0370157395000682
doi:http://dx.doi.org/10.1016/0370-1573(95)00068-2.

[99] William H. Press, Saul A. Teukolsky, William T. Vetterling and Brian P. Flannery. *Numerical Recipes in C++*. Cambridge, 2002.

[100] I Prigogine and J Marechal. 'The influence of differences in molecular size on the surface tension of solutions. IV'. In: *Journal of Colloid Science* 7.2 (1952), pp. 122 –127.
http://www.sciencedirect.com/science/article/pii/009585225290055X
doi:http://dx.doi.org/10.1016/0095-8522(52)90055-X.

[101] R Core Team. *R: A Language and Environment for Statistical Computing*. R Foundation for Statistical Computing. Vienna, Austria, 2013.
http://www.R-project.org/.

[102] Karine Ragil, Jacques Meunier, Daniel Broseta, Joseph O. Indekeu and Daniel Bonn. 'Experimental Observation of Critical Wetting'. In: *Phys. Rev. Lett.* 77 (8 1996), pp. 1532–1535.
https://link.aps.org/doi/10.1103/PhysRevLett.77.1532
doi:10.1103/PhysRevLett.77.1532.

[103] L.E. Reichl. *A Modern Course in Statistical Physics*. Physics textbook. Wiley, 2009.
https://books.google.co.uk/books?id=H_4qxPazAYEC.

[104] D. Ross, D. Bonn and J. Meunier. 'Observation of short-range critical wetting'. In: *Nature* 400.6746 (1999), pp. 737–739.
http://dx.doi.org/10.1038/23425
doi:10.1038/23425.

[105] M. Rubinstein and R.H. Colby. *Polymer Physics*. OUP Oxford, 2003.
http://books.google.co.uk/books?id=RHksknEQYsYC.

[106] J. Rysz, A. Budkowski, A. Bernasik, J. Klein, K. Kowalski, J. Jedliński and L. J. Fetters. 'Wetting transition in a binary polymer blend'. In: *EPL (Europhysics Letters)* 50.1 (2000), p. 35.
http://stacks.iop.org/0295-5075/50/i=1/a=035.

[107] Elise Fanny Delphine Sabattié. *Oligomer/polymer mixtures as model adhesives: Impact of compatibility on surface segregation behaviour*. Durham theses, Durham University, 2018.
http://etheses.dur.ac.uk/12459/.

[108] Elise F. D. Sabattie, Jos Tasche, Mark R. Wilson, Maximilian W. A. Skoda, Arwel Hughes, Torsten Lindner and Richard L. Thompson. 'Predicting oligomer/polymer compatibility and the impact on nanoscale segregation in thin films'. In: *Soft Matter* 13 (19 2017), pp. 3580–3591.
http://dx.doi.org/10.1039/C7SM00048K
doi:10.1039/C7SM00048K.

[109] Tsukasa Sato, Kazutaka Katayama, Takaki Suzuki and Tomoo Shiomi. 'UCST and LCST behaviour in polymer blends containing poly(methyl methacrylate-statstyrene)'. In: *Polymer* 39.4 (1998), pp. 773 –780.
http://www.sciencedirect.com/science/article/pii/S003238619700339X
doi:http://dx.doi.org/10.1016/S0032-3861(97)00339-X.

[110] S.L. Savage and H.M. Markowitz. *The Flaw of Averages: Why We Underestimate Risk in the Face of Uncertainty*. Wiley, 2009.
https://books.google.co.uk/books?id=2lsLAQi0LlcC.

[111] J. M. H. M. Scheutjens and G. J. Fleer. 'Statistical theory of the adsorption of interacting chain molecules. 2. Train, loop, and tail size distribution'. In: *The Journal of Physical Chemistry* 84.2 (1980), pp. 178–190. http://dx.doi.org/10.1021/j100439a011 doi:10.1021/j100439a011. arXiv:http://dx.doi.org/10.1021/j100439a011.

[112] I. Schmidt and K. Binder. 'Model calculations for wetting transitions in polymer mixtures'. In: *J.Physique* 46 (1985), pp. 1631–1644. doi:http://dx.doi.org/10.1051/jphys:0198500460100163100.

[113] M. Sferrazza, C. Xiao, R. A. L. Jones, D. G. Bucknall, J. Webster and J. Penfold. 'Evidence for Capillary Waves at Immiscible Polymer/Polymer Interfaces'. In: *Phys. Rev. Lett.* 78 (19 1997), pp. 3693–3696. http://link.aps.org/doi/10.1103/PhysRevLett.78.3693 doi:10.1103/PhysRevLett.78.3693.

[114] Tomoo Shiomi, Katsumi Kohno, Kohji Yoneda, Tetsuo Tomita, Masamitsu Miya and Kiyokazu Imai. 'Thermodynamic interactions in the poly(vinyl methyl ether)-polystyrene system'. In: *Macromolecules* 18.3 (1985), pp. 414–419. http://dx.doi.org/10.1021/ma00145a020 doi:10.1021/ma00145a020. arXiv:http://dx.doi.org/10.1021/ma00145a020.

[115] Kenneth R. Shull. 'End-Adsorbed Polymer Brushes in High- and Low-Molecular-Weight Matrices'. In: *Macromolecules* 29.7 (1996), pp. 2659–2666. http://dx.doi.org/10.1021/ma951290k doi:10.1021/ma951290k. arXiv:http://dx.doi.org/10.1021/ma951290k.

[116] Kenneth R. Shull. 'Theory of end adsorbed polymer brushes in polymeric matrices'. In: *The Journal of Chemical Physics* 94.8 (1991), pp. 5723–5738. http://scitation.aip.org/content/aip/journal/jcp/94/8/10.1063/1.460456 doi:http://dx.doi.org/10.1063/1.460456.

[117] Kenneth R. Shull and Edward J. Kramer. 'Mean-field theory of polymer interfaces in the presence of block copolymers'. In: *Macromolecules* 23.22 (1990), pp. 4769–4779. http://dx.doi.org/10.1021/ma00224a005 doi:10.1021/ma00224a005. arXiv:http://dx.doi.org/10.1021/ma00224a005.

[118] Ullrich Steiner, Jacob Klein, Erika Eiser, Andrzej Budkowski and Lewis J. Fetters. 'Complete Wetting from Polymer Mixtures'. In: *Science* 258.5085 (1992), pp. 1126–1129. http://science.sciencemag.org/content/258/5085/1126 doi:10.1126/science.258.5085.1126. arXiv:http://science.sciencemag.org/content/258/5085/1126.full.pdf.

[119] Gert Strobl. '*Colloquium* : Laws controlling crystallization and melting in bulk polymers'. In: *Rev. Mod. Phys.* 81 (3 2009), pp. 1287–1300. http://link.aps.org/doi/10.1103/RevModPhys.81.1287 doi:10.1103/RevModPhys.81.1287.

[120] Augustinus J. M. Sweere and Johannes G. E. M. Fraaije. 'Accuracy Test of the OPLS-AA Force Field for Calculating Free Energies of Mixing and Comparison with PAC-MAC'. In: *Journal of Chemical Theory and Computation* 13.5 (2017). PMID: 28418655, pp. 1911–1923. http://dx.doi.org/10.1021/acs.jctc.6b01106 doi:10.1021/acs.jctc.6b01106. arXiv:http://dx.doi.org/10.1021/acs.jctc.6b01106.

[121] Hajime Tanaka. 'Universality of Viscoelastic Phase Separation in Dynamically Asymmetric Fluid Mixtures'. In: *Phys. Rev. Lett.* 76 (5 1996), pp. 787–790.
http://link.aps.org/doi/10.1103/PhysRevLett.76.787
doi:10.1103/PhysRevLett.76.787.

[122] *The Chemistry Unified Language Interface (Culgi), version 11.* Culgi B.V. The Netherlands, 2004-2017.

[123] L.R.G. Treloar. *The Physics of Rubber Elasticity.* Oxford Classic Texts in the Physical Sciences. OUP Oxford, 2005.
https://books.google.com/books?id=-iyDehYpoAQC.

[124] A. Werner, M. Müller, F. Schmid and K. Binder. 'Effect of long-range forces on the interfacial profiles in thin binary polymer films'. In: *The Journal of Chemical Physics* 110.2 (1999), pp. 1221–1229.
http:
//scitation.aip.org/content/aip/journal/jcp/110/2/10.1063/1.478164
doi:http://dx.doi.org/10.1063/1.478164.

[125] Ronald P. White and Jane E. G. Lipson. 'Chain fluids: Contrasts of theoretical and simulation approaches, and comparison with experimental alkane properties'. In: *The Journal of Chemical Physics* 131.7 (2009), p. 074109.
http://dx.doi.org/10.1063/1.3200925
doi:10.1063/1.3200925.
arXiv:http://dx.doi.org/10.1063/1.3200925.

[126] Ronald P. White and Jane E. G. Lipson. 'Polymer Free Volume and Its Connection to the Glass Transition'. In: *Macromolecules* 49.11 (2016), pp. 3987–4007.
http://dx.doi.org/10.1021/acs.macromol.6b00215

doi:10.1021/acs.macromol.6b00215.

arXiv:http://dx.doi.org/10.1021/acs.macromol.6b00215.

[127] Ronald P. White, Jane E. G. Lipson and Julia S. Higgins. 'How Pure Components Control Polymer Blend Miscibility'. In: *Macromolecules* 45.21 (2012), pp. 8861–8871.

http://dx.doi.org/10.1021/ma3018124

doi:10.1021/ma3018124.

arXiv:http://dx.doi.org/10.1021/ma3018124.

[128] Ronald P. White, Jane E. G. Lipson and Julia S. Higgins. 'New Correlations in Polymer Blend Miscibility'. In: *Macromolecules* 45.2 (2012), pp. 1076–1084.

http://dx.doi.org/10.1021/ma202393f

doi:10.1021/ma202393f.

arXiv:http://dx.doi.org/10.1021/ma202393f.

[129] Kenny Q. Ye. 'Orthogonal Column Latin Hypercubes and Their Application in Computer Experiments'. In: *Journal of the American Statistical Association* 93.444 (1998), pp. 1430–1439.

http://www.tandfonline.com/doi/abs/10.1080/01621459.1998.10473803

doi:10.1080/01621459.1998.10473803.

arXiv:http:

//www.tandfonline.com/doi/pdf/10.1080/01621459.1998.10473803.

[130] Arun Yethiraj. 'Entropic and Enthalpic Surface Segregation from Blends of Branched and Linear Polymers'. In: *Phys. Rev. Lett.* 74 (11 1995), pp. 2018–2021.

http://link.aps.org/doi/10.1103/PhysRevLett.74.2018

doi:10.1103/PhysRevLett.74.2018.